

RCA Review

RECEIVED FROM
NASA LIBRARY
AMES RESEARCH CENTER
MAR 25 1980
COPY NO. 1
MOFFETT FIELD, CALIF

December 1979

Volume 40 No. 4

RCARCI 40(4) 369-456 (1979)

RCA Review, published quarterly in March, June, September and December by RCA Research and Engineering, RCA Corporation, Princeton, New Jersey 08540. Entered as second class matter July 3, 1950 under the Act of March 3, 1879. Second-class postage paid at Princeton, New Jersey, and at additional mailing offices. Effective January 1, 1978, subscription rates as follows: United States and Canada: one year \$8.00, two years \$14.00, three years \$18.00; in other countries, one year \$8.60, two years \$15.20, three years \$19.80. Single copies (except for special issues) up to five years old \$3.00.

Contents

- 371 Carrier Generation, Recombination, and Transport in Amorphous Silicon Solar Cells**
Richard Williams and Richard S. Crandall
- 390 Collimated Electron Trajectory in a Nonuniform Transverse Magnetic Field**
K. K. N. Chang
- 397 Shear Viscosity-Temperature-Shear Rate Relations for Flame Retardant Impact Polystyrene Melts**
Wendell M. Lee and Hollis V. Becker
- 416 A Survey of Corrosion Failure Mechanisms in Microelectronic Devices**
George L. Schnable, Robert B. Comizzoli, Werner Kern, and Lawrence K. White
- 447 Patents**
- 449 Authors**
- 452 Index to Volume 40, 1979**

RCA Corporation

E. H. Griffiths President and Chief Executive Officer

Editorial Advisory Board

Chairman, J. J. Tietjen RCA Laboratories

N. L. Gordon RCA Laboratories

G. C. Hennessy RCA Laboratories

E. O. Johnson RCA Research Laboratories, Inc.

H. Kressel RCA Laboratories

W. Merz Laboratories RCA, Ltd.

K. H. Powers RCA Laboratories

L. A. Shottliff International Licensing

T. O. Stanley, RCA Laboratories

W. M. Webster RCA Laboratories

Secretary, Charles C. Foster RCA Laboratories

Editor Ralph F. Cialone

Associate Editors

D. R. Higgs Missile and Surface Radar Division

C. Hoyt Consumer Electronics

T. King RCA Research and Engineering

R. Mausler National Broadcasting Company

M. Rosenthal RCA Americom, Inc.

J. Schoen Solid-State Division

M. G. Pietz Government and Commercial Systems

W. S. Sepich Commercial Communications Systems Division

J. E. Steoger RCA Service Company

D. Tannenbaum Government Communications Systems

© RCA Corporation 1980. All rights reserved, except that express permission is hereby granted for the use in computer-based and other information-service systems of titles and abstracts of papers published in RCA Review.

Carrier Generation, Recombination, and Transport in Amorphous Silicon Solar Cells*

Richard Williams and Richard S. Crandall

RCA Laboratories, Princeton, N.J. 08540

Abstract—The discovery of the amorphous silicon solar cell has stimulated work in many laboratories to develop a cheap, efficient, and practical cell. The ability to deposit large-area thin films of this material, with its high optical absorption and relatively good electron lifetime, offers great promise for the development of solar cells. However, the charge-carrier generation and transport are quite different from that found in the more familiar single-crystal silicon. A proper design for a solar cell must take these differences into account. We discuss charge-carrier generation, recombination, and transport through insulator layers, and show how these affect solar cell performance.

Introduction

When solar cells become available in large areas at low cost, they will make a significant contribution to our energy needs. An important step in this direction has been the discovery of the amorphous silicon solar cell.¹ Efforts to develop this cell are now underway in several laboratories.²⁻⁸ The amorphous silicon material, a-Si:H, is really an alloy that may contain as much as 30% hydrogen. Its optical properties and the generation and transport of carriers are quite different from what one observes in the more familiar crystalline Si solar cell.^{9,10} In this paper we review the properties of a-Si(H) solar cells, emphasizing carrier generation, transport, and recombination.

* Research reported herein was sponsored jointly by RCA Laboratories, Princeton, N.J. and the Department of Energy, Oakland, Ca., under Contract No. ET-78-C-03-2219.

a-Si:H Versus Crystalline Si Solar Cells

The different optical and transport properties of a-Si(H) and crystalline Si result in very different values of useful thickness for the two kinds of solar cell. Fig. 1 shows this, schematically, for Schottky barrier solar cells on n-type material. For crystalline Si solar cells, the total wafer thickness is typically $250\ \mu\text{m}$. For a donor concentration of $2 \times 10^{15}\ \text{cm}^{-3}$, the Schottky barrier thickness or depletion width W is $1.0\ \mu\text{m}$, whereas the minority carrier (hole) diffusion length may be $100\ \mu\text{m}$. Much of the useful light in the visible and near infrared spectrum penetrates into the crystal well beyond the Schottky barrier before it is absorbed. For blue light ($5400\ \text{\AA}$) the penetration depth of a photon before absorption is $1.4\ \mu\text{m}$, and for red light ($8000\ \text{\AA}$) it is $10\ \mu\text{m}$. These distances are indicated by arrows in Fig. 1(a). The quantum efficiency for free-carrier production is nearly 1, both in the barrier and in the field-free region beyond. Since most of the light is absorbed in the field-free region, the minority carriers must diffuse to the barrier, where they are swept to the collecting electrode by the electric field in the barrier. For light in the visible part of the spectrum, the collection efficiency is high, since the minority-carrier diffusion length, L_p , is much greater than the penetration depth of the light. Only a few of the carriers recombine before being collected. Collection efficiency can be increased by making cells with suitable gradients of the donor concentration. This builds in a modest electric field that

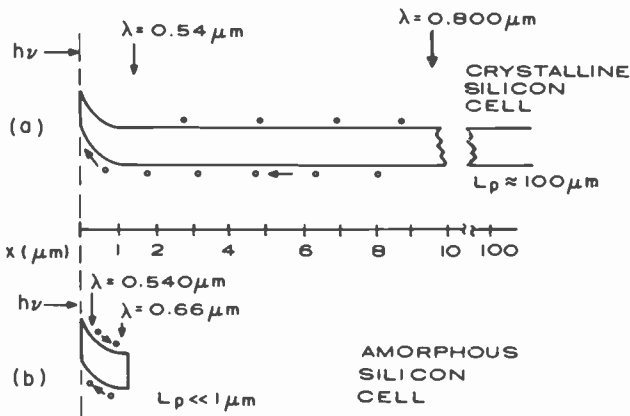


Fig. 1—Comparison of the dimensions of solar cells made of single crystal silicon and a-Si(H): (a) Single crystal solar cell. The light penetrates far beyond the barrier region. The penetration depths for red and blue light are indicated by arrows. (b) a-Si(H) solar cell. This cell is much thinner than the single crystal cell and the optical absorption constant is larger. Arrows show penetration depths for red and blue light.

favors the transit of minority carriers to the strong field region of the barrier.

Fig. 1 (b) shows the contrasting properties of a solar cell made from a-Si:H. The total cell thickness is typically $1\ \mu\text{m}$ and, in a good cell, W will be at least half of the total thickness. This is truly a thin-film device. Even though the layer of active material is very thin, light absorption is adequate, because the optical absorption constant α is much larger, through the visible range, than it is for crystalline silicon.¹¹ Penetration depths for two wavelengths are indicated in Fig. 1 (b). Much of the light is absorbed within the barrier region where there is a high electric field. If this were not the case, the cell could not function with a useful efficiency. The reason for this is that, in a-Si(H), the photoexcitation of free holes and electrons requires an electric field in addition to light. As a result, only the light absorbed in the barrier makes a significant contribution to the solar cell current. Once separated, holes and electrons move off in opposite directions to the electrodes. Some reach the electrodes and others recombine before doing so.

If we want to compare their behavior in solar cells, the essential distinction to make between crystalline and amorphous silicon is that between a good semiconductor and a low-mobility photoconductor. The crystalline silicon solar cell makes effective use of the high mobility, good minority-carrier lifetime, and long diffusion length that have helped to make silicon the material of choice in semiconductor device technology. It suffers somewhat from the disadvantage that the optical absorption is not very strong. To get high absorption, the cell must be thick, using more of an expensive material than one would like. The a-Si(H) fits more comfortably into the family of low-mobility photoconductors that are at the heart of electrostatic copying¹² and television-camera-tube technology.¹³ High optical absorption and our ability to deposit large areas offer the promise of thin-film solar cells that can be fabricated cheaply and still have useful efficiency. Low mobility and the other effects that go with it will mean that material control and careful design must be combined to achieve a workable solar cell with a-Si(H). In what follows, we discuss some of the physics involved, making use of photoconductor terminology and ideas.¹⁴ We begin with the first thing that happens in a solar cell—production of free electrons and holes.

Carrier Generation

Many workers have indicated that Coulomb attraction between hole and electron plays an important part in the photoexcitation of carriers.¹⁵⁻²⁰ This effect, often called "geminate recombination," is important in materials that have low carrier mobilities. In selenium and anthracene,

for example, it limits the efficiency of free-carrier production to low values. Mobility in a-Si(H) is also low. The microscopic mobility is the important quantity for geminate recombination. It is estimated²¹ to lie in the range 1–10 cm²/V-sec. Shallow trapping leads to drift mobilities that are several orders of magnitude less than the microscopic mobility.²²

Fig. 2 shows the energy levels in a-Si(H) that are involved in excitation and recombination. The optical band gap is approximately 1.7 eV.¹¹ The attraction between electron and hole puts them in a potential well that is Coulombic at large distances. At room temperature, for example, this attractive energy is equal to kT at a distance of 46 Å. Luminescence experiments^{23–26} indicate that there is a bound state, possibly involving a defect, about 0.3 eV below the ionization limit.

As an example of the excitation process we consider an electron excited by a 2.0-eV photon into a level 0.3 eV above the ionization limit. The electron will move with a velocity v , which is related to the electron's effective mass m^* (assumed to be equal to the free electron mass) and its excess energy U above the ionization limit by

$$v = (2U/3m^*)^{1/2} = 1.9 \times 10^7 \text{ cm/sec.} \quad [1]$$

The electron is then scattered by phonon emission or absorption after a time, τ_s , that can be estimated from the usual relation between scattering time and the mobility, μ ,

$$\mu = e\tau_s/m^*, \quad [2]$$

When μ is 1 cm²/V-sec, $\tau_s = 6 \times 10^{-16}$ sec. When $\mu = 1000$ cm²/V-sec,

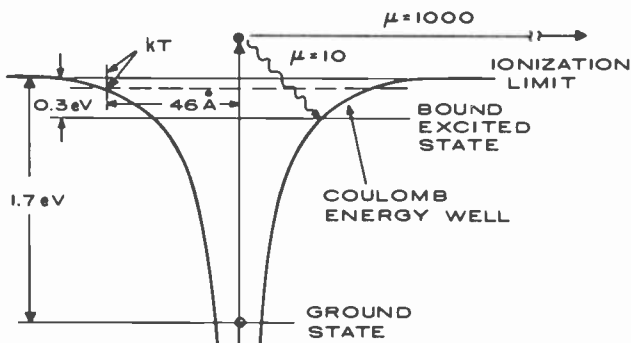


Fig. 2—Energy well due to the attraction between an electron and a hole in a-Si(H). The ionization limit is given by the optical band gap of 1.7 eV. Luminescence data indicate that there is a bound level ~ 0.3 eV below the ionization limit. The shape of the potential energy well is Coulombic at large distances, but is probably quite different when the electron and hole are very close together. Energy loss by high-mobility and low mobility electrons is shown.

$\tau_s = 6 \times 10^{-13}$ sec. The electron moves a distance L_s before it is scattered, where

$$L_s = v\tau_s. \quad [3]$$

For the scattering length in a-Si(H), we estimate $L_s = 1.1 \text{ \AA}$; in a good semiconductor, such as crystalline Si, $L_s = 1100 \text{ \AA}$.

In a high-mobility material the electron is well beyond the reach of the attractive force before it is scattered for the first time. Therefore, it has no chance to lose energy within the potential energy well, and all the electrons excited above the threshold ionization energy become free carriers. In a low-mobility material the electron begins to lose energy while it is still strongly attracted to the hole. It will lose energy until it has fallen to the highest bound electronic state. This is about 0.3 eV below the ionization limit, and since, by hypothesis, the electron starts out with an energy 0.3 eV above the ionization limit, it must lose altogether 0.6 eV to reach the bound state. Taking the dominant optical phonon energy as 0.05 eV, the electron must emit 12 phonons to do this. It may either absorb or emit phonons, but emission will predominate so that this will require a time somewhat larger than $12\tau_s$. During this time it diffuses a distance L_D given by

$$L_D^2 \cong D(12\tau_s) \cong \frac{\mu k T^*}{e} 12\tau_s. \quad [4]$$

T^* is the average electron temperature during the energy-loss process. The electron begins with kinetic energy of 0.3 eV and rapidly loses it by successive phonon emissions. To make a rough estimate, we take a T^* that corresponds to the median energy during this process, such that $kT^* = 0.15$ eV. Using this, together with $\mu = 1 \text{ cm}^2/\text{V-sec}$ and $\tau_s = 6 \times 10^{-16}$ sec, gives us an estimate for L_D of 3.2 \AA . If $\mu = 10 \text{ cm}^2/\text{V-sec}$, $L_D = 32 \text{ \AA}$. Therefore, improving the mobility can make a significant improvement in collection efficiency.

By this rapid energy loss, an excited electron in a low-mobility material falls back into the Coulomb well and does not separate from its companion hole. In the bound excited state, it can recombine with the hole, with or without emission of light, or it may ionize thermally. In selenium and anthracene the probability of thermal ionization at room temperature is small. The photoconductivity quantum yield is small, unless a high electric field is applied. In a high field, the electron and hole can be torn apart by field ionization and the quantum yield increases.

The competition between recombination and ionization can be expressed by a kinetic equation containing the rates p_i (for ionization, which may be thermal or field assisted), p_r (for radiative recombination), and p_n (for nonradiative recombination). The quantum yield, η_i , for ionization is

$$\eta_I = p_i / (p_i + p_r + p_n). \quad [5]$$

The quantum yield, η_L , for luminescence is

$$\eta_L = p_r / (p_i + p_r + p_n). \quad [6]$$

For a-Si(H) at room temperature η_L is small, indicating that $(p_i + p_n) \gg p_r$. In high mobility semiconductors at room temperature η_I may be nearly unity. In this case, $p_i \gg (p_n + p_r)$. In a-Si(H) and other low-mobility materials η_I can be very low because of the rapid energy loss and capture in the Coulombic well that we described above. For the electron caught in the well, the most likely alternatives available are nonradiative recombination and thermal ionization. If there is also a high electric field, then field-assisted thermal ionization also becomes important.

Field-Assisted Thermal Ionization

To escape from its well, the electron must be thermally excited over a barrier. The electric field lowers this barrier. The effect is well-known and is illustrated by Fig. 3. The problem has been treated^{17 19,27} by applying the Frenkel-Poole model²⁸ for the field-assisted escape of an electron from a bound state. The escape rate, $p_i(E)$, contains three basic terms. One of these is an attempt frequency, ν . The second term, $\exp(-\epsilon_i/kT)$, expresses the thermal ionization contribution in relation to the binding energy, ϵ_i , in the absence of a field. The field, E , acts by lowering the barrier that the electron must get over to escape. It comes into the third term, $\exp(\sqrt{E/E_f})$, where E_f is a constant at a given temperature. The complete equation for the escape rate is

$$p_i(E) = \nu \exp\left(\frac{-\epsilon_i}{kT}\right) \exp\left(\sqrt{\frac{E}{E_f}}\right). \quad [7]$$

In a solar cell, some of the light is absorbed in the high-field region of

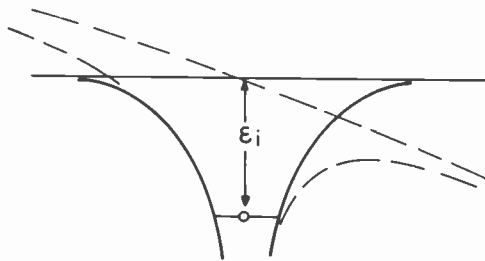


Fig. 3—Effect of an electric field on the potential well. The field lowers the barrier and allows faster thermal ionization.

the Schottky barrier and some penetrates beyond. Eq. [7] applies in either case. Some free carriers can be generated in the field-free region by purely thermal ionization. Those that diffuse to the barrier will then be collected. There is experimental evidence²⁹ that the diffusion length for holes is much less than the barrier thickness in a-Si(H) solar cells. This, together with the lower ionization efficiency in the field-free region, means that diffusion plays only a small part in the collection of carriers.

Both dark and photoconductivity of a-Si(H) depend on electric field³¹ for fields above 10^4 V/cm. The data fit Eq. [7] and can be explained as field-lowering of a barrier to thermal ionization. Field-quenching of the luminescence^{20,25} of a-Si(H) can be understood by similar considerations. The electric field facilitates thermal ionization of electron-hole pairs before they can recombine radiatively.

These effects are important to solar cell performance because they determine the magnitude of the solar cell collection efficiency, η_{sc} . We define η_{sc} as the number of electron charges passing through the cell for each absorbed photon. It has a maximum value of 1 and depends on wavelength and the field, $E(x)$, in the barrier. The barrier field depends on the depletion width, W , and the potential difference across the barrier. For an ideal Schottky barrier,

$$E(x) = 4\pi N_s \frac{eW}{\epsilon_s} \left(1 - \frac{x}{W}\right) = E_{max} \left(1 - \frac{x}{W}\right). \quad [8]$$

Here N_s is the concentration of ionized donors in the barrier, e is the electronic charge, ϵ_s is the dielectric constant, and x is the distance into the barrier measured from the metal contact where the field has its maximum value. By combining Eq. [8] with Eqs. [5] and [7] we can show that the molecular quantum efficiency, η_{sc} , depends on W in the following way:²⁷

$$\eta_{sc} = \alpha(W - W_0). \quad [9]$$

This expression applies only to the case of uniform light absorption when $\alpha W \ll 1$. W_0 depends weakly on W , but is nearly constant. To a good approximation,

$$W_0 = \frac{\pi^2 E_f \epsilon_s}{6N_s e}, \quad [10]$$

where

$$E_f = \pi K (kT)^2 e^{-3}. \quad [11]$$

We have data for η_{sc} as a function of W for many a-Si(H) solar cells.³² They confirm that Eq. [9] is a correct description. W can be varied, in

a given solar cell, by varying the applied voltage. We determined W from measurements of small-signal capacitance using a measuring frequency of 100 kHz. In the following section, we will discuss the validity of capacitance measurements for the determination of W . Fig. 4 shows the dependence of collection efficiency on depletion width for excitation with He-Ne laser light. The line through the data points obeys Eq. [9]. The results of Fig. 4 and similar data on other samples give strong evidence that free-carrier generation takes place mainly in the Schottky barrier, and that we are dealing with the geminate recombination process treated above.

Details of the data are consistent with the picture we have developed. For example, at a given level of illumination, the magnitude of W_0 is fixed. However, it varies with illumination because N_s varies. The product $N_s W_0$, however, should be independent of intensity, since E_f and ϵ_s are material properties independent of light. By varying light intensity, we can vary N_s by two orders of magnitude. At the same time, the product $N_s W_0$ remains constant, within experimental error.

Barrier Thickness

Hole diffusion lengths in a-Si(H) are short.²⁹ Therefore, collection of free carriers takes place mainly in the depletion layer where there is a high field. The depletion width depends on solar cell bias and on light intensity. For an ideal Schottky barrier,

$$W = \left(\frac{2e\epsilon_s V}{N_s} \right)^{1/2}. \quad [12]$$

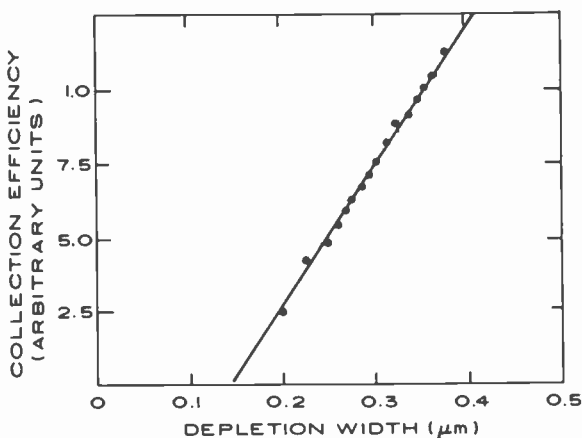


Fig. 4—Photocurrent quantum yield, η_{sc} , as a function of the barrier thickness, W , for a Pt-a-Si(H) solar cell.

V is the total voltage drop across W and N_s is the space charge, assumed uniform. N_s can depend on light level, because holes and electrons are not necessarily trapped in equal numbers. Usually, more holes than electrons are trapped and, with increasing light intensity, there is an increase in N_s along with a decrease in η_{sc} . Both η_{sc} and N_s vary weakly with light intensity, I . We show an example of this in Fig. 5 where we have plotted N_s versus I for a Pt-a-Si(H) Schottky-barrier solar cell illuminated with uniformly absorbed light. To determine N_s , we measure the capacitance C as a function of applied voltage and use Eq [12]. The data, plotted on a log-log scale, fit a straight line with a slope of $1/4$.

We want to use this relation to test the consistency of the values of W that we determined from capacitance measurements and that went into our determination of N_s . To do this, we have measured the photocurrent, j_p , as a function of I for the same sample used for Fig. 5. The photoconductivity can be related to N_s by a simple conventional model and the results compared with those that we get from capacitance data. If the results are consistent, this supports the validity of capacitance measurements as a tool to measure W .

The photoconductivity depends on N_s because the lifetime of majority

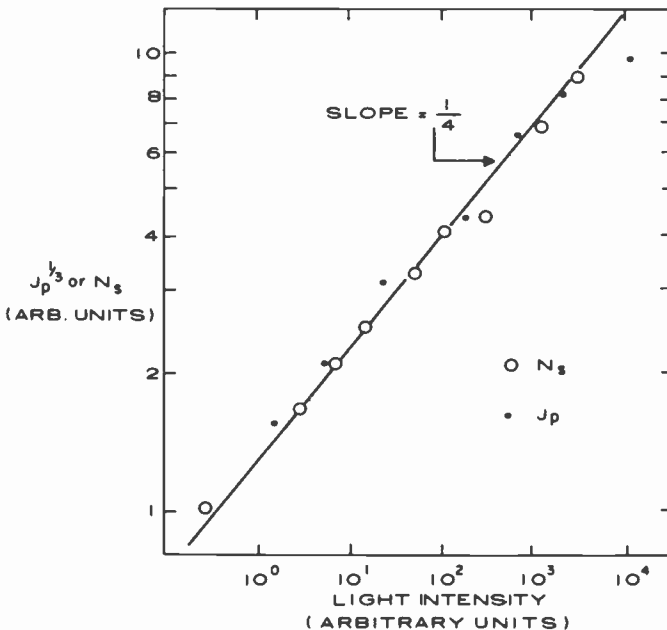


Fig. 5—Dependence of space-charge density, N_s , and photocurrent, j_p , on light intensity, I . Circles show N_s ; dots show $j_p^{1/3}$ for Pt-a-Si(H) solar cell. Further details of the experiment are described in the text.

carrier electrons is determined by their recombination with trapped holes. Specifically, the electron lifetime, τ_c , is proportional to $1/N_s$. We can relate j_p to the photogeneration rate G for free hole-electron pairs, the mobility μ , and the sample length L by

$$j_p = \frac{eG\mu\tau_c V}{L}. \quad [13]$$

Since G is proportional to light intensity we can write, for the overall intensity dependence, $j_p \propto (I/N_s) \propto I^{3/4}$. Thus, j_p should vary with light intensity as $I^{3/4}$. A sublinear variation of j_p with light intensity has previously been reported³³ for a-Si(H). We have done a different kind of measurement, using a solar cell under forward bias to determine the Ohmic secondary current as a function of I . The results are plotted in Fig. 5, as the quantity $j_p^{1/3}$. According to the above arguments, this should be proportional to $I^{1/4}$. The graph shows that this is, indeed, the case. The good agreement between these data and the theoretical model supports the validity of capacitance measurements as a tool to determine W .

Another way to estimate the depletion layer thickness is to measure collection efficiency for different wavelengths of light. If efficient collection takes place only within the depletion layer, then we can expect a close relation between η_{sc} and the penetration depth of the light. By comparing values of W estimated this way with those obtained from capacitance measurements on the same sample, we can make a further consistency check. In one case^{5,33} η_{sc} was found to be proportional to the penetration depth of the light. In another kind of experiment, j_{sc} was measured for different wavelengths, along with the slope of the j - V curve near $V = 0$. We can relate these data to W by assuming that collection is confined to the barrier region.³⁴ Again, values of W were in good agreement with those determined from capacitance measurements on the same sample. Therefore, we conclude that capacitance measurements on illuminated samples, using a measuring frequency around 10^5 Hz, give a valid measure of W .

Measurements of capacitance at low frequencies often indicate a much smaller W than one would infer from other measurements on the same sample, such as optical properties. This may be due either to deep states in the silicon or to an oxide layer at the interface.³⁵ There has been some controversy^{36,37} about the proper interpretation of capacitance measurements in a-Si:H diodes. One problem is that C depends strongly on the measuring frequency, particularly at very low frequencies. Part of this is due to the emptying and filling of the high concentration of states that lie deep in the forbidden gap. At high frequencies these states cannot follow the ac measuring signal and make no contribution to the measured

C. The series capacitance of the oxide layer that is often found between metal and semiconductor begins to dominate at low frequencies. Most of the controversy centers around measurements made in the *dark*. In this case, the Fermi level is near midgap and deep states near the Fermi level make an important contribution. Results on samples measured under *illumination* are usually simpler to interpret. The Fermi level is now closer to the conduction band and the dielectric relaxation time is shorter, 10^{-8} sec in sunlight. There is now enough charge in shallow centers to follow a measuring signal of 10^5 Hz, and the resistance of material in series with the barrier is not a problem. At the same time, the deep centers do not respond. In this way, differential capacitance measurements can give a true measure of W if the measuring frequency and experimental conditions are properly chosen. At too low a frequency, the series capacitance of the oxide will complicate the interpretation.

Carrier Recombination in the Barrier

As we have shown above, most of the photovoltaic current is due to carriers excited in the barrier region. What happens to the free electron and hole once they are formed? The separated carriers move off in opposite directions to be collected at the electrodes. Ideally, all would reach the contacts and give a current flow equivalent to one electron passing all the way through the sample for each hole-electron pair excited by the light. In practice, electrons and holes may recombine along the way and never reach the electrodes. This reduces the current by the ratio of the distance travelled before recombination to the total solar-cell thickness. We would expect little direct recombination of holes and electrons with each other in the barrier. The high field that prevents geminate recombination acts to prevent recombination of the free carriers once they are separated. However, more complicated processes make take place, such as capture by a neutral center, followed by recombination.

We can understand some of the possible effects of recombination on solar cell performance by reference to Fig. 6. The barrier region is similar to an insulator with one blocking contact and one Ohmic contact. Both holes and electrons can *leave* freely through the contacts, but only electrons can *enter* freely. If there is no trapping or recombination, every free hole and electron produced leaves the barrier and makes its full contribution to the photovoltaic current. This is the ideal behavior, and it is achieved in silicon single-crystal solar cells to a high degree of approximation. In a-Si(H) there is shallow trapping²² to complicate this picture and, possibly, significant recombination. Where there is shallow trapping, carriers jump in and out of traps repeatedly. The drift mobility

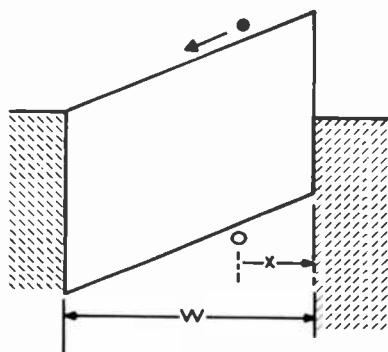


Fig. 6—Mott barrier.

is greatly reduced. Nevertheless, carriers can reach the contacts and make their full contribution to the current. Recombination is more serious. How serious depends on how far carriers go, on the average, before recombining. In insulator physics this distance is defined as the "Schubweg," the product of mobility, μ_p , electric field, E , and recombination lifetime. We consider holes with recombination lifetime, τ_p :

$$S = \mu E \tau_p. \quad [14]$$

The effect on the solar cell current can be shown by a simple analysis. For this, we use as the model a "Mott Barrier"³⁸, shown in Fig. 6. It is the same as the usual Schottky barrier, except that the field within the barrier is constant. This has little effect on the physics, but makes the problem mathematically simpler. Actually, this model is a good description of the best solar cells.

We consider a separated electron-hole pair, formed at a distance x from the interface by the combined action of the barrier field and light. The probability that the electron will reach the interface before recombination is $\exp(-x/S)$. By averaging this over all values of x through the barrier thickness, W , we get the fraction, f , which is the ratio of the actual current to that which would flow if all carriers passed all the way through the barrier. For simplicity, we take the case in which carriers are produced uniformly through the barrier.³⁹ Then

$$f = \frac{\int_0^W e^{-x/S} dx}{\int_0^W dx} = (S/W) (1 - e^{-W/S}). \quad [15]$$

Table 1 shows the magnitude of this function for several values of S/W .

Table 1—Ratio of Actual Current to Current that Would Flow If All Carriers Passed All the Way through the Barrier, f , for Several Values of S/W

S/W	f
0.1	0.1
0.5	0.43
1.0	0.63
2.0	0.79
10	0.95

The schubweg must be several times W to avoid significant reduction of the solar cell current and efficiency due to recombination. For highest efficiency one needs $S/W \cong 10$. This means that the concentration of recombination centers must be controlled.

We can estimate the upper limit to the concentration of recombination centers that can be tolerated in a solar cell without loss of efficiency. In a good a-Si(H) solar cell, W is 10^{-4} cm and the barrier height is 1 eV, giving a mean field in the barrier of 10^4 V/cm. If we take $\mu_p \sim 1$ cm²/V-sec and, $S/W = 10$, then $\tau_p \geq 10^{-7}$ sec. τ_p is related to the concentration, N_r , of recombination centers, their capture cross-section, σ , and the thermal velocity, v_{th} , of the electron or hole by

$$\frac{1}{\tau_p} = N_r v_{th} \sigma. \quad [16]$$

The order of magnitude of v_{th} is 10^7 cm/sec, giving us the criterion that $N_r \sigma$ should be less than 1 for a good solar cell. For a neutral center, σ is typically $10^{-15} - 10^{-16}$ cm². For this kind of recombination center, the concentration can be of order $10^{15} - 10^{16}$ cm⁻³ without deterioration of solar cell performance, but the concentration must not be allowed to exceed this range.

To apply the above ideas to an actual solar cell, we need some way to measure S/W . We cannot easily measure this for holes, but useful information can be gained by measuring S/W for electrons. This can be done by measuring the saturation photocurrent of the cell under reverse bias and the Ohmic secondary photocurrent under forward bias. The saturation reverse current gives the number of hole-electron pairs generated per unit time by the light. Under forward bias there may be photoconductive gain, leading to a larger photocurrent. The ratio of the forward current to the saturation reverse current is equal to S/W and is proportional to the applied voltage. Fig. 7 shows photoconductivity data obtained in this way.

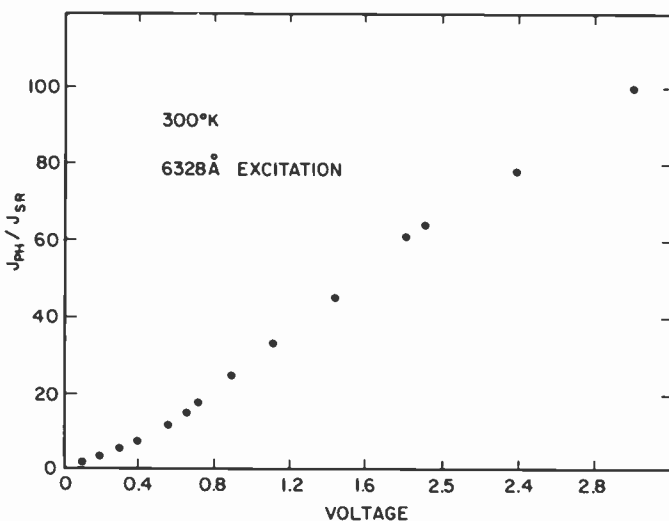


Fig. 7—Ratio of forward-bias photocurrent j_{ph} to saturation reverse current j_{SR} as a function of applied voltage.

Metal-Insulator-Semiconductor Devices

Silicon Schottky Barrier diodes often have a thin layer of insulating oxide between metal and semiconductor. This may either be grown intentionally or appear naturally during device fabrication. In air at room temperature, a 10 \AA thick layer of oxide grows in 1 minute, increasing to 20 \AA within a few days. The oxide has a significant effect on electron transport across the interface, and on solar cell performance. To assure solar cell uniformity and the desired results, growth of the oxide must be either carefully controlled or eliminated. Some of the results on a-Si(H) solar cells can only be explained by the presence of such an oxide layer. For example, some Pt-a-Si(H) Schottky barrier diodes under 1 Sun illumination have $V_{oc} \geq 0.80$ volt. According to the ideal diode formula, V_{oc} is related to the short-circuit current, j_{sc} , and the saturation current, j_0 ,

$$V_{oc} = \frac{kT}{e} \ln \left(\frac{j_{sc}}{j_0} \right). \quad [17]$$

For good diodes, j_{sc} is around 10^{-2} amp/cm² and j_0 is 10^{-12} amp/cm². Thus, V_{oc} should be 590 mV. The larger V_{oc} actually found can most easily be explained by assuming that there is an insulating layer at the surface.

The effect of an insulating layer on solar cell performance has been

discussed in several articles.⁴⁰⁻⁴³ We will use a simplified model to show the essential physics of the effect on V_{oc} and will point out some of the limitations involved. Fig. 8(a) shows a metal–semiconductor interface and 8(b) shows the same interface with a thin insulating layer between metal and semiconductor. We assume that the presence of the insulator does not change the amount of band-bending in the semiconductor. In both cases, there is an exchange current of electrons back and forth due to thermionic emission over the barrier. The magnitude of the current in either direction is j_0 . In Fig. 8(a) all electrons that reach the interface with enough energy to get over the semiconductor barrier pass on through the interface unimpeded. A photoexcited hole is also shown passing freely through the interface. The oxide layer is an obstacle to the free passage of electrons through the interface. In Fig. 8(b) most of the electrons that arrive at the interface are reflected by the insulator, even though they have enough energy to get over the semiconductor barrier. Some can tunnel through the insulator with a probability given

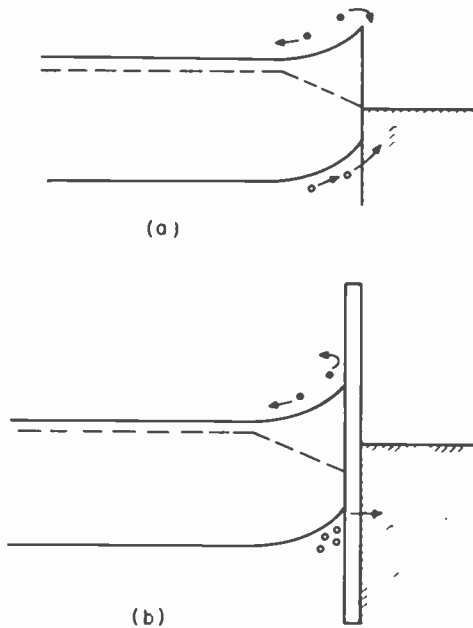


Fig. 8—Schottky barriers with and without intermediate oxide layer: (a) No oxide layer. There is no obstruction to free passage of holes and electrons between metal and semiconductor, provided they have enough energy to get over the semiconductor barrier. (b) Oxide layer turns back most carriers that arrive. Some get through by tunneling. Effects on electrons and holes are different because holes are concentrated at the interface by the barrier field.

by the transmission coefficient, t . We assume that t has the same magnitude for both electrons and holes. However, what happens to electrons and holes is different. When an electron arrives from the semiconductor side, it is reflected and diffuses away from the interface. For this reason, only a small fraction, t , of the electrons coming to the interface can pass through. This is not the case for the holes. When they reach the interface they are confined there by the barrier field. They collide with the interface again and again, eventually getting through, even if t is very small. Furthermore, the recombination probability is small during their stay near the interface, because the electron concentration at the top of the barrier is small. As a result, it may be possible for nearly all the holes that reach the interface to pass on through, even for small t . The effect on V_{oc} comes about because we have reduced j_0 to tj_0 , while making little or no change in j_{sc} . In the example introduced above, V_{oc} would, ideally, be 590 mV in the absence of an insulating layer. With the insulating layer,

$$V_{oc} = \frac{kT}{e} \ln \left(\frac{j_{sc}}{tj_0} \right). \quad [18]$$

To bring V_{oc} up to the 800 mV actually observed requires that $t = 2.5 \times 10^{-4}$. For this, the insulating layer must be about 10 Å thick. To produce a uniform, stable layer of this thickness is a considerable achievement in technology.⁴⁴

It seems paradoxical that one can increase solar cell efficiency by putting in an obstacle to electron transport through the interface. It is possible because the barrier separates holes and electrons, so that j_0 can be reduced without changing j_{sc} . How far can one go, in principle, to increase solar cell efficiency in this way? There is the practical difficulty of making the thin insulator and several limitations based on the physics:

- (1) Once the bands in the semiconductor are flattened under illumination, nothing more can be gained.
- (2) Charge Separation: Holes confined near the insulator interface are imaged by an equal number of electrons that collect on the opposite side of the insulator for electrostatic reasons. This gives an electric field across the insulator and a voltage drop that is subtracted from the useful output voltage of the cell.
- (3) Recombination: Some of the confined holes may recombine with electrons in the semiconductor, reducing the current in the cell. We will make some estimates of the effects of these last two processes.

Charge Separation: The electrostatic problem can be analyzed by

considering the lifetime, τ_{pi} , that a hole spends confined near the interface before tunneling through the insulator. The number N_p of holes cm^{-2} is related to j_{sc} by

$$\frac{N_p}{\tau_{pi}} = \frac{j_{sc}}{e} \quad [19]$$

For numerical estimates we take $j_{sc} = 16 \text{ mA/cm}^2$. We can estimate τ_{pi} from t and an attempt frequency, ν :

$$\frac{1}{\tau_{pi}} = \nu t. \quad [20]$$

We assume that ν is $1 \times 10^{14} \text{ sec}^{-1}$ and calculate the values of N_p and τ_{pi} that correspond to any given value of t . For a given N_p we can calculate the voltage drop, V_{ox} , across the insulator if we know its thickness and dielectric constant. We assume that an insulator 15 \AA thick having a dielectric constant of 4.0 gives $t = 10^{-7}$. Table 2 shows the relation between t , N_p , τ_{pi} , and V_{ox} that we get in this way.

As long as t is larger than 10^{-8} the build-up of charge due to the holes waiting to get through the layer of insulator will be negligible and will not affect the collection of current in short-circuit operation. At the same time, the reduction in j_0 achieved by the presence of the insulating layer will be substantial.

Recombination: When a solar cell without an insulator layer, Fig. 8(a), operates at the maximum power point, the flow of holes to the surface is accompanied by a smaller current of electrons going in the same direction. Holes and electrons enter the metal and recombine. As a result, the net current at the maximum power point is less than j_{sc} . For an ideal diode, the current lost to this kind of recombination is about 7% of j_{sc} .

In the MIS diode, Fig. 8(b), most of the electrons that arrive at the insulator from the semiconductor side are reflected. However, it is possible for them to recombine with the holes localized near the interface. This decreases the current and the solar cell efficiency. To estimate the amount of recombination, we assume that the holes are localized in a plane at the interface, and that they have a capture cross-section, σ_c , for

Table 2 — The Relation Between t , N_p , τ_{pi} , and V_{ox}

t	N_p (cm^{-2})	τ_{pi} (sec)	V_{ox} (volt)	$N_p S_{max}$
10^{-3}	10^6	10^{-11}		10^{-7}
10^{-6}	19^9	10^{-8}		10^{-4}
10^{-7}	10^{10}	10^{-7}	7×10^{-4}	10^{-3}
10^{-8}	10^{11}	10^{-6}	8×10^{-3}	10^{-2}
10^{-9}	10^{12}	10^{-5}	10×10^{-1}	10^{-1}
10^{-10}	10^{13}	10^{-4}	11×10^{-1}	1

electrons. The largest effect would be for a Coulomb attractive cross-section σ_{max} , which is of the order 10^{-13} cm². On each square centimeter of interface, a fraction, $N_p \sigma_{max}$, is blocked out by recombination centers having this capture cross-section. This product, $N_p \sigma_{max}$, gives the fraction of all electrons striking the surface that recombine. As we described above, in the absence of an insulating layer, all electrons that reach the surface recombine. As long as $N_p \sigma_{max} \ll 1$, recombination of electrons with the holes at the surface will not be a serious problem in the MIS diode. The last column of Table 2 shows $N_p \sigma_{max}$ as a function of t . For values of $t > 10^{-8}$ this kind of recombination does not reduce the performance of the solar cell.

Summary

The optical and transport properties of amorphous silicon are quite different from those of crystalline silicon. Solar cells of amorphous silicon must be carefully designed to take advantage of its special properties. Geminate recombination is of special importance. To achieve high efficiencies the depletion width must be controlled. We have shown that the depletion width can be determined by making proper use of capacitance measurements.

References:

- ¹ D. E. Carlson and C. R. Wronski, "Amorphous Silicon Solar Cell," *Apply. Phys. Lett.*, **28**, p. 671 (1976).
- ² I. Solomon, J. Kiettle, and D. Kaplan, "Influence of Interface Charges on Transport Measurements in Amorphous Silicon Films," *J. de Physique*, **39**, p. 1241, (1978).
- ³ J. I. B. Wilson, J. McGill, and S. Kinmond, "Amorphous Silicon MIS Solar Cells," *Nature*, **272**, p. 152 (1978).
- ⁴ W. E. Spear, P. G. LeComber, S. Kinmond, and M. H. Brodsky, "Amorphous Silicon P-N Junction," *Appl. Phys. Lett.*, **28**, p. 105 (1976).
- ⁵ B. T. Debney, "Model for Amorphous Silicon Solar Cells," *Solid State and Electronic Dev.*, Special Issue, **S-15**, June 1978.
- ⁶ S. R. Ovshinsky and A. Madan, "A New Amorphous Silicon-Based Alloy for Electronic Applications," *Nature*, **276**, p. 482 (1978).
- ⁷ Y. Hamakawa, H. Okamoto, and Y. Nitta, "A New Type of Amorphous Silicon Photovoltaic Cell Generating More than 2.0 V," *Appl. Phys. Lett.*, **35**, p. 187 (1979); M. J. Thompson, J. Allison, M. M. Al-Kaisi, *Solid State Electron Devices*, **2**, (1978); B. Abeles, G. D. Cody, T. Tiedje, and C. R. Wronski, "Dependence of Electronic Properties of Glow Discharge Produced SiH_x Films on Deposition Conditions," 21st Electronic Materials Conf., Boulder, Colo., June 17, 1979.
- ⁸ Y. Kuwano, *J. Electronic Engineering*, **16**, p. 65 (1979).
- ⁹ S. M. Sze, *Physics of Semiconductor Devices*, Wiley-Interscience, New York (1969), p. 643.
- ¹⁰ H. J. Hovel, *Semiconductors and Semimetals*, Academic Press, New York, Ed. by R. K. Willardson and A. C. Beer, Vol. 11, "Solar Cells" (1975).
- ¹¹ P. J. Zanzucchi, C. R. Wronski, and D. E. Carlson, "Optical and Photoconductive Properties of Discharge Produced Amorphous Silicon," *J. Appl. Phys.*, **48**, p. 5227 (1977).
- ¹² R. M. Schaffert, *Electrophotography*, Focal Press, New York (1965).
- ¹³ A. Rose, *Vision, Human and Electronic*, Plenum Press, New York (1973).
- ¹⁴ A. Rose, *Concepts in Photoconductivity and Allied Problems*, Interscience, New York (1963).
- ¹⁵ R. H. Batt, C. L. Braun, and J. F. Hornig, "Field and Temperature Dependent Recombination in Anthracene," *Appl. Optics Suppl.*, p. 20 (1969).

- ¹⁶ E. A. Davis and N. F. Mott, "Conduction in Non-crystalline Systems versus Conductivity, Optical Absorption, and Photoconductivity in Amorphous Semiconductors," *Phil. Mag.*, **22**, p. 903 (1970).
- ¹⁷ M. D. Tabak and P. J. Warter, "Field Controlled Photogeneration and Free Carrier Transport in Amorphous Selenium Films," *Phys. Rev.*, **173**, p. 899 (1968).
- ¹⁸ D. M. Pai and S. W. Ing., "Photogeneration of Carriers in Vitreous Selenium," *Phys. Rev.*, **173**, p. 729 (1968).
- ¹⁹ E. A. Davis, "Optical Absorption, Transport, and Photoconductivity in Amorphous Selenium," *J. Non-Crystalline Solids*, **4**, p. 107, (1970).
- ²⁰ R. A. Street, "Phonon Interaction in the Luminescence of Amorphous Silicon," *Phil. Mag.*, **38**, p. 1337 (1978).
- ²¹ P. G. LeComber and W. E. Spear, "Electronic Transport in Amorphous Silicon Films," *Phys. Rev. Lett.*, **25**, p. 509 (1970).
- ²² A. Moore, "Electron and Hole Drift Mobility in Amorphous Silicon," *Appl. Phys. Lett.*, **31**, p. 762 (1977).
- ²³ C. Tsang and R. A. Street, "Recombination in Plasma-Deposited Amorphous Si:H. Luminescence Decay," *Phys. Rev.*, **319**, p. 3027 (1979).
- ²⁴ T. M. Searle, T. S. Nashashibi, I. G. Austin, R. Devonshire, and G. Lockwood, "Radiative and Non-Radiative Tunnelling in Glow Discharge and Sputtered Amorphous Silicon," *Phil. Mag.*, **B39**, p. 389 (1979).
- ²⁵ J. I. Pankove and D. E. Carlson, "Electroluminescence in Amorphous Silicon," *Appl. Phys. Lett.*, **29**, p. 620 (1976).
- ²⁶ D. Engemann and R. Fischer, "Radiative and Non-Radiative Recombination in Amorphous Silicon," *Proc. Fifth Int'l Conf. on Amorphous and Liquid Semiconductors*, Garmisch-Partenkirchen, Springer, Berlin (1973).
- ²⁷ R. S. Crandall, "Field-Dependent Quantum Efficiency in Hydrogenated Amorphous Silicon," DOE Contract ET-78-C-03-2219, Quarterly Report #2, April 1979.
- ²⁸ J. Frenkel, *Tech. Phys., USSR*, **5**, p. 685 (1938).
- ²⁹ D. Staebler, "Hole Diffusion Length Measurements in Discharge-Produced a-SiH," 8th Int'l Conf. on Amorphous and Liquid Semiconductors, Cambridge, Mass., Aug. 27, 1979.
- ³⁰ T. Suzuki, M. Hirose, S. Ogase, and Y. Osaka, "Electrical Transport and Photoconductivity in Amorphous Silicon," *Phys. Stat. Sol.*, **42**, p. 337 (1977).
- ³¹ R. S. Crandall, "Band Tail Absorption in Hydrogenated Amorphous Silicon," to be published in *Proc. of Conf. on Amorphous and Liquid Semiconductors*, Edinburgh, Scotland, Ed. by W. E. Spear.
- ³² R. S. Crandall, R. Williams, and B. E. Tompkins, "Collection Efficiency Measurements on a-Si:H Solar Cells," *J. Appl. Phys.*, **50**, p. 5506 (1979).
- ³³ C. Wronski, "Electronic Properties of Amorphous Silicon in Solar Cell Operation," *IEEE Trans. Electron Dev.*, **ED-24**, p. 351 (1977).
- ³⁴ G. Swartz and R. Williams, unpublished work.
- ³⁵ I. Balberg and D. E. Carlson, "Tunneling in Hydrogenated Amorphous Silicon," *Phys. Rev. Lett.*, **43**, p. 58 (1979).
- ³⁶ G. H. Dohler and M. Hirose, "Determination of the Electronic Density of States in Amorphous Semiconductors from Capacitance-Voltage Measurements," *Proc. Conf. on Amorphous and Liquid Semiconductors*, Edinburgh, Scotland, Ed. by W. E. Spear; C. R. Wronski and T. Tiedge, to be published in *Proc. Eighth Int'l Conf. on Amorphous and Liquid Semiconductors*, Cambridge, Mass. (1979).
- ³⁷ W. E. Spear, P. G. LeComber, and A. J. Snell, *Phil. Mag.*, **B38**, p. 303 (1979).
- ³⁸ N. F. Mott and Gurney, *Electronic Processes in Ionic Crystals*, Dover Publications, N.Y. (1964), p. 179.
- ³⁹ H. Hecht, *Zeits. fur Physik*, **77**, p. 235 (1932).
- ⁴⁰ H. C. Card and E. H. Roderick, "Studies of Tunnel MOS Diodes I. Interface Effects in Silicon Schottky Diodes," *J. Phys.*, **D4**, p. 1589 (1971).
- ⁴¹ R. J. Stirn and Y. C. M. Yeh, "A 15% Efficient Antireflection-Coated Metal-Oxide-Semiconductor Solar Cell," *Appl. Phys. Lett.*, **27**, p. 95 (1975).
- ⁴² M. A. Green, F. D. King and J. Shewchun, "Minority Carrier MIS Tunnel Diodes and Their Application to Electron- and Photo-Voltaic Energy Conversion I. Theory," *Solid State Electronics*, **17**, p. 551 (1974).
- ⁴³ R. B. Godfrey and M. A. Green, "655 mV Open-Circuit Voltage, 17.6% Efficient Silicon MIS Solar Cells," *Appl. Phys. Lett.*, **34**, p. 790 (1979).
- ⁴⁴ A. M. Goodman and J. M. Breece, "Thin Tunnelable Layers of Silicon Dioxide Formed by Oxidation of Silicon," *J. Electrochem. Soc.*, **117**, p. 982 (1970).

Collimated Electron Trajectory in a Nonuniform Transverse Magnetic Field

K. K. N. Chang

RCA Laboratories, Princeton, N.J. 08540

Abstract—The Gabor collimator, which involves a correcting magnetic lens for keystone distortion, has not been explored, except in terms of a complex geometry, since its conception. A model for a simple, yet practical, collimator is proposed. The model features a transverse magnetic field, linear in one direction and hyperbolic in the other. A sweeping electron beam, in transversing the transverse field of a right polarity, is collimated. Full collimation occurs at a maximum field that varies as a function of the initial slope of the entering beam. The collimated trajectory is simulated by computer and computed results have been substantiated by measurements.

Introduction

Transverse magnetic fields have been widely used in cathode-ray tubes to deflect electron beams. One important application is the use of a nonuniform magnetic field to correct for trapezoidal distortion in a two-dimensional image display. Gabor* proposed a strong convergent magnetic lens for this purpose. This and other similar proposals have not been explored in the past except in terms of a complex geometry.

The energy of a drift electron during deflection under the influence of a magnetic field is conserved. The magnetic field is generally three-dimensional in space and becomes quite complex when it is nonuniform.

* D. Gabor, "Magnetic Electron Lenses," U.S. Patent 2,872,607, Feb. 3, 1959, and D. Gabor, P. R. Stuart, and P. G. Kalman, "A New Cathode Ray Tube for Monochrome and Color Television," *Institute of Electrical Engineering*, p. 581, Paper No. 2661R, May 1958.

If one chooses a simple particular geometry of the magnet, however, the nonuniformity may be assumed to be two-dimensional, and the electron motion can then be analyzed using a simple ordinary differential equation.

This paper proposes such a model. The model is used to examine the nature of the field distribution, and the electron trajectory is computed for a given set of boundary conditions. The computation is then compared with experimental results.

Model

The magnetic lens geometry employed (Fig. 1) is a symmetrical slot-shaped structure of two continuous parallel-plate pole pieces. Two magnets, either permanent magnets or electromagnets, supply the magnetic field B_z in the slot in an opposite direction with respect to the center of the magnet (Fig. 2). The following assumptions are made: (1) The field considered is z directional and limited only in the plane $z = 0$, i.e., the midplane between two parallel pole pieces. (2) The concerned electron trajectories of interest are confined in the x - y plane, $z = 0$. (3) The field distribution is linear in the x direction and hyperbolic and symmetric in the y direction. Thus,

$$B_z(x,y) = B_0 \frac{x}{x_d} \operatorname{sech} k_0 y, \quad [1]$$

where k_0 is a constant.

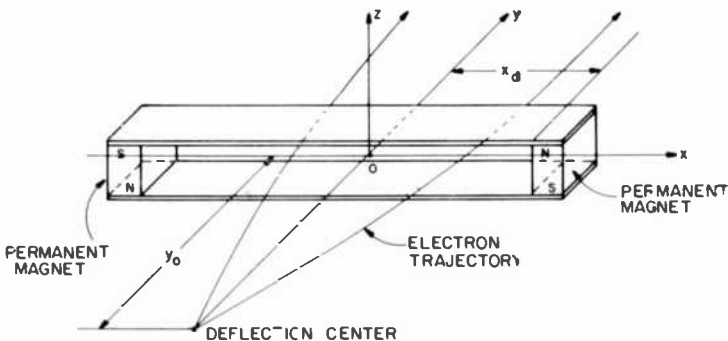


Fig. 1—A magnetic collimator.

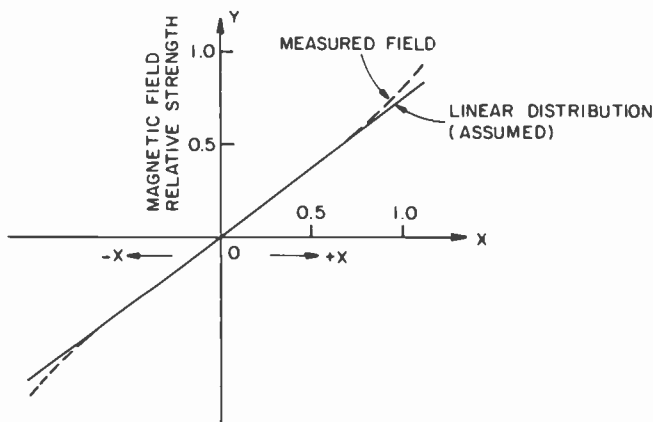


Fig. 2—Field distribution of a magnetic collimator along the x axis.

Analysis

Electron motion in a nonuniform transverse magnetic field (Eq. [1]) is described by the following force equations:

$$\begin{aligned} \frac{d\dot{x}}{dt} &= w_z(x,y) \dot{y} \\ \frac{d\dot{y}}{dt} &= -w_z(x,y) \dot{x}, \end{aligned} \quad [2]$$

where \dot{x} and \dot{y} are the velocity components and $w_z(x,y) = (e/m)B_z(x,y)$ is the cyclotron frequency, e/m being the electron charge-to-mass ratio.

The solution of interest is the electron trajectory in the x - y plane. To arrive at such a solution, one must transform the time variable t into the coordinate variable y . The transformation proceeds as follows. The trajectory velocity v_0 , the time derivative of the trajectory length l , is considered for drifting electrons under influence of a transverse magnetic field, i.e.,

$$v_0^2 = \left(\frac{dl}{dt}\right)^2 = \dot{x}^2 + \dot{y}^2. \quad [3]$$

If the trajectory slope is designated as $x' = \tan\theta = dx/dy$, one formulates from Eq. [2]

$$\frac{\dot{y}\ddot{x} - \dot{y}\dot{x}}{\dot{y}^2} = \dot{y} \frac{d}{dy} \left(\frac{\dot{x}}{\dot{y}}\right) = \dot{y} \frac{d}{dy} \left(\frac{dx}{dy}\right) = w_z(1 + x'^2)$$

which leads to*

$$\frac{d}{d\bar{y}} \left(\frac{dx}{dy} \right) = (1 + x'^2)^{3/2} \left(\frac{w_0}{v_0} y_0 \right) \bar{x} \operatorname{sech} \bar{k}\bar{y} \quad [4]$$

where $\bar{x} = x/x_d$, $\bar{y} = y/y_0$, and $\bar{k} = k_0 y_0$, x_d and y_0 being the maximum values. Integration of Eq. [4] yields

$$\begin{aligned} \left[\frac{x'}{\sqrt{1+x'^2}} \right]_{\bar{y}=\bar{y}} \left[\frac{x'}{\sqrt{1+x'^2}} \right]_{\bar{y}=-1} &= \sin\theta - \sin\theta_0 \\ &= \int_{-1}^{\bar{y}} \frac{w_0}{v_0} y_0 \bar{x} \operatorname{sech} \bar{k}\bar{y} d\bar{y}, \end{aligned} \quad [5]$$

where θ_0 is the initial trajectory angle.

The definite integral of Eq. [5] can be replaced by

$$\int_{-1}^{\bar{y}} \frac{w_0}{v_0} y_0 \bar{x} \operatorname{sech} \bar{k}\bar{y} d\bar{y} = \frac{1}{x_d y_0} \int_0^{\text{Area}} \frac{w_0}{v_0} y_0 (\operatorname{sech} \bar{k}\bar{y}) dA, \quad [6]$$

which is the total flux linkage of a magnetic field $(w_0/v_0)y_0(\operatorname{sech} \bar{k}\bar{y})$ in the region of interest. Thus, Eq. [5] shows that the change of the sine function of the slope angle θ from its initial value is related to the flux linkage.

Also, from Eq. [4], the radius of curvature, as expected, varies inversely as the magnetic field and the horizontal distance \bar{x} .

Both Eqs. [4] and [5] are nonlinear equations. The trajectory can, however, be readily calculated with the aid of a computer.

Results

Two crucial measurements were made to confirm the validity of the concept of the magnetic collimation. A permanent-magnet lens of the geometry shown by Fig. 1 was built 8 inches wide by $1/2$ inch deep by $1/4$ inch high. Fig. 2 shows the z -directional field along the x axis. The measured dotted curve is in a good agreement with the assumed solid curve. The measured z -directional field at a given x plane is plotted as a dotted curve in Fig. 3. The theoretical hyperbolic simulation is shown by a solid curve. These curves are also in a good agreement, particularly near the x axis. Experiments were made with such a magnetic lens using a 5 kV deflecting electron beam. With a fixed magnetic field, correction of trapezoidal distortion was found to be better than 10%.

The computer simulation of Eqs. [4] and [5] was carried out with the initial boundary condition that when $\bar{x}_0 = 0$ and $\bar{y}_0 = -1$

$$\left(\frac{dx}{dy} \right) = \tan\theta_0.$$

* This key trajectory equation was originally deduced from Eq. [2] through a different but somewhat involved mathematical manipulation and then verified by R. W. Klopfenstein of these Laboratories, who suggested the alternative simple derivation that is presented here. Identical results can also be achieved by changing the variable from time to trajectory length in the manner

$$x = v_0^2 \frac{d^2 x}{dt^2} = v_0^2 \frac{dy}{dl} \frac{d}{dy} \left(\frac{x'}{\sqrt{1+x'^2}} \right) = w_z v_0 \frac{dy}{dl}$$

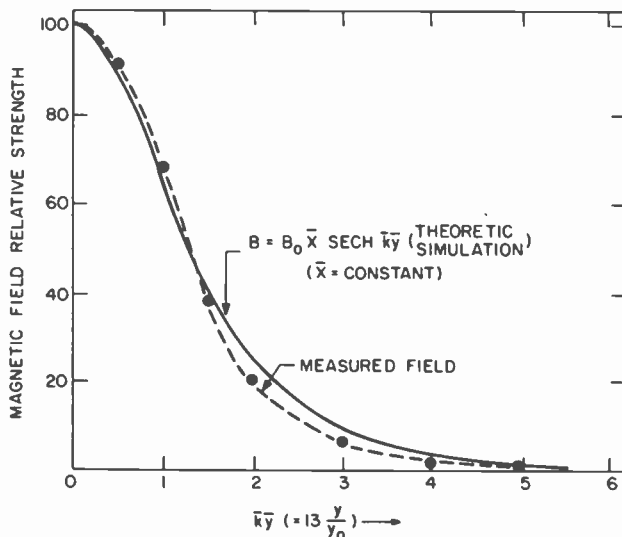


Fig. 3—Field distribution of a magnetic collimator at a given x plane.

At a constant normalized magnetic field of $(w_0/v_0)y_0 = 3.18$, trajectories at various initial angles were computed and plotted as shown in Fig. 4. The trapezoidal distortion is also of the order of 10%, and in agreement with experimentally measured values. Further simulation shows that if the normalized maximum magnetic field varies with the initial slope as indicated by Fig. 5, trajectories are fully collimated into parallel lines, as shown by the dotted lines in Fig. 4.

Discussion

A varied maximum magnetic field as described above can be used to collimate trapezoidal distortion. This effect can be further explored by the following simple analysis. According to Eq. [5], a parallel trajectory ($\theta = 0$) requires a flux linkage equal to the sine function of the initial deflection angle. Assume that the integrand, the y -dependent magnetic field, in Eq. [6] is replaced by an average but constant magnetic field α_{ave} such that

$$\int_0^{\text{Area}} \left(\frac{1}{x_d y_0} \right) \left(\frac{w_0}{v_0} y_0 \right) (\text{sech } \bar{k} \bar{y}) dA = \int_0^{\text{Area}} \alpha_{ave} d\bar{A} = \alpha_{ave} \bar{A},$$

where $\bar{A} = A/(x_d y_0)$. The region of area A can be approximated as a trapezoid ABCD, as shown in Fig. 4, whose area is proportional to the initial slope $S_0 = \tan \theta_0$.

Thus,

$$\alpha_{ave} A = c \alpha_{ave} S_0 = \sin \theta_0 = \frac{S_0}{\sqrt{1 + S_0^2}}$$

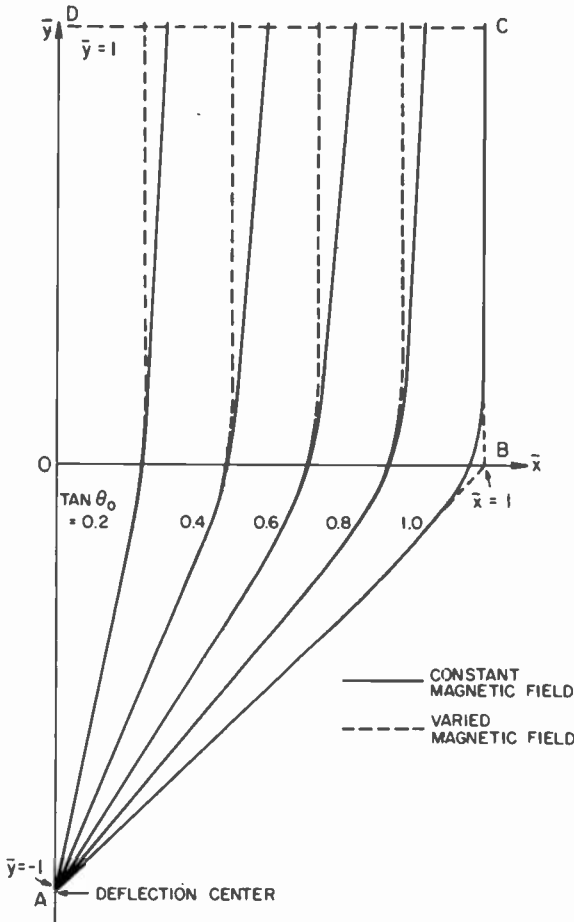


Fig. 4—Collimated electron trajectories in a magnetic collimator.

$$\text{and } \alpha_{ave} = \frac{1}{c\sqrt{1+S_0^2}}$$

where c is a proportional constant. The average normalized field α_{ave} , which is a measure of the normalized peak field $(w_0/v_0)y_0$, is plotted as a dotted curve in Fig. 5. Normalized at the initial tangent, $\tan\theta_0 = 1$, the approximated field is in remarkable agreement with the exact one.

The correction of the trapezoidal distortion by full collimation is applied here to the case of a magnetic lens with a linear field in the x direction and a hyperbolic field in the y direction. Such a collimation may be generalized to other magnetic structures of different field configurations. The general rule is that the bending angle of the electron beam

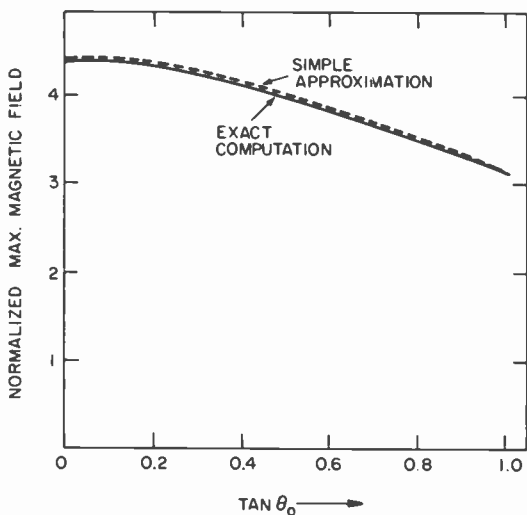


Fig. 5—Maximum magnetic field as a function of initial slope for a collimated beam.

is closely related to the flux linkage, although the required varied field function may appear more complicated than that attained in Fig. 5.

Conclusion

The concept of employing a nonuniform magnetic field for keystone correction of a deflecting electron beam in a two-dimensional image display has been fully explored. This field, linear in one dimensional and hyperbolic in the other, is produced in a slot-shaped structure of two continuous parallel-plate pole pieces. Theory predicts that for a full collimation, the average magnetic field (α_{avr}) must increase with the decrease of the initial slope S_0 of the deflecting beam in the manner of $\alpha_{avr} \propto 1/\sqrt{1 + S_0^2}$. Experimental results have substantiated the prediction.

Acknowledgment

The author wishes to acknowledge the programming of Y. Y. Hsieh for the computer solution of the nonlinear ordinary differential equation. He also wishes to express his gratitude to H. J. Prager and S. Weisbrod for assistance in the measurements.

Shear Viscosity–Temperature–Shear Rate Relations for Flame-Retardant Impact Polystyrene Melts

Wendell M. Lee

RCA Laboratories, Princeton, NJ 08540

Hollis V. Becker

RCA Consumer Electronics, Indianapolis, IN 46201

Abstract—A power-law equation is described that is suitable for computing the apparent shear viscosities of a commercial flame-retardant impact polystyrene resin at injection molding temperatures and shear rates. The equation applies for shear rates above 100 sec^{-1} , and it is based on the properties of apparent shear viscosity-versus-shear rate master curves. Master curves were developed by applying the method of reduced variables; they were produced by superpositions of graphical representations of the results from capillary extrusion rheometer studies at different temperatures: 204, 218, 232, and 246°C. The applicability of the reduced variable principle is demonstrated for this morphologically complex resin by melt flow, and apparent shear viscosity-versus-shear stress, and shear rate master curves for a reference temperature of 232°C (450°F).

1. Introduction

The pressure flow characteristics of molten polymers are of interest to polymer rheologists and plastics processors; the reasons for their interest differ significantly. Polymer rheologists are concerned with the physics of polymer flow, while the processor's interests are primarily economic and arise from his role as the fabricator of plastics into articles of commercial value. Frequently, these articles are produced by injection

molding, which, although it is one of the more complex plastics processing methods, is the most versatile in terms of the variety of items that can be produced economically. The favorable features of injection molding have created, understandably, a broad desire to better comprehend the dynamics of this process.

There has been recent activity in modeling the process that takes place during injection molding.¹⁻⁸ In many cases, these studies have required equations that are able to represent the rheological properties of molten viscoelastic fluids; this has been especially true for computer simulations of the injection molding process. Before the current interest in simulating plastic processing methods, a considerable effort had been expended in developing plastics rheological equations of state, sometimes called constitutive equations. Han *et al.*⁹ have appraised some of the rheological models as they apply to the flow properties of molten plastics.

Some rheological parameters that are of interest and importance in polymer processing are the non-Newtonian viscosity, normal stress differences, and the melt elastic moduli. However, the current levels of development in computer simulation of injection molding require primarily the response of the non-Newtonian shear viscosity parameter to the plastic melt temperature, rate of shear, and, infrequently, the pressure.

The present paper considers a flame-retardant high-impact polystyrene's (FRHIPS) non-Newtonian shear viscosity response to the variables of temperature and rate of shear. The equation developed is a form of the power-law, and it is applicable at the higher shear rates such as those experienced during the filling of injection molds. Equations of the type described here may be developed from the appropriate melt rheology results if Ferry's¹⁴ method of reduced variables can be applied successfully to the data. The methodology employed to handle the data is the usual superpositioning of double logarithmic shear stress-versus-shear rate curves, i.e., melt flow curves generated for different melt temperatures.

We believe the results presented to be the first reported on the successful application of superposition to polymer systems as complicated as the present FRHIPS resin, which is used to injection mold TV receiver cabinets. In addition, we consider the construction of master curves for an important viscosity function, the steady-state apparent shear viscosity. The dependence of this viscosity function on shear stress and shear rate is demonstrated.

Mendelson has reported on the successful applications of the superposition procedures to the melt flow curves of olefin polymers^{10,11} and poly(1-butene) and ethylene-vinyl acetate (EVA) copolymers.¹² Recently, his studies were extended to more complicated polymer systems¹³

and he demonstrated that a generalized melt viscosity-temperature dependence exists for polystyrene (PS), styrene-acrylonitrile (SAN) copolymers, and two high-impact polystyrenes (HIPS).

In the light of Mendelson's reported success in temperature reducing the melt flow curves of the complicated two-phase SAN and HIPS polymers into their master curves, our steady-state capillary rheology data were reexamined and the melt flow curves tested for their capacities to superimpose. The primary reason for this reexamination was to test the ability of our rheology plots to form master curves. Master curves contain considerable amounts of information on the dependences of material parameters, such as viscosity, on the temperature, time, and the rates of shear.

One simple procedure for constructing master curves is by the application of the method of reduced variables to the appropriate graphical representations of the melt rheology data. The method of reduced variables has been used extensively in the present study.

2. Theory

Poiseuille's equation expresses the volumetric steady-state flow rate of Newtonian liquids through tubes of length L and diameter D . The equation may be solved for the coefficient of viscosity, a proportionality constant relating the shear stress and shear rate. In this form, the equation's parameters may be arranged conveniently into terms defining the shear stress and shear rate in the liquid at the tube walls. The expression describing the relation between these parameters is

$$\tau = \mu \dot{\gamma}, \quad [1]$$

where τ is the shear stress, $\dot{\gamma}$ the shear rate, and μ the Newtonian viscosity of the fluid, which is a constant.

The viscosities of non-Newtonian fluids, such as plastic melts, are not independent of the rates of shear. However, the concept and equations of Newtonian or ideal flow may be retained by restricting the definitions of certain parameters. The viscosities of non-Newtonian liquids are instantaneous quantities, defined for specific shear stresses and the corresponding shear rates. The calculated viscosities are called apparent viscosities and are denoted by η_a :

$$\eta_a = \tau_w / \dot{\gamma}_w, \quad [2]$$

where the subscript w indicates values at the wall. Eq. [2] expresses the apparent viscosity of the fluid in terms of the experimentally measurable parameters, τ_w and $\dot{\gamma}_w$. The shear parameters are usually plotted as

double logarithmic shear stress-versus-shear rate curves. These plots are called melt flow curves, and they are constructed to represent the rheological properties of polymer melts at different temperatures.

Shortly before the appearance of the dilute solution theories for flexible-coil polymer molecules, Ferry¹⁴ developed empirically what is currently known as the method of reduced variables. The method is essentially a procedure for superimposing, at fixed temperature, plots that have been constructed for different temperatures, in order to define the values of a parameter over an extended range of a variable. Generally, the data used to construct the individual plots are limited to a somewhat narrow experimental range. Although the principle was applied first to polymer solutions, it was soon extended to undiluted (bulk) polymers. For bulk polymers, the earlier concentration parameter was replaced by the polymer density ρ .

Ferry made the following assumptions in developing the empirical method of reduced variables.

- (1) All moduli associated with the i modes of chain motion are proportional to the absolute temperature and the material density at that temperature.
- (2) Every relaxation time τ_i for every motion mode i has the same temperature dependence.

The effect of assumption (2) is that a change of temperature from a given reference temperature T_R to another temperature T requires multiplying all τ_i by the same factor. Ferry called this multiplier the shift factor. It is denoted by the symbol a_T . Ferry applied the above assumptions to an earlier expression derived for the steady flow viscosity by Alfrey and Doty¹⁵ and obtained for the viscosity at the new temperature T

$$\eta = a_T \frac{T\rho}{T_R\rho_R} \eta_R. \quad [3]$$

Here, T is in degrees Kelvin and the measured viscosity $\eta_R = \sum_i \eta_i$, the sum of the viscosities of the i individual states. Eq. [3] may be rearranged to define a_T ,

$$a_T = \frac{\eta}{\eta_R} \frac{T_R\rho_R}{T\rho}, \quad [4]$$

or to define the viscosity at the arbitrarily selected reference temperature, T_R ,

$$\eta_R = \frac{\eta}{a_T} \frac{T_R\rho_R}{T\rho}. \quad [5]$$

Eq. [5] is an important expression, whose use becomes clearer in subse-

quent discussions. Ferry successfully applied his empirical assumptions to other viscoelastic functions, but these expressions are not included in the present study.

Papers by Rouse,¹⁶ Bueche,¹⁷ and Zimm¹⁸ on the behaviors of flexible coil polymers in dilute solutions appeared several years after Ferry's development of the method of reduced variables. These dilute polymer solution theories offered, in fact, partial theoretical justification for the soundness of Ferry's empirical assumptions and for the forms of his reduced equations.

The results of the three theories were essentially equivalent in their abilities to predict the properties of certain flexible polymers in solution. Although each theory developed differently, each treated the coiled polymer molecule as connected statistical units, selected to assure the proper end-to-end Gaussian coil behavior. The theories were developed for polymer molecules in solvent environments, but they could be applied to undiluted (bulk) polymers by redefining the friction coefficients.

Expressions for the relaxation times of the different modes of motion for the polymer molecules were derived in the theories of Rouse and Zimm. In the Rouse theory, the relaxation time for the undiluted polymer may be expressed as

$$\tau_p = \frac{6\eta M}{\pi^2 p^2 \rho RT}, \quad [6]$$

where τ_p is the relaxation time for the p th mode of motion, η is the viscosity, and M is the polymer's molecular weight and ρ its density. Eq. [6] shows that the temperature dependence of the relaxation time τ_p is controlled primarily by the viscosity, although this dependence is partly explicit and partly through the temperature dependence of the density. Passaglia¹⁹ has shown that the ratio of the relaxation time at temperature T , for the p th mode of motion, to that of the same relaxation at some reference temperature T_R can be expressed as

$$\frac{\tau_p(T)}{\tau_p(T_R)} = \frac{\eta}{\eta_R} \frac{T_R \rho_R}{T \rho} = a_T \quad [7]$$

$$a_T = \frac{\eta}{\eta_R} \frac{T_R \rho_R}{T \rho}. \quad [8]$$

Eq. [7] shows that the ratios of relaxation times are independent of the mode parameter p for temperatures T and T_R . Therefore, the relaxation time ratios for these two temperatures are constant and the same for all the relaxation times. Eq. [8] is the same as Eq. [4], the earlier empirically derived expression by Ferry.

The magnitude of the shift factor a_T is defined by the displacement of a curve at temperature T along a prescribed coordinate route to su-

perimpose it on a similar curve at an arbitrarily selected reference temperature T_R . The value of a_T is less than unit if $T > T_R$, greater than unity if $T < T_R$, and, of course, unity at $T = T_R$.

Mendelson¹⁰ has reported an expression that defines a_T in terms of the shear rates at two different temperatures. The equation expressing this relationship is

$$a_T = \frac{\dot{\gamma}_w(T_R)}{\dot{\gamma}_w(T)} \quad \text{at constant } \tau_w. \quad [9]$$

Eq. [9] indicates that a_T may be calculated from shear rates at constant stress but different temperatures. a_T may also be determined by the superposition of melt flow curves generated at different temperatures. This procedure requires shifting the $T \neq T_R$ melt flow curves along the shear rate coordinate, at constant shear stress, until the curves superimpose and form the composite or the master curve at the reference temperature T_R .

Eq. [9] may be expressed in its logarithmic form as

$$\log \dot{\gamma}_w(T_R) = \log \dot{\gamma}_w(T) + \log a_T. \quad [10]$$

This expression shows that the logarithm of the shift factor, or $\log a_T$, is the magnitude of the displacement of a melt-flow curve from its position at temperature T to one that superimposes the melt-flow curve at some arbitrary reference temperature T_R .

Similarly, Eq. [8] may be written

$$a_T = \frac{\eta_a(T)}{\eta_a(T_R)} \quad \text{at constant } \tau_w, \quad [11]$$

where η_a is the apparent shear viscosity and the factor $T_R \rho_R / T \rho$ has been taken to be essentially unity. The assumption that the factor is unity is frequently justified by the fact that melt viscosity data usually encompass a limited elevated temperature range. Within this temperature range, phase changes in the molten fluid are usually absent; exceptions are the crystalline polymers or filled polymers with components that have melting temperatures, T_M , or phase transitions within the temperature range under study. In its logarithmic form, Eq. [11] may be written

$$\log \eta_a(T_R) = \log \eta_a(T) - \log a_T. \quad [12]$$

Eqs. [10] and [12] are approximate logarithmic forms of the reduced shear rate and apparent shear viscosity variables. These reduced variables are used in the temperature reductions of steady flow melt rheology

plots to produce the corresponding composite or master curve. In fact, several important master curves of the viscoelastic functions can be obtained by plotting double logarithmically the appropriate reduced variables.

One of these plots is the rheologically important master curve obtained by plotting the reduced variables $\eta_a(T_R)$ and $\dot{\gamma}_w(T_R)$. These master curves begin with plots of $\log\eta_a(T)$ ($T_R P_R/T_p$) or $\log\eta_a(T)$ against $\log\dot{\gamma}_w(T)$ for the different temperatures. The individual temperature plots are then temperature reduced to produce the desired master curve at an arbitrary reference temperature T_R .

The temperature dependence of the shift factor a_T represents the basic effect of temperature on the viscoelastic properties of polymers. A graphical representation of this temperature dependence may follow no simple analytical form. The plots may be complicated or simple curves of a_T or $\log a_T$ versus temperature. The functional dependence of a_T on temperature is frequently taken to follow some known analytical expression. One such expression is the common Arrhenius equation.

Eqs. [9] and [11] show that, for fixed T and T_R , the same value of a_T is obtained with either $\dot{\gamma}_w$ or η_a as the variable. One criterion for the applicability of the method of reduced variables is satisfied if the a_T values for different variables and functions are the same. That is, the same shift factor, a_T , must superimpose all the viscoelastic functions for a given temperature. A second crucial test of the method is one that requires exact matching of the slopes of adjacent unreduced curves.

In cases where the method of reduced variables applies, it serves to separate the complicated dependence of a viscoelastic function on both shear rate (frequency, time) and temperature into a function of shear rate (frequency, time) alone and one of temperature alone. From a practical viewpoint, it is important that the reverse of the temperature-reduction or superposition procedures can be performed, i.e., the master curve may be "unreduced" or resolved.

3. Experiment

3.1. Apparatus and Materials

The resin used in this study was a flame-retardant high-impact polystyrene, TMDH-5171.* The resin is a modified styrenic toughened with rubber particles. It was reported²⁰ to contain 7–15% rubber (a polybu-

tadiene elastomer),²¹ 11–13% decabromodiphenyl oxide, and 4–5% antimony trioxide. Particulate decabromodiphenyl oxide and antimony trioxide make up the resin's additive flame-retardant package. It is very likely that small quantities of antioxidants, stabilizers, and lubricants are present.

The melt viscosity properties of the FRHIPS were determined at six elevated temperatures, 163°C (325°F) to 246°C (475°F), using an Instron Capillary Extrusion Rheometer. The capillary die dimensions were diameter $D = 0.0502$ inches and length $L = 2.0095$ inches; the included entry angle was 90° and the L/D ratio was 40. A minimum of two experimental runs with different samples were made at each temperature. The plunger loads for the experiments generally agreed to within 5%, except at the lower loads where the differences were greater. An average of the load values was used as input for the shear stress computations.

Instron rheometers are constant rate capillary extrusion instruments. They operate on the principle of a plunger forcing the molten polymer from a thermostatted reservoir through a capillary die forming an extrudate that exists into the air. The plunger is driven mechanically at a preselected constant velocity, but the selected velocity is variable in increments. Shear stress and shear rate at the capillary walls are determined by the plunger's load and velocity and the reservoir and capillary dimensions. The steady flow apparent shear viscosity, Eq. [2], is the significant parameter obtained from the results of measurements on capillary extrusion rheometers.

A Fortran IV computer program²² was used to compute the wall shear stresses, τ_w , and shear rates, $\dot{\gamma}_w$, along with other pertinent viscosity parameters. The shear stresses, shear rates, flow index, and partially corrected apparent shear viscosities were the portions of the output used. Shear rates were corrected by applying the Weissenberg-Rabinowitsch-Mooney correction. The customary Bagley corrections were not made. Thus, the apparent shear viscosities are partially corrected. The failure to take into account end corrections does not affect the superposition of curves. However, the application of the correction would change the values of the constants in equations for the master curve, Eq. (18). Qualitative estimates of the correction indicate that the magnitudes of the highest measured shear stresses would be reduced by about 8%.²³ The curves of this study were drawn empirically.

* The FRHIPS TMDH-5171 was originally manufactured by the Union Carbide Corporation. This polystyrene is now manufactured by Gulf Oil Chemicals Company, whose designation for the resin is MH-5171.

3.2. Curve Shifting Procedures

The procedures described below were used to shift or superimpose the curves for different temperatures to form composite plots or master curves.

For the case of the melt flow curves, Fig. 1, the flow curve for each temperature was shifted horizontally at a constant shear stress (6.0×10^5 dynes/cm²) until it superimposed on the melt flow curve at the selected reference temperature, $T_R = 232^\circ\text{C}$ (450°F). For each melt flow curve, the magnitude of this horizontal shift is $\log a_T$, from which the value of the shift factor can be determined for temperatures T and T_R . A melt flow master curve, such as that shown in Fig. 2, is obtained on shifting each melt flow curve in the manner described.

By procedures analogous to those described for the melt flow curves, double logarithmic $\eta_a(T)$ versus τ_w curves, Fig. 4, were temperature reduced at constant stress to produce the $\eta_a(T_R)$ versus τ_w master curve at 232°C (450°F), shown in Fig. 5. In this case, the shifts occurred vertically along a constant stress of 6.0×10^5 dynes/cm². The ordinate of Fig. 5 contains the reduced apparent shear viscosity, $\eta_a(T_R)$, a reduced variable that is defined by a rearranged form of Eq. [11], $\eta_a(T_R) = \eta_a(T)/a_T$. Again, $\log a_T$ is equal to the magnitude of the vertical displacement of the $\eta_a(T)$ versus τ_w curves from T to T_R .

A third set of temperature reducible plots is the rheologically important $\eta_a(T)$ versus $\dot{\gamma}_w(T)$ curves, plotted logarithmically for different

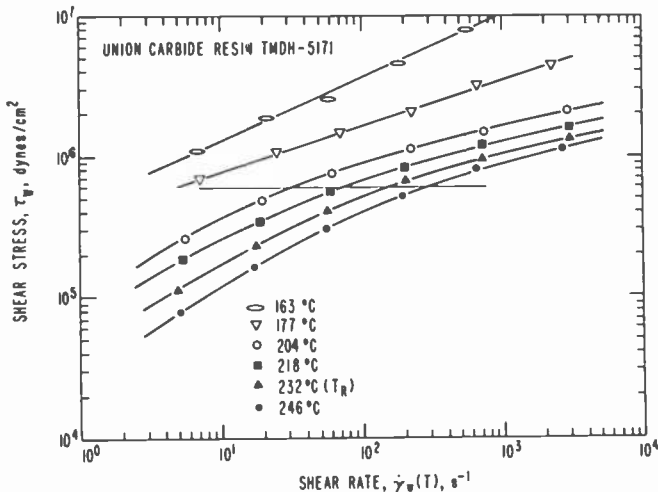


Fig. 1—Shear stress-versus-shear rate melt flow curves at various temperatures for a flame-retardant impact polystyrene.

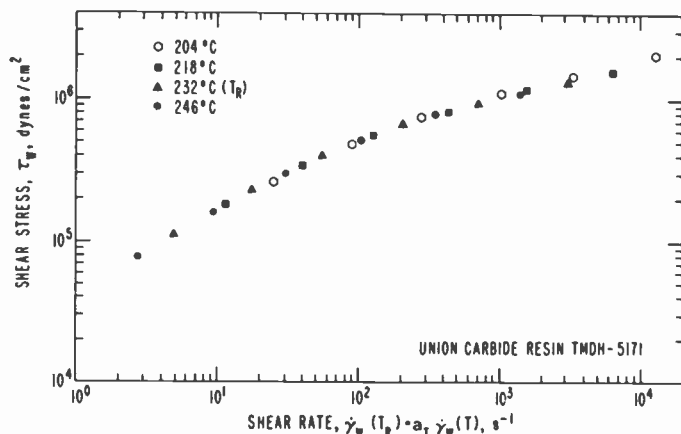


Fig. 2—Melt flow master curve at reference temperature $T_R = 232^\circ\text{C}$ for a flame-retardant impact polystyrene.

temperatures, T . A set of these curves is shown in Fig. 6. These plots were temperature reduced to form a master curve at T_R by shifting each along the appropriate direction of a line with slope -1 until they superimposed on the curve for the arbitrarily selected reference temperature. The reference curve is shown in Figs. 6 and 7 as \blacktriangle 's. A master curve produced by the temperature reduction of the plots of Fig. 6 is shown in Fig. 7.

The master curve of Fig. 7 is, of course, the equivalent of plotting the reduced variables $\eta_a(T_R)$ and $\dot{\gamma}_w(T_R)$ as the ordinate and abscissa, respectively. These reduced variables are defined by rearranged forms of Eqs. [9] and [11]. The reduced shear rate is defined as $\dot{\gamma}_w(T_R) = a_T \dot{\gamma}_w(T)$ and the reduced apparent shear viscosity as $\eta_a(T_R) = \eta_a(T)/a_T$. According to these definitions of the variables, each experimental point with coordinates $[\eta_a(T), \dot{\gamma}_w(T)]$ may be temperature reduced to its master curve coordinates $[\eta_a(T_R), \dot{\gamma}_w(T_R)]$ by dividing each $\eta_a(T)$ by the appropriate a_T value and multiplying the corresponding $\dot{\gamma}_w(T)$ by the same value of a_T .

4. Results

Fig. 1 shows melt flow curves that depict the melt viscosity characteristics of the FRHIPS at six different temperatures. At the lowest temperatures, 163°C (325°F) and 177°C (350°F), the melt flow curves are approximately linear and could be represented by one or two power-law expressions. In the 163°C (325°F) to 246°C (475°F) range, the melt flow curves of this flame-retardant polystyrene exhibit distinctly non-Newtonian flow characteristics. Flow curves at the four highest temperatures

may be represented by three constant quadratic expressions that are logarithmic in the shear rate variable. The form of these expressions is

$$\log \tau_w(T) = C_0(T) + C_1 \log \dot{\gamma}_w(T) + C_2 [\log \dot{\gamma}_w(T)]^2. \quad [13]$$

An inspection of Fig. 1 indicates that the melt flow curves at the two lowest temperatures cannot be made to superimpose by applying any of the common shifting procedures described. However, the melt flow curves for the four highest temperatures do temperature reduce to form useful melt flow master curves. Using the curve shifting methods that were described earlier, the curves of Fig. 1 were shifted along the shear rate coordinate, at constant shear stress, until they superimposed to produce the 232°C (450°F) melt flow master curve shown in Fig. 2.

The melt flow master curve in Fig. 2 represents the flow properties of the TMDH-5171 resin at 232°C (450°F). It extends the useful shear rate range roughly a decade beyond the shear rates that could be measured experimentally.

At first glance, the master curve in Fig. 2 appears to be an ordinary melt flow curve constructed with a large number of data points collected at 232°C. This appearance is deceiving because the master curve contains information on the flow properties of the FRHIPS resin at other shear rates and temperatures. The apparent extension of the shear rate range by about a decade may be traced to the influence of the reduced shear-rate variable, $a_T \dot{\gamma}_w(T)$, which is governed by the temperature dependent shift factor a_T .

Values for $\log a_T$ were determined by the melt flow curve shifts necessary to produce the 232°C (450°F) master curve. The values for $\log a_T$ and those for a_T computed from them, along with the values for a_T from Eq. [9], are given in columns 2-4 of Table 1. Certain assumptions were made concerning the properties of the shift factor a_T . One such assumption was that the shift factor's dependence on temperature is defined by the Arrhenius equation. That is, $\log a_T$ was taken to be a linear function of the reciprocal absolute temperature. A plot of $\log a_T$ versus $1/T^\circ\text{K}$ is shown in Fig. 3, where the line was drawn empirically forcing

Table 1—Shift Factor a_T Values for a Flame-Retardant Impact Polystyrene*

Temp. (°C)	$\tau_w - \dot{\gamma}_w$ Curves			$\eta_a - \tau_w$ Curves			a_T Average Value
	Curve Shifting Log a_T	Eq. [9] a_T	Eq. [9] a_T	Curve Shifting Log a_T	Eq. [11] a_T	Eq. [11] a_T	
204	0.698	4.99	4.73	0.666	4.64	4.85	4.80
218	0.365	2.32	2.21	0.332	2.15	2.14	2.21
232	0.0	1.00	1.00	0.0	1.00	1.00	1.00
246	-0.226	0.59	0.59	-0.258	0.55	0.55	0.57

* Union Carbide injection molding resin TMDH-5171.

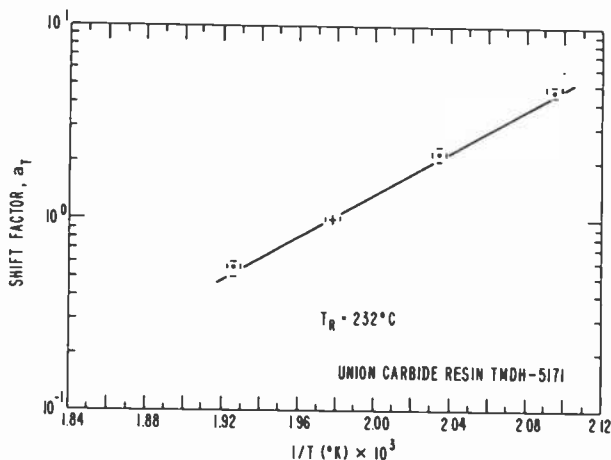


Fig. 3—Superposition shift factors a_T versus reciprocal of absolute temperature for a flame-retardant impact polystyrene

the fit through the reference point. The plot is linear showing that the assumed exponential, or Arrhenius relation, is obeyed. An expression for this exponential temperature dependence is

$$a_T = A \exp(E_{\tau_w}/RT), \quad [14]$$

where T in degrees Kelvin, R the gas constant, and A a factor that depends on the reference temperature. The constant E_{τ_w} is the shift factor's activation energy. It is equivalent to the activation energy for viscous flow at constant shear stress. The slope of the curve of Fig. 3 was used to calculate for the FRHIPS resin the magnitude of its activation energy for viscous flow. The value for the activation energy is about 25 kcal/mole, which is reasonably close to the 25.5 kcal/mole value reported by Mendelson¹³ for the flow activation energies of the complex two-phase SAN and HIPS polymers.

The shift-factor temperature dependence for the FRHIPS may be expressed by the following equations.

$$\log a_T = -10.78 + 5.44 \times 10^3 \left(\frac{1}{T} \right), \quad \text{at } 232^{\circ}\text{C} (505^{\circ}\text{K}), \quad [15]$$

or

$$a_T = 1.66 \times 10^{-11} \exp(25,000/RT), \quad \text{at } 232^{\circ}\text{C} (505^{\circ}\text{K}). \quad [16]$$

Eqs. [15] and [16] are expected to define the a_T values for different $T - T_R$ combinations over a conservative 60°C temperature range (200 - 260°C) based on the 232°C reference temperature. Melt viscosity

measurements on the resin at 260°C (500°F) are prevented by rapid thermal degradation of the polymer at elevated temperatures. It is important that equations be developed for computing the values of the plastic parameters at these higher temperatures, since the actual injection molding operations can produce resin temperatures of 260°C (500°F).

According to Eq. [2], a fluid's apparent viscosity is defined as τ_w divided by the corresponding $\dot{\gamma}_w$. This apparent shear viscosity may be plotted against the shear parameters to reveal some useful shear viscosity dependences. One set of curves is the logarithmic plots of apparent shear viscosity, $\eta_a(T)$, versus the shear stress, τ_w . However, $\eta_a(T)$ versus τ_w curves are seldom used. Plots of this type can be generated for different temperatures to produce a family of curves such as the ones shown in Fig. 4. These curves were temperature reduced to produce the 232°C $\eta_a(T_R)$ versus τ_w master curve shown in Fig. 5, using the shifting procedures described earlier. For this case, the shifts of the curves occurred vertically at a constant stress value of 6.0×10^5 dynes/cm². Again, the magnitudes of these vertical displacements were the $\log a_T$ values for the temperature reductions. The $\log a_T$ values, as well as the a_T values derived from them and from Eq. [11], are given in columns 5–7 of Table 1. Column 8 of Table 1 contains the average a_T values obtained with the values of columns 3, 4, 6, and 7.

An important set of viscosity curves is that produced by plotting logarithmically the apparent shear viscosity function, $\eta_a(T)$, against the

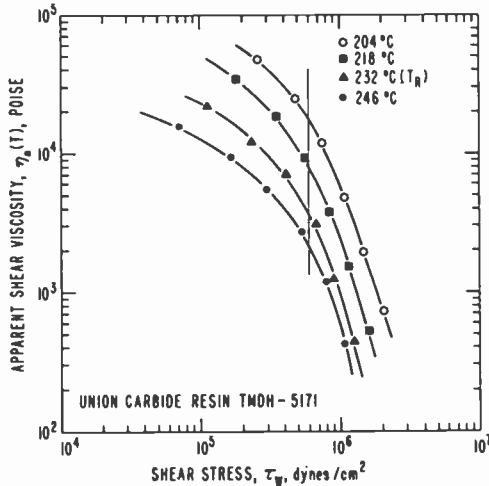


Fig. 4—Apparent shear viscosity versus shear stress curves at various temperatures for a flame-retardant impact polystyrene.

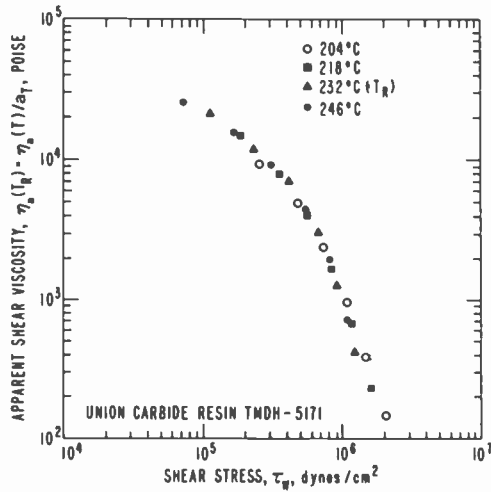


Fig. 5—Apparent shear viscosity at 232°C versus shear stress master curve for a flame-retardant impact polystyrene.

shear rate variable, $\dot{\gamma}_w(T)$. These plots are constructed for different temperatures and their characteristic shapes reveal the fluid viscosity dependence on the rate of shear.

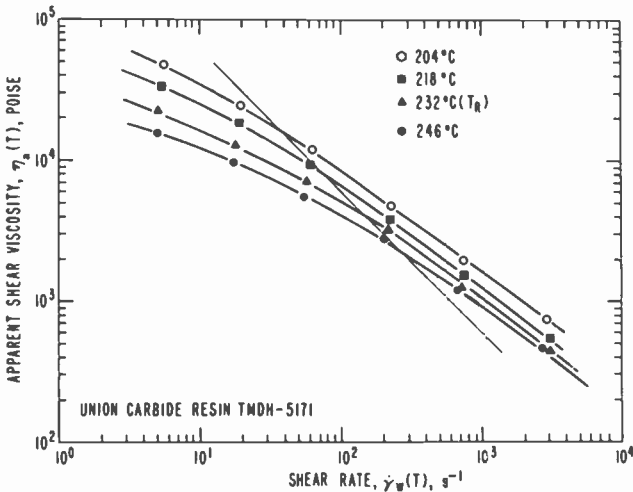


Fig. 6—Apparent shear viscosity versus shear rate curves at various temperatures for a flame-retardant impact polystyrene.

Fig. 6 shows, for the flame-retardant polystyrene resin TMDH-5171, the logarithmic apparent shear viscosity-versus-shear rate curves for four temperatures. A line with slope -1 is also shown in this figure. It is along this line that the individual curves must be displaced to achieve proper superposition and the formation of a master curve at the 232°C reference temperature. Fig. 7 is the 232°C master curve produced by the temperature reduction of the curves in Fig. 6. The master curve in Fig. 7 is constructed with two reducible variables, $\eta_a(T_R)$ and $\dot{\gamma}_w(T_R)$, and expressions for these are shown on the coordinates of the master curve. In fact, this master curve could be constructed by applying the appropriate average shift factor values from Column 8, Table 1, to the data for the curves of Fig. 6.

The master curve in Fig. 7 shows that the shear rate range has been extended about a decade beyond the range that bounds the experimental curves of Fig. 6. The highest shear rates of the master curve exceed $10,000 \text{ sec}^{-1}$, and they are into the range of shear rates commonly experienced in gates in injection molding. Apparent shear viscosity values at these large shear rates must be accepted cautiously because viscous heating of the flowing fluid becomes significant. The curves of Figs. 6 and 7 have not been corrected for viscous heating effects. In the past, corrections for the effects of shear heating have been cumbersome and difficult to apply. Hieber²⁵ reported recently on corrections to capillary rheometer data that take into account the effects of shear heating the fluid.

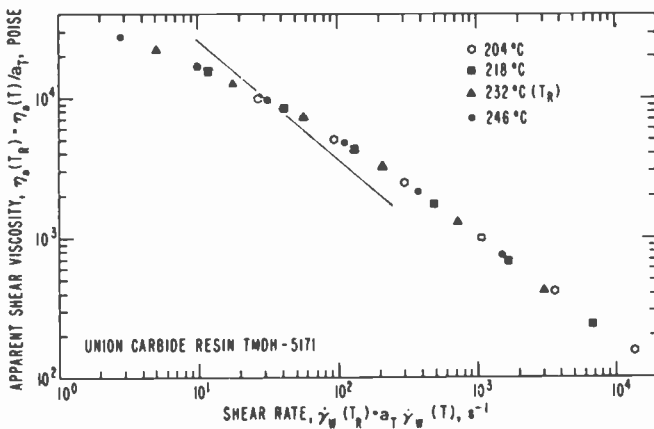


Fig. 7—Apparent shear viscosity at 232°C versus shear rate master curve for a flame-retardant impact polystyrene.

5. Discussion

Results of the present study show that the method of reduced variables can be applied to at least one morphologically and compositionally complex commercial flame-retardant styrene resin, a resin used to injection mold TV receiver cabinets. Graphical forms of the melt viscosity data were temperature reduced by superposition to produce three types of master curves, demonstrating the applicability of the principle to this FR resin. The melt flow and melt flow master curves of Figs. 1 and 2, respectively, are frequently used to represent the flow behaviors of molten plastics. The rheologically important curves are log-log plots of the apparent shear viscosity versus shear rate, $\eta_a(T)$ versus $\dot{\gamma}_w(T)$. Fig. 6 shows this set of curves and Fig. 7 gives the 232°C master curve resulting from the temperature reduction.

Inspection of the $\eta_a(T_R)$ versus $\dot{\gamma}_w(T_R)$ master curve in Fig. 7 indicates, quite convincingly, the general viscosity characteristics of pseudoplastic, or shear thinning, fluids. This reversible decrease in viscosity with increasing rates of shear is the key material characteristic that enables the molten plastic to be pushed easily and economically through intricate geometric channels to form complex molded plastic parts.

Further inspection of Fig. 7 reveals linearity of the log-log plot and suggests that the resin's viscosity dependence on shear rate may be expressed as some form of the power-law. At shear rates of 200–10,000 sec^{-1} , the magnitudes of the viscosity of the TMDH-5171 resin at 232°C at different shear rates are represented satisfactorily by the following power-law expression:²⁴

$$\eta_a(T_R) = \eta_a^0(T_R) \left(\frac{\dot{\gamma}_w(T_R)}{\dot{\gamma}_w^0(T_R)} \right)^{n-1}, \quad [17]$$

where $\dot{\gamma}_w^0(T_R)$ is the reference shear rate. This shear rate and the corresponding shear stress determine the magnitude of the reference viscosity, $\eta_a^0(T_R)$. The factor n of the exponent is the fluid flow index, defined as the apparent slope of the melt flow curve in the region where the power-law is applicable.

Values for some of the parameters in Eq. [17] were determined by selecting a mid-range power-law reference shear rate of $1.0 \times 10^3 \text{ sec}^{-1}$ for $\dot{\gamma}_w^0(T_R) = \dot{\gamma}_w^0(232)$. The reference viscosity, $\eta_a^0(232)$, is therefore 1.0×10^3 poise, determined from the 232°C master curve (Fig. 7). A value of 0.26 was determined for the flow index, n , at the reference shear rate. Substituting these values into Eq. [17] gives

$$\eta_a(232) = 1.0 \times 10^3 [1.0 \times 10^{-3} \times \dot{\gamma}_w(232)]^{-0.74}. \quad [18]$$

Eq. [18] represents the FRHIPS resin viscosity dependence on shear rate

over a limited shear rate range, at the 232°C melt temperature. Melt viscosity values calculated with Eq. [18] are accurate to within 6% over the shear rate range of 150–9000 sec⁻¹. Shear rates of this magnitude are frequently experienced in the filling stages of injection molding.

The capacity of master curves to reproduce the parent plots or similar plots at arbitrary temperatures is an important practical feature of these curves. Since the master curve contains information on the values of the coordinate variables within defined boundary limits, the master curve may be “unreduced” or resolved to produce, at different temperatures, curves having the characteristics of the parent plots. The resolution of the master curve is carried out with the aid of the shift factor a_T . The shear viscosity of the resin at temperature T is defined as the product of the shear viscosity at the reference temperature and the appropriate shift factor value. This definition of the apparent shear viscosity at temperature T may be written

$$\eta_a(T) = \eta_a(T_R)a_T, \quad [19]$$

a rearranged form of Eq. [11]. Eq. [19] shows that the resolution of the reduced viscosity function occurs in the vertical direction only. The horizontal component in the resolution of the master curve in Fig. 7 involves the reduced shear rate, defined as

$$\dot{\gamma}_w(T_R) = a_T \dot{\gamma}_w(T), \quad [20]$$

a form of Eq. [9]. The resolution of $\eta_a(T_R)$ versus $\dot{\gamma}_w(T_R)$ master curves into extended $\eta_a(T)$ versus $\dot{\gamma}_w(T)$ plots involves shifting the master curve along the directions of a line with slope -1 , while maintaining the same point of intersection on the master curve. The line is actually one representing constant stress, in this case 6.0×10^5 dynes/cm².

Substituting Eq. [20] for the $\dot{\gamma}_w(T_R)$ term in Eq. [17] gives

$$\eta_a(T_R) = \eta_a^0(T_R) \left(\frac{\dot{\gamma}_w(T)a_T}{\dot{\gamma}_w^0(T_R)} \right)^{n-1},$$

which, when substituted for $\eta_a(T_R)$ in Eq. [19], gives

$$\eta_a(T) = \eta_a^0(232) \left(\frac{\dot{\gamma}_w(T)}{\dot{\gamma}_w^0(232)} \right)^{n-1} a_T^n. \quad [21]$$

Here the parameters $\eta_a^0(232)$, $\dot{\gamma}_w^0(232)$, and a_T are based on the properties of the master curve at the reference temperature, 232°C (505°K). The appropriate a_T value is calculated with Eq. [16] by replacing T with the plastic's melt temperature.

Substitution of values for the constants in Eq. [21] gives

$$\eta_a(T) = 1.0 \times 10^3 [1.0 \times 10^{-3} \times \dot{\gamma}_w(T)]^{-0.74} a_T^{0.26}, \quad [22]$$

an equation based on the master curve (Fig. 7). Computer simulations

of injection molding require values for the shear viscosities of plastic melts for a variety of mold filling conditions. Eq. [22] may be used to calculate the shear viscosity of the commercial FRHIPS for different melt temperatures and shear rates. Presumably, simple equations with the form of Eq. [22] could be developed for other complex commercial resins, if the method of reduced variables can be applied to the melt viscosity data.

Eq. [22] expresses for the FRHIPS the magnitude of its apparent shear viscosity for arbitrarily selected shear rates and temperatures. Both the shear rate and temperature variables must be within the limits for which the power-law and the method of reduced variables are applicable, and these limits are not necessarily the experimental limits of the parent curves used in the construction of the master curve. In fact, it is desirable to have the limits of applicability extend beyond the experimental restrictions on the original data, particularly in the direction of higher temperatures and shear rates for injection molding. Injection molding operations frequently expose the molten plastic to temperatures higher than those of the melt viscosity experiments, usually for times of 60 seconds or less.

Eq. [22] limits computations of the shear viscosity to the higher shear rate range, and, indeed, these shear rates are the ones of interest in modeling and computing plastic flow during injection molding. However, it appears that the procedures described could be applied to give the correct temperature dependences to some of the more complicated equations, such as the ones used to represent the apparent shear viscosities of polymer melts over the spectrum of shear rates.

6. Acknowledgments

The authors are indebted to A. W. Jessup, Jr., for writing the computer program and to K. I. Maijala for performing the viscosity measurements.

References:

- ¹ S. Kenig, *Injection Molding of Thermoplastics*, Ph.D. Thesis, McGill University (1972).
- ² J. L. Berger and C. G. Gogos, "A Numerical Simulation of the Cavity Filling Process with PVC in Injection Molding," *Polym. Eng. Sci.*, **13**, p. 102 (1973).
- ³ K. K. Wang, S. F. Shen, J. F. Stevenson, C. A. Hieber, and S. Chung, First Progress Report, "Computer-Aided Injection Molding System," Cornell University, Ithaca, N.Y., (1975), NSF Grant No. ATA-7411490.
- ⁴ G. Williams and H. A. Lord, "Mold-Filling Studies for the Injection Molding of Thermoplastic Materials. Part I: The Flow of Plastic Materials in Hot- and Cold-Walled Circular Channels," *Polym. Eng. Sci.*, **15**, p. 553 (1975).
- ⁵ H. A. Lord and G. Williams, "Mold-Filling Studies for the Injection Molding of Thermoplastic Materials. Part II: The Transient Flow of Plastic Materials in the Cavities of Injection-Molding Dies," *Polym. Eng. Sci.*, **15**, p. 569 (1975).

- ⁶ M. R. Kamal, Y. Kuo, and P. H. Doan, "The Injection Molding Behavior of Thermoplastics in Thin Rectangular Cavities," *Polym. Eng. Sci.*, **15**, p. 863 (1975).
- ⁷ J. L. White, "Fluid Mechanical Analysis of Injection Mold Filling," *Polym. Eng. Sci.*, **15**, p. 44 (1975).
- ⁸ J. F. Stevenson, C. A. Hieber, A. Galskoy, and K. K. Wang, "An Experimental Study and Simulation of Disc Filling by Injection Molding," *Soc. Plastics Eng. Tech. Papers, 34th ANTEC*, Atlantic City, N.J., p. 382, April 1976.
- ⁹ C. D. Han, K. U. Kim, N. Siskovic, and C. R. Huang, "An Appraisal of Rheological Models as Applied to Polymer Melt Flow," *Rheol. Acta.*, **14**, p. 553 (1975).
- ¹⁰ R. A. Mendelson, "Polyethylene Melt Viscosity Shear Rate-Temperature Superposition," *Trans. Soc. Rheol.*, **9**, p. 53 (1965).
- ¹¹ R. A. Mendelson, "On the Temperature Dependence of the Melt Viscosity of Crystalline Polypropylene," *J. Polym. Sci., Polymer Letters*, **5**, p. 295 (1967).
- ¹² R. A. Mendelson, "Prediction of Melt Viscosity Flow Curves at Various Temperatures for Some Olefin Polymers and Copolymers," *Polym. Eng. Sci.*, **8**, p. 235 (1968).
- ¹³ R. A. Mendelson, "A Generalized Melt-Viscosity-Temperature Dependence for Styrene and Styrene-Acrylonitrile Based Polymers," *Soc. of Plastics Engineers Tech. Papers, 34th ANTEC*, Atlantic City, N.J., April 1976, p. 344; R. A. Mendelson, "A generalized Melt Viscosity-Temperature Dependence for Styrene and Styrene-Acrylonitrile Based Polymers," *Polym. Eng. Sci.*, **16**, p. 690 (1976).
- ¹⁴ J. D. Ferry, "Mechanical Properties of Substances of High Molecular Weight. VI: Dispersion in Concentrated Polymer Solutions and its Dependence on Temperature and Concentration," *J. Amer. Chem. Soc.*, **72**, p. 3746 (1950); J. D. Ferry, E. R. Fitzgerald, M. F. Johnson, and L. D. Grandine, Jr., "Mechanical Properties of Substances of High Molecular Weight. X: The Relaxation Distribution Function in Polyisobutylene and Its Solutions," *J. Appl. Phys.*, **22**, p. 717 (1951); J. D. Ferry, *Viscoelastic Properties of Polymers*, 2nd Ed., John Wiley and Sons, N.Y. (1970), Chapter 11, "Dependence of Viscoelastic Behavior on Temperature and Pressure."
- ¹⁵ T. Alfrey and P. Doty, "The Methods of Specifying the Properties of Viscoelastic Materials," *J. Appl. Phys.*, **16**, p. 700 (1945).
- ¹⁶ P. E. Rouse, Jr., "A theory of the Linear Viscoelastic Properties of Dilute Solutions of Coiling Polymers," *J. Chem. Phys.*, **21**, p. 1272 (1953).
- ¹⁷ F. Bueche, "The Viscoelastic Properties of Plastics," *J. Chem. Phys.*, **22**, p. 603 (1954); F. Bueche, "Influence of Rate of Shear on the Apparent Viscosity of (A) Dilute Polymer Solutions and (B) Bulk Polymers," *J. Chem. Phys.*, **22**, p. 1507 (1954).
- ¹⁸ B. H. Zimm, "Dynamics of Polymer Molecules in Dilute Solution: Viscoelasticity, Flow-Birefringence, and Dielectric Loss," *J. Chem. Phys.*, **24**, p. 269 (1956).
- ¹⁹ E. Passaglia, in *Engineering Design of Plastics*, E. Baer Ed., Reinhold Publishing Co., N.Y. (1964), Chap. 3, "Viscoelastic Behavior and Time-Temperature Relations."
- ²⁰ Union Carbide Corp.
- ²¹ L. Korsakoff and W. M. Lee, private communication.
- ²² A. W. Jessup, Jr., and W. M. Lee, Computer Program developed from Flowcharts in *Computer Programs for Plastics Engineers*, I. Klein and D. I. Marshall, eds., Reinhold Book Corp., N.Y. (1968), Chapter 2.1 by S. F. Dieckman, "Characterization of Polymer Melt Flow Properties by Applying Rabinowitsch and Bagley Corrections to Capillary Viscometric Data," and Chapter 3.1 by R. A. Mendelson, "Viscoelastic Functions from Capillary Flow Data."
- ²³ W. M. Lee, unpublished results.
- ²⁴ J. M. McKelvey, *Polymer Processing*, John Wiley and Sons, N.Y. (1962), Chapter 2, Table 2-4.
- ²⁵ C. A. Hieber, "Thermal Effects in the Capillary Rheometer," *Rheol. Acta.*, **16**, p. 553 (1977).

A Survey of Corrosion Failure Mechanisms in Microelectronic Devices*

George L. Schnable, Robert B. Comizzoli, Werner Kern, and
Lawrence K. White

RCA Laboratories, Princeton, NJ 08540

Abstract—This paper surveys published information on corrosion processes that lead to degradation or failure of microelectronic devices. Consideration is given to both cathodic and anodic corrosion phenomena in aluminum-metallized devices and to electrolysis effects in gold metallization systems. The types of passivation layers that are used over the metallization pattern are outlined, and the adverse effects of localized defects in passivation layers are indicated. The implications of moisture and of contaminants on the reliability of devices both in hermetic and in plastic packages are reviewed. An extensive list of references to pertinent techniques for characterizing thin-film materials and for studying thin-film corrosion effects is included.

Introduction

Corrosion of the thin-film metal structures in microelectronic solid-state components, such as integrated circuits, constitutes a major cause of failure. These metal structures, which usually consist of either aluminum or gold, may comprise electrical contacts to the semiconductor, interconnect lines, and bonding pads for wire or solder connections. Except for the bonding pads, these structures are almost always coated with an inorganic glassy and/or organic polymeric protective insulator layer that

* This work was supported by Rome Air Development Center under contract No. F30602-78-C-0276 and by RCA Laboratories.

provides both mechanical and chemical protection of the device. These passivating films, if defect-free, can be very effective in preventing corrosion of underlying thin-film resistors or conductors. However, localized structural defects in the protective coatings, or the presence of unprotected metal areas such as the bonding pads, render the metal vulnerable to corrosive attack by chemicals from the ambient, such as a plastic encapsulant or the atmosphere in a defective hermetic device enclosure.

The corrosion of aluminum metal in solid-state devices is frequently accelerated in the presence of contaminants such as moisture, chloride ions, and sodium ions. Galvanic corrosion effects can be more severe because in some structures a small-area aluminum anode is in contact with a large-area gold-wire cathode. In gold-metallized devices, a possible reliability problem is electrochemical deplating and the redeposition of gold under electrically biased conditions at high relative humidity, especially at elevated temperatures. This corrosion mechanism can be accelerated by trapped moisture and contaminants in cracks and pinholes in deposited protective glass layers over gold film areas. Conventional corrosion science has been primarily concerned with the bulk properties of materials and is of limited use in understanding and explaining the thin-film processes on a microscopic scale that are of concern in solid-state components.

Available Information on Passivation, Corrosion and Related Effects

This survey considers corrosion effects in hermetically-sealed packages and in plastic-encapsulated structures. References on devices ranging in complexity from discrete transistors to complex monolithic and hybrid structures are included. The survey also includes a number of references on analytical techniques for characterizing thin-film materials and for studying thin-film corrosion effects.

A considerable amount of information is available on corrosion of thin metal films of the type used to fabricate solid-state electronic devices. An alphabetical listing of references given at the end of the paper [1-252] provides a survey of the type of information that is available in the published literature on device failure mechanisms, corrosion studies, and on pertinent surface and thin-film analysis techniques. A few very recent references which appeared after preparation of the original manuscript have also been provided [253-272].

In general, emphasis has been given to the inclusion of more recent references rather than to very extensive citations of early literature, since the reference list contains a number of recent reviews and bibliographies [184, 185, 242], including reviews on silicon device passivation [112, 113,

198, 200, 201], on corrosion [58, 59, 67, 234, 235, 255, 260], electrode potentials [18, 175, 176, 212], electrochemistry of aluminum [4, 136] and gold [197], and on surface and thin-film analytical techniques [57, 99, 100, 121, 253, 265].

A considerable amount of pertinent published information exists on the corrosion of aluminum metal in silicon devices in both hermetic and plastic packages [20, 21, 47, 65, 103, 104, 118, 120, 158, 165, 180, 186], on defects in passivation layers [15, 22, 23, 48, 109, 110, 114, 137, 201, 256], and on general corrosion phenomena [26, 67, 120, 175, 176, 177, 234, 235]. Much information is also available on methods of studying [24, 58, 59, 123, 129, 176] and preventing [2, 35, 67, 95, 101, 111, 122, 255, 260] corrosion of aluminum [4, 14, 25, 26, 27, 28, 29, 35, 49, 51, 135, 136, 138], aluminum-copper alloys [78, 156, 219, 225, 232], and gold [53, 68, 197]. Corrosion studies of aluminum and aluminum alloys have been performed on bulk samples and on thin-film samples immersed in various electrolyte solutions. A number of studies of the corrosion of thin-film metallization in test structures with patterned metal electrodes have also been made [47, 129, 193, 195, 196, 256].

Materials Used in Microelectronic Device Fabrication

Aluminum metal is the material most widely used for the metallization of silicon devices. It finds wide application in integrated circuits and small-signal transistors, as well as in many silicon power devices.

Many manufacturers use aluminum that contains a small percentage of silicon to minimize penetration at contacts to the single-crystal silicon substrate, and to reduce a tendency to form hillocks due to the recrystallization of aluminum during contact alloying. In devices fabricated by the deposition of pure aluminum on wafers, solid-state dissolution of silicon occurs at contact cuts during alloying; the lateral diffusion of silicon in the aluminum then results in an appreciable concentration of Si in the Al, even at distances over 20 μm away from the contact cuts. Some manufacturers use aluminum with a small percentage of copper to reduce susceptibility to electromigration effects. Al-Si-Cu alloys have also been employed. In some devices a thin layer of titanium has been used under the aluminum to reduce penetration at contact cuts. The conditions used for deposition of the Al metal films can exert considerable effect on the properties of the deposited films [36, 242, 243], including grain size, metallic impurity content, oxygen content, stress [124], surface roughness, and tendency to recrystallize and form hillocks during alloying and other subsequent processing steps [268].

Gold is widely used in discrete transistors, in certain integrated circuits [72, 73, 74, 75, 86, 116, 117], and as the top layer in beam-lead-type me-

tallization systems [33, 221] consisting of Ti-Pt-Au or Ti-Pd-Au. The gold layer may be deposited by vacuum evaporation or by electroplating.

Inorganic passivation layers that are used on integrated circuits include chemically vapor deposited phosphosilicates [199, 201], rf-sputtered silicon dioxide [201], and plasma deposited silicon nitride [154, 189, 215, 216, 263, 271].

Organic coatings over silicon devices that have been used include epoxy, silicone, parylene [87, 107, 108], and polyimide [79] materials. Conformal coatings are frequently used in hybrid devices [246]. Photolithographically-delineated polyimide films have been used to passivate monolithic device structures.

Plastic encapsulating materials that are used for integrated circuits include epoxy [65, 76, 93, 165, 180, 213, 261] (particularly novolac epoxy), silicone [10, 40, 44, 85], and silicone-epoxy [150, 213, 224] materials. Various additives, such as fillers [55], and flame retardants [247] in the case of some epoxy formulations, may be present in the encapsulant system.

Thin-Film Metal Corrosion as a Cause of Failure of Microelectronic Components

Corrosion effects may be classified as chemical (no bias involved), electrochemical (electrodes serve as cathode and anode when bias is applied), and galvanic (dissimilar metals). All of these corrosion effects can be factors in reliability of solid-state devices. Corrosion effects in some cases are particularly significant at localized sites such as capillaries. In some environments, the chemical corrosion of exposed metal in bonding-pad areas can be the ultimate cause for device failure. Even 25- μm aluminum bond wires have corroded under certain conditions [17].

Aluminum Metallization and its Corrosion

Corrosion of aluminum metal in integrated circuits can occur at anodic sites and/or at cathodic sites. Failures due to anodic corrosion are frequently observed in chloride-contaminated structures. Failures due to cathodic corrosion are predominant when the phosphorus content of the phosphosilicate glass is too high.

Cathodic corrosion of aluminum metal in semiconductor devices has been studied extensively [21, 47, 65, 84, 120, 165, 167, 168, 201, 239, 257].

The effects of moisture [34, 47, 118, 158, 165], of sodium ions [118, 168, 257], of chloride ions [120], and of the phosphorus content of the overlying phosphosilicate glass [47, 111, 167] have been reported.

In many cases, devices fail because of the corrosion of aluminum metal in regions near bonding pads. In such devices, localized defects in the passivation glass are the sites at which the corrosion begins. The exposed metal at the defect serves as one electrode, and an adjacent bonding pad of opposite polarity serves as the opposite electrode. Obviously, anode and cathode currents are equal. However, since the defects in the glass are small, whereas adjacent exposed metal in the bond-pad area is large, the current density at the exposed metal at the defect is high. At such high current densities, localized pH increases at the cathode can result in appreciable current efficiency for dissolution of aluminum metal.

The most commonly encountered failure mode due to chemical interaction of dielectric with metallization is metal corrosion at the glass/aluminum interface. This is brought about by the leaching of P_2O_5 from phosphosilicate glass by moisture, especially during pressure-cooker testing or life tests under electrical bias in high humidity [167]. The P_2O_5 reacts with moisture, forming phosphoric acid [165], which readily attacks the aluminum. Excessively high phosphorus concentration in a phosphosilicate layer under the Al metal, such as a flowed phosphosilicate layer in silicon-gate MOS devices [199] or an emitter glass in bipolar circuits [52], can also result in undesirable corrosion effects.

The phosphorus concentration in phosphosilicate layers used for passivation of aluminum-metallized integrated circuits is a very important factor in tensile stress and also in increasing susceptibility of exposed aluminum metal to corrosion. Accordingly, a number of analytical techniques, such as sheet resistivity of p-type silicon wafers after heat treatment [19, 39], x-ray fluorescence [81], and infra-red spectroscopy [111], have been developed specifically to determine the phosphorus content in deposited phosphosilicate films.

Both aluminum and gold films on integrated circuits are in tension at room temperature [217] and also under most usage conditions. Since aluminum metal is known to undergo stress corrosion cracking [26], tensile stress in the aluminum film may be a factor in the rate at which an aluminum line corrodes to an electrical open, or becomes reduced in cross-sectional area to the point of failure due to electromigration (current-induced mass transport) or some other mechanism.

Surface contamination [13, 152] prior to encapsulation is sometimes a factor in device reliability. Aluminum is, for example, extremely prone to electrolytic corrosion [236] in the presence of water and/or certain impurities (such as sodium ions, fluoride ions, and chloride ions), even during its deposition and processing [35, 232]. Other contaminants can

increase the electrical conductivity at the passivation layer-plastic interface, and thus increase electrolytic corrosion rates.

Gold Metallization and Its Corrosion

While the basic failure mechanism in gold metallization systems is usually a result of dendrite formation at the cathode, anodic reactions in gold-metallized devices are important because reactions at the anode are the source for gold-containing ions which are ultimately reduced to elemental gold at the cathode. The presence of contaminants such as chloride ions (or other complexing agents for gold such as bromide ions, iodide ions, or cyanide ions) [197, 212] determines whether the anode reaction results in the dissolution of gold metal to form ions rather than the evolution of oxygen or formation of an insoluble gold hydroxide; the last two processes occur in an aqueous system free of complexing agents for gold.

In a variety of devices, the formation of gold dendrites at cathodes has been reported [82, 86, 139, 141, 143, 203, 210]. Formation of a voluminous $\text{Au}(\text{OH})_3$ reaction product [68], which has sufficient conductivity to cause failure due to leakage between conductors, has recently been reported [259].

A number of authors have compared gold metallization systems to aluminum systems for use in manufacture of plastic-encapsulated integrated circuits [72, 73, 74, 75, 76, 249]. Several papers have reviewed the mechanisms leading to failures characteristic of beam-lead sealed-junction semiconductor devices [33, 70, 86, 143, 193].

Defects in Passivation Layers

Analysis of failed microelectronic devices frequently reveals corrosion due to a number of factors, one of which is defects in the passivation layer over the metal.

Structural defects in inorganic glassy passivation layers include cracks, pinholes, inadequate edge coverage of metal lines, and other localized defects [15, 22, 23, 94, 103, 111, 114, 126, 137, 201, 256, 257, 264, 270]. Cracks originate because of excessive tensile stress in the deposited film, or because of tensile stresses when the device is subjected to elevated temperatures during subsequent device processing, since the thermal coefficient of expansion of the aluminum or gold film is considerably higher than that of phosphosilicate glass or of plasma-deposited nitride. Cracks can also be caused by the recrystallization of aluminum at elevated temperatures (particularly over large metal areas), by contact

printing, and by impact during chip handling [15, 22, 109, 110, 114, 201].

Pinholes in dielectric films can be formed during the process of etching open the bonding pads. These may result from pinholes in the resist film as spun on, from excessively large hillocks in the Al film, from inadequate coverage of the resist over the edges of topological steps, from dust or defects in the photomask, or by wafer handling or contact printing.

Most chemically vapor deposited SiO_2 or phosphosilicate passivation glass films (but not plasma-deposited silicon nitride films) are in tensile stress at room temperature and at device usage conditions. When the passivation layer is strongly adherent to the underlying metal, the tensile stress is uniformly distributed. If, however, a crack forms in the dielectric, then the tensile stress in the passivation layer exerts a localized tensile force on the underlying metal at the bottom of the crack. The result could be enhanced corrosion due to stress corrosion cracking. Somewhat similarly, when an area of dielectric is removed by etching and adjacent areas are protected by photoresist, the tensile stress in the dielectric film can result in the application of a tensile force to the underlying metal at the edge of the delineated area of the passivation layer. This type of situation occurs when the passivation layer is removed from bonding-pad areas, and occurs in the circuit itself due to any defects in the photoresist film or photomask that permit localized etching of pinholes over metal lines in the circuit.

Defects in organic coatings may arise because of cracks formed due to tension in the films, inadequate coverage of topological steps or hillocks in metal, or poor adhesion to the underlying metal. Cracks in organic coatings frequently exist over areas in which there is no underlying metal, as well as over metallized regions of a silicon device.

Generally, deposited passivation layers adhere well to thermally-grown SiO_2 and to aluminum, but have limited adhesion to gold metallization. In regions where the Au metallization lines pass over topological steps in the underlying dielectric, tensile stresses in the deposited passivation film may tend to cause localized lifting of the passivation film.

Plasma-deposited silicon nitride films, which usually contain appreciable amounts [216] of dissolved as well as chemically-bonded hydrogen, are sometimes susceptible to blistering effects during life testing at elevated temperatures [112].

In laboratory studies, controlled defects of various types have been generated in the insulator layer over the metal for corrosion studies. Special photomasks have been used to prepare exact openings of different geometries by photolithographic techniques to simulate, for example, pinholes. Cracks have been formed by thermal stress treatments of the test samples in such a way that the density of cracks in a given

film/substrate combination can be related to the temperature level and rate of temperature change [111, 114]. A microhardness testing instrument has also been used to introduce indentations to various depths in glass layers over aluminum at accurately selectable specific sites, such as aluminum interconnect lines at critical locations [256]. Defects simulating mechanical impact damage encountered in integrated circuits have been formed by this technique. The extent of the damage can be controlled by the pressure applied by the diamond stylus.

Various levels of stress in deposited dielectric films of specified composition and thickness on a given substrate have been attained by performing the chemical vapor deposition process at specific temperatures and rates of deposition [111, 114]. A number of techniques are available for assessing the integrity of dielectric layers [48, 109, 110, 270].

Plastic Encapsulation

Moisture and other contaminants can enter plastic packages either along the interface between the device leads and the plastic [180], or through the bulk of the plastic [61, 165, 180, 241]. Device geometry and fabrication techniques, as well as the composition of the plastic, determine the relative importance of these two types of paths.

A number of authors have studied the relative effects of temperature, relative humidity, and applied voltage on reliability of plastic-encapsulated devices. Accelerated stress conditions [71, 134, 170, 196, 198, 200, 229, 252] such as 85°C/85% relative humidity [21, 65, 76, 104, 144, 145, 165, 180, 200, 205, 247, 252], autoclave (pressure cooker) [145, 247] tests, or controlled corrosive chemical ambients [66, 70, 193, 195] have been used to assess susceptibility of plastic-encapsulated devices to corrosion. The failure rate under these accelerated conditions, as well as under equipment usage conditions in humid ambients [85], is determined by a large number of factors, including the metal deposition process, passivation layer composition and integrity, surface contamination level, lead frame geometry [65], plastic encapsulant used, molding conditions and thermal history, as well as by the conditions of test during the accelerated testing sequence. The procedure used to cure the plastic materials used can be very important, since improperly cured adhesives and coating or encapsulation materials may contribute to increased corrosion rates. Because of relative differences in the thermal coefficients of expansion of the lead materials and the encapsulation plastics, the thermal history of the parts prior to subjecting them to a moist ambient can also be a factor in susceptibility to ingress of moisture along device leads.

Moisture can cause large changes in the surface conductivity of inor-

ganic dielectrics [6, 7, 8, 45, 46, 97, 131, 142]. Moreover, encapsulation materials are sometimes a source of ionic and polar materials, which have adverse effects on semiconductor device reliability. In several studies, failure was attributed to moisture-induced conduction at the interface between two dielectrics [32, 206].

Power dissipation in plastic-encapsulated devices during field usage can result in lower corrosion rates because the heat generated results in water desorption at device surfaces [52, 84, 153].

Hermetic Encapsulation

Although serious problems of aluminum corrosion occur in plastic encapsulated devices, especially during life testing at high humidity, even hermetic packages can be problematic. Hermetic packages may have leaks, may contain entrapped moisture or other ionizing impurities from inadequate processing or sealing, or, for chip attachment or conformal coatings, may include epoxy adhesives that release polar contaminants [230, 233, 245]. All of these materials may contribute to metal corrosion.

Moisture problems in hermetic packages are of considerable concern [5, 56, 132, 148, 149, 157, 209, 220, 231, 248], and sensors have been developed to monitor the water content inside hermetic packages [131].

Laboratory Studies of Corrosion

There are various ways in which electrode reactions can be studied [163, 177], including techniques in which the perturbed variable is the potential, the current, or the charge. In potentiostatic methods, the electrode potential is displaced from the reversible value, and current, charging, or electrical impedance is measured. In galvanostatic methods, a continuous current is passed, and potential measurements are made. Measurements can be made on a steady-state or a transient basis. In some cases ac is superimposed on a dc potential. In any case, an operational amplifier with a very high input impedance (field-effect-transistor input) is used to drive a meter or a recorder.

In corrosion studies, it is desirable to perform some measurements under conditions of high irreversibility of the electrode process (with the polarization potential exceeding 0.05V). In such cases the Tafel equation applies. Extrapolation of the straight section of the Tafel line can then be used to determine the exchange current. The series resistance of the structures on silicon test devices is high, and thus high-frequency measurements of the type frequently used for bulk metal samples cannot be used.

Corrosion or oxidation studies of thin-film metals have utilized a number of specialized techniques, such as use of ellipsometry, quartz crystal microbalance [128, 129], measurement of resistivity changes [47, 129, 213], and measurements of corrosion currents in structures consisting of parallel, closely-spaced conductor lines [21, 256, 257]. The measurement of corrosion current dependence on relative humidity is complicated by long-term hysteresis effects [192, 196].

In structures in which electrolysis processes are occurring, localized changes in the pH [31, 92, 147, 187, 266] may be a very important factor in determining electrode processes and in determining whether corrosion reactions proceed at a significant rate.

In studies of electronic device stability in hostile environments, various techniques have been used to apply contaminants to solid-state devices. One of the simplest is to dip the device into a very dilute solution, such as an aqueous sodium chloride solution for Na^+ and Cl^- ions or an aqueous sodium bicarbonate solution for Na^+ ions. This technique, in addition to simplicity, has the advantage of simulating effects that would occur in device processing when liquids containing contaminants are used for etching, resist stripping, or other operations. Where cracks, pinholes, tunnels, blisters, or other defects occur in passivation layers, processing liquids penetrate these defect sites by capillary action and are difficult to remove in subsequent rinsing operations. The net result is that the concentration of contaminant is not uniform over the device surface, but is substantially higher at defect sites. Since the surfaces of test devices that have been exposed to room air are invariably hydrophobic, the addition of a small amount of a water-soluble nonionic surfactant or suitable polar solvent is used to achieve uniform wetting and provide a uniform concentration of contaminants on the defect-free surfaces [256, 257].

Evaporation techniques have been used to apply a known concentration of contaminants, such as NaCl , to device surfaces. The amount deposited per unit area can be closely controlled.

In some corrosion studies, the contaminant has been applied as one of the constituents in the moist atmosphere to which the devices were subjected. For example, atmospheres containing 1 ppm of chlorine gas have been used in studies. Other gaseous contaminants [1] have included HCl , HBr , H_2S , SO_2 and NH_3 . Other studies have subjected structures to salt solution treatments or to salt sprays.

In the absence of halide contamination, Al-metallized devices in which moisture is available for corrosion typically fail because of cathodic corrosion. Alkali contamination of the surface of the passivation layer is believed to be a factor in cathodic corrosion, permitting the pH at the cathode to locally increase to values in excess of a pH of 8. The pH of the

electrolyte is a very important factor in corrosion of both gold and aluminum [266]. Examination of Pourbaix (potential-pH) diagrams [175, 176, 177, 222] can lead to an increased understanding of the importance of pH effects.

References:

- [1] W. H. Abbott, "Air Pollution and Failure Mechanisms of Electronic Interfaces," *Electrochem. Soc. Ext. Abstr.*, 78-2, p. 657 (Oct. 1978).
- [2] M. F. Abd Rabbo, J. A. Richardson, and G. C. Wood, "A Study of the Effects of Inhibitive and Aggressive Ions on Oxide-Coated Aluminum Using Secondary Ion Mass Spectrometry," *Corrosion Sci.*, 16, p. 677 (1976).
- [3] R. Alkire and D. Siitari, "The Location of Cathodic Reaction During Localized Corrosion," *J. Electrochem. Soc.*, 126, p. 15 (1979).
- [4] R. S. Alwitt, "The Aluminum-Water System," in J. W. Diggle and A. K. Vijh, eds., *Oxides and Oxide Films*, Vol. 4, Marcel Dekker, Inc., New York, 1976, pp. 169-254.
- [5] L. K. Anderson, "Some Package Reliability Implications of Current Trends in Large Scale Silicon Integrated Circuits," *16th Ann. Proc. Reliab. Phys.*, p. 121 (1978).
- [6] S. Anderson and D. D. Kempton, "Some Phenomena Related to the Hydrophobicity of Silicate Glasses and Adsorbed Oxygen," *J. Amer. Ceram. Soc.*, 43, p. 484 (1960).
- [7] P. A. Arutyunov and K. A. Keidzhyan, "The Use of Test Structures in Assessing the Quality and Reliability of LSI Circuits," *Sov. Microelectron.*, 6 (6), p. 390 (Nov./Dec. 1977).
- [8] Y. Awakuni and J. H. Calderwood, "Water Vapour Adsorption and Surface Conductivity in Solids," *J. Phys. D: Appl. Phys.*, 5, p. 1035 (1972).
- [9] C. M. Bailey, "Effects of Burn-in and Temperature Cycling on the Corrosion Resistance of Plastic Encapsulated Integrated Circuits," *15th Ann. Proc. Reliab. Phys.*, p. 120 (1977).
- [10] C. M. Bailey, Jr., "Reliability of Plastic Encapsulated Integrated Circuits," *Proc. Symp. Plastic Encapsulated/Polymer Sealed Semiconductor Devices for Army Equipment* (US Army ER-ADCOM, Fort Monmouth, N.J), p. 97 (1978).
- [11] C. M. Bailey, Jr., "Reliability of Plastic Encapsulated Integrated Circuits," *Proc. Tech. Program Int. Microelectron. Conf.* (Anaheim, CA/New York, NY), p. 246 (1978).

- [12] C. M. Bailey, "Plastic Encapsulated ICs: A Reliability Evaluation," *Electron. Pkg. Prod.*, **18** (6), p. 129 (June 1978).
- [13] M. K. Balazs, "The Identification of Contaminants and Their Sources in the Processing of Semiconductor Integrated Circuits," *Proc. ATFA-77*, pp. 42-47 (Sept. 1977).
- [14] C. B. Barger and R. B. Givens, "Localized Corrosion of Aluminum: Blister Formation as a Precursor of Pitting," *J. Electrochem. Soc.*, **124**, p. 1845 (Dec. 1977).
- [15] J. J. Bart, "Analysis of Deposited Glass Layer Defects," *13th Ann. Proc. Reliab. Phys.*, p. 128 (1975).
- [16] J. J. Bart, "Scanning Electron Microscopy for Complex Microcircuit Analysis," *16th Ann. Proc. Reliab. Phys.*, p. 108 (1978).
- [17] J. J. Bart and E. A. Doyle, Jr., "An Avionic System Long-Term Microcircuit Corrosion Problem," *GOMAC (Government Microcircuits Applications Conference) Proc.*, pp. 80-83 (Nov. 1976).
- [18] R. G. Bates, *Determination of pH—Theory and Practice*, 2nd ed., John Wiley & Sons, Inc., New York, 1973.
- [19] C. Beck, "Phosphorus Concentration in Low Temperature Vapor Deposited Oxide," *Solid State Technol.*, **20**(12), p. 58 (Dec. 1977).
- [20] H. M. Berg and W. M. Paulson, "The Factors Affecting Aluminum Corrosion in Plastic Semiconductor Packages," *Electrochem. Soc. Ext. Abstr.*, **77-1**, p. 33 (May 1977).
- [21] H. M. Berg and W. M. Paulson, "Aluminum Corrosion in Plastic-Encapsulated Devices," *Proc. Symp. Plastic Encapsulated/Polymer Sealed Semiconductor Devices for Army Equipment (US Army ERADCOM, Fort Monmouth, NJ)*, p. 197 (1978).
- [22] R. G. Berger, K. M. Gardiner, and N. A. Sinclair, "Manufacturing Handling and Semiconductor Reliability," *Proc. Tech. Program Int. Microelectron. Conf. (West/East)*, p. 173 (1976).
- [23] R. G. Berger, Jr., and A. J. Gregoritsch, "Induced Passivation Defect Study," *13th Ann. Proc. Reliab. Phys.*, p. 121 (1975).
- [24] U. Bertocci and R. W. Shideler, "Detection and Analysis of Electrochemical Noise for Corrosion Studies," *Electrochem. Soc. Ext. Abstr.*, **78-2**, p. 336 (Oct. 1978).
- [25] A. Berzins, R. T. Lawson, and K. J. Mirams, "Aluminum Corrosion Studies III: Chloride Adsorption Isotherms on Corroding Aluminum," *Austral. J. Chem.*, **30**, p. 1891 (1977).
- [26] W. W. Binger, E. H. Hollingsworth, and D. O. Sprowls, "Resistance to Corrosion and Stress Corrosion," in *Aluminum*, Vol. 1, K. R. Van Horn, ed., *Properties, Physical Metallurgy and Phase Diagrams*, American Society for Metals, Metals Park, OH, 1967, pp.

209-254.

- [27] F. D. Bogar and R. T. Foley, "The Influence of Chloride Ion on the Pitting of Aluminum," *J. Electrochem. Soc.*, **119**, p. 462 (April 1972).
- [28] H. Bohni and H. H. Uhlig, "Environmental Factors Affecting the Critical Pitting Potential of Aluminum," *J. Electrochem. Soc.*, **116**, p. 906 (July 1969).
- [29] A. P. Bond, G. F. Bolling, H. A. Domian, and H. Biloni, "Microsegregation and Tendency for Pitting Corrosion in High Purity Aluminum," *J. Electrochem. Soc.*, **113**, p. 773 (Aug. 1966).
- [30] G. W. Brassell and D. R. Fancher, "Electrically Insulative Adhesives for Hybrid Microelectronic Fabrication," *IEEE Trans. Components Hybr. Mfg. Technol.*, **CHMT-1**, p. 192 (June 1978).
- [31] B. F. Brown, C. T. Fujii, and E. P. Dahlberg, "Methods for Studying the Solution Chemistry Within Stress Corrosion Cracks," *J. Electrochem. Soc.*, **116**, p. 218 (Feb. 1969).
- [32] G. A. Brown, K. Lovelace, and C. Hutchins, "A Process Control Test for Lateral Charge Spreading Susceptibility," *11th Ann. Proc. Reliab. Phys.*, p. 203 (1973).
- [33] U. C. Brown and J. R. Sim, "Failure Mechanisms in Beam Lead Semiconductors," *Proc. 27th Electronic Comp. Conf.*, p. 188 (May 1977); *IEEE Trans. Parts Hybr. Pkg.*, **PHP-13**, p. 225 (Sept. 1977).
- [34] G. F. Cerofolini and C. Rovere, "The Role of Water Vapour in the Corrosion of Microelectronic Circuits," *Thin Solid Films*, **47**, p. 83 (1977).
- [35] C. C. Chang, D. B. Fraser, M. J. Grieco, T. T. Sheng, S. E. Haszko, R. E. Kerwin, R. B. Marcus, and A. K. Sinha, "Aluminum Oxidation in Water," *J. Electrochem. Soc.*, **125**, p. 787 (May 1978).
- [36] C. C. Chang, T. T. Sheng, D. V. Speeney, and D. B. Fraser, "Si Depth Profile and Contaminants in Si-Doped Al Film," *J. Appl. Phys.*, **47**, p. 1790 (May 1976).
- [37] N. J. Chaplin and A. J. Masessa, "Reliability of Epoxy and Silicone Molded Tape-Carrier Silicon Integrated Circuits With Various Chip-Protective Coatings," *16th Ann. Proc. Reliab. Phys.*, p. 187 (1978).
- [38] G. T. Cheney et al., "Special Issue on Device Reliability," *IEEE Trans. Electron Devices*, **ED-26**, p. 1 (Jan. 1979).
- [39] K. Chow and L. G. Garrison, "Phosphorus Concentration of Chemical Vapor Deposited Phosphosilicate Glass," *J. Electrochem. Soc.*, **124**, p. 1133 (July 1977).
- [40] A. Christou, "Assessment of Silicone Encapsulants for Hybrid

- Integrated Circuits (HIC)," *IEEE Trans. Parts Hybr. Pkg.*, **PHP-13**, p. 298 (Sept. 1977).
- [41] A. Christou, "Reliability Aspects of Moisture and Ionic Contamination Diffusion Through Hybrid Encapsulants," *Proc. Tech. Progr. Int. Microelectron. Conf.* (Anaheim, CA/New York, NY), p. 237 (1978).
- [42] A. Christou, "Moisture Diffusion Through Hybrid-Circuit Encapsulants," *Electronic Pkg. Prod.*, **19** (4), p. 91 (April 1979).
- [43] A. Christou, J. R. Griffith and W. Wilkins, "Reliability Testing of Fluorinated Polymeric Materials (FNP) for Hybrid Encapsulation," *16th Ann. Proc. Reliab. Phys.*, p. 194 (1978).
- [44] A. Christou and W. Wilkins, "Assessment of Silicone Encapsulation Materials: Screening Techniques," *15th Ann. Proc. Reliab. Phys.*, p. 112 (1977).
- [45] R. B. Comizzoli, "Bulk and Surface Conduction in CVD SiO₂ and PSG Passivation Layers," *J. Electrochem. Soc.*, **123**, p. 386 (March 1976).
- [46] R. B. Comizzoli, "Surface and Bulk Electrical Conduction in Low-Deposition-Temperature Si₃N₄ and Al₂O₃ Films for Silicon Devices," *RCA Rev.*, **37**, p. 473 (Dec. 1976).
- [47] R. B. Comizzoli, "Aluminum Corrosion in the Presence of Phosphosilicate Glass and Moisture," *RCA Rev.*, **37**, p. 483 (Dec. 1976).
- [48] R. B. Comizzoli, "Nondestructive, Reverse Decoration of Defects in IC Passivation Overcoats," *J. Electrochem. Soc.*, **124**, p. 1087 (July 1977).
- [49] S. M. de DeMicheli, "The Electrochemical Study of Pitting Corrosion of Aluminum in Chloride Solutions," *Corrosion Sci.*, **18**, p. 605 (1978).
- [50] N. F. De Rooij, R. J. S. Sieberdink, and R. M. Tromp, "An Investigation of the Hydration Properties of Chemically Vapour-Deposited Silicon Dioxide Films By Means of Ellipsometry," *Thin Solid Films*, **47**, p. 211 (1977).
- [51] G. A. DiBari and H. J. Read, "Electrochemical Behavior of High Purity Aluminum in Chloride Containing Solutions," *Corrosion-NACE*, **27**, p. 483 (Nov. 1971).
- [52] H. K. Dicken, "Cost and Reliability Trends of Plastic Encapsulated Integrated Circuits," *Proc. Symp. Plastic Encapsulated/Polymer Sealed Semiconductor Devices for Army Equipment* (US Army ERADCOM, Fort Monmouth, NJ), p. 130 (1978).
- [53] B. S. Duncan and R. P. Frankenthal, "Effect of pH on the Rate of Corrosion of Gold in Acid Sulfate Solutions," *J. Electrochem. Soc.*, **126**, p. 95 (Jan. 1979).

- [54] G. H. Ebel, "Failure Analysis Techniques Applied in Resolving Hybrid Microcircuit Reliability Problems," *15th Ann. Proc. Reliab. Phys.*, p. 70 (1977).
- [55] M. Edwards, "Effects of Fillers on Electrical Performance of Semiconductor Grade Liquid Epoxy Systems," *Proc. Tech. Program Int. Microelectron. Conf.* (Anaheim, CA/New York, NY), p. 232 (1978).
- [56] A. Ertel and H. J. Perlstein, "The Hermeticity Hoax," *Proc. 1978 Ann. Reliab. Maint. Symp.*, p. 448 (Jan. 1978).
- [57] C. A. Evans, Jr., and R. J. Blattner, "Modern Experimental Methods for Surface and Thin-Film Chemical Analysis," *Ann. Rev. Mater. Sci.*, 8, p. 181 (1978).
- [58] U. R. Evans, *The Corrosion and Oxidation of Metals*, Edward Arnold Publishers, Ltd., London, England (1960).
- [59] U. R. Evans, *The Corrosion and Oxidation of Metals*, 2nd Suppl. Vol., Edward Arnold Publishers, Ltd., London, England (1976).
- [60] D. R. Fancher and R. G. Horner, "Hybrid Package Hermeticity and Moisture Level Monitoring," *Proc. 1978 Int. Microelectron. Symp.*, p. 114, ISHM (Sept. 1978).
- [61] L. G. Feinstein, "Failure Mechanism in Molded Microelectronic Packages," *NEPCON/West—NEPCON/East*, 1979 (preprint); *Semiconductor International*, 2, No. 7, p. 51 (Sept. 1979).
- [62] A. V. Ferris-Prabhu, "Contaminant Induced Aging in Integrated Circuit Packages," *Proc. 28th Electronic Comp. Conf.*, p. 1 (Apr. 1978).
- [63] J. A. Ferro, "An Accelerated Method for Effective Process Control of Plastic Encapsulated Nichrome PROMS," *15th Ann. Proc. Reliab. Phys.*, p. 125 (1977).
- [64] P. J. Ficalora and D. Y. Shih, "The Effect of Hydrogen on Rate of Formation of Intermetallics in the Cu-Sn, Ag-Sn, and Ni-Sn Systems," *17th Ann. Proc. Reliab. Phys.*, p. 87 (1979).
- [65] M. J. Fox, "A Comparison of the Performance of Plastic and Ceramic Encapsulations Based on Evaluation of CMOS Integrated Circuits," *Microelectron. Reliab.*, 16(3), p. 251 (1977).
- [66] J. P. Franey, "Trace Gas Flow Control Using Polymer Permeation," *Electrochem. Soc. Ext. Abstr.*, 78(2), p. 659 (Oct. 1978).
- [67] R. P. Frankenthal, "Corrosion in Electronic Applications," in R. Sard, H. Leidheiser, Jr., and F. Ogburn, eds., *Properties of Electrodeposits—Their Measurement and Significance*, The Electrochemical Society, Princeton, NJ, 1975, pp. 142-169.
- [68] R. P. Frankenthal and W. H. Becker, "Corrosion Failure Mechanisms for Gold Metallizations," *Electrochem. Soc. Ext. Abstr.*, 78(2), p. 661 (Oct. 1978).

- [69] R. P. Frankenthal and D. E. Thompson, "Electrochemical Behavior of Electronic Materials," pp. 90-92 in R. Baboian, ed., *Electrochemical Techniques for Corrosion*, Natl. Assoc. Corrosion Engineers, 1977.
- [70] F. N. Fuss and C. T. Hartwig, "Corrosion of Solder-Coated Ti-Pd-Au Thin-Film Conductors in a Moist Chlorine Atmosphere," *Proc. 27th Electronic Components Conf.*, p. 72 (May 1977).
- [71] T. R. Gagnier and E. M. Kimball, "Storage Reliability Verification Testing Program for Plastic Encapsulated Integrated Circuits," *Proc. Symp. Plastic Encapsulated/Polymer Sealed Semiconductor Devices for Army Equipment* (US Army ERADCOM, Fort Monmouth, NJ), p. 108 (1978).
- [72] L. J. Gallace, "Reliable Plastic-Packaged IC's and Power Transistors," *Proc. Symp. Plastic Encapsulated/Polymer Sealed Semiconductor Devices for Army Equipment* (US Army ERADCOM, Fort Monmouth, NJ), p. 168 (1978).
- [73] L. J. Gallace, L. A. Jacobus, E. J. Pffner, and C. A. West, "Accelerated Reliability Evaluation of Trimetal Integrated Circuit Chips in Plastic Packages," *IEEE Trans. Components Hybr. Mfg. Technol.*, CHMT-2, p. 172 (June 1979).
- [74] L. J. Gallace, H. J. Khajezadeh, and A. S. Rose, "Accelerated Reliability Evaluation of Trimetal Integrated Circuit Chips in Packages," *16th Ann. Proc. Reliab. Phys.*, p. 224 (1978).
- [75] L. J. Gallace, H. Khajezadeh, and A. S. Rose, "High-Reliability Low-Cost Integrated Circuit Plastic Packages," *GOMAC-78*, Monterey, CA, Nov. 14, 1978, p. 267.
- [76] L. J. Gallace, H. L. Pujol, and G. L. Schnable, "CMOS Reliability," *Proc. 27th Electronic Components Conf.*, p. 496 (May 1977); *Microelectron. Reliab.*, 17(2), p. 287 (1978).
- [77] J. R. Galvele, "Transport Processes and the Mechanism of Pitting of Metals," *J. Electrochem. Soc.*, 123, p. 464 (April 1976).
- [78] J. R. Galvele and S. M. de DeMicheli, "Mechanism of Intergranular Corrosion of Al-Cu Alloys," *Corrosion Sci.*, 10, p. 795 (1970).
- [79] A. J. Gregoritsch, "Polyimide Passivation Reliability Study," *14th Ann. Proc. Reliab. Phys.*, p. 228 (1976).
- [80] A. J. Gregoritsch, "Double Level Metallurgy Defect Study," *16th Ann. Proc. Reliab. Phys.*, p. 28 (1978).
- [81] C. Grilletto, "An X-Ray Fluorescence Technique for the Rapid Determination of Phosphorus in PSG Film," *Solid State Technol.*, 20 (2), p. 27 (Feb. 1977).
- [82] F. J. Grunthamer, T. W. Griswold, and P. J. Clendening, "Migratory Gold Resistive Shorts: Chemical Aspects of a Failure Mech-

- anism," *13th Ann. Proc. Reliab. Phys.*, p. 99 (1975).
- [83] E. B. Hakim, "U.S. Army Panama Field Test of Plastic Encapsulated Devices," *Microelectron. Reliab.*, 17(3), p. 387 (1978).
- [84] E. B. Hakim and B. Reich, eds., *Proc. Symp. Plastic Encapsulated/Polymer Sealed Semiconductor Devices for Army Equipment*, US Army ERADCOM, Fort Monmouth, NJ (1978).
- [85] E. B. Hakim and H. A. Schauer, "Panama Field Test Results of Plastic Encapsulated Devices," *Proc. Symp. Plastic Encapsulated/Polymer Sealed Semiconductor Devices for Army Equipment* (US Army ERADCOM, Fort Monmouth, NJ), p. 67 (1978).
- [86] E. B. Hakim and J. R. Shappirio, "Failure Mechanisms in Gold Metallized Sealed Junction Devices," *Solid State Technol.*, 18(4), p. 66 (April 1975).
- [87] L. D. Hanley and J. H. Martin, "A Test of Parylene as a Protective System for Microcircuitry," *13th Ann. Proc. Reliab. Phys.*, p. 53 (1975).
- [88] M. L. Harding, "Non-Hermetic Packaging for Commercial Hybrid Microcircuits," *Proc. Symp. Plastic Encapsulated/Polymer Sealed Semiconductor Devices for Army Equipment* (US Army ERADCOM, Fort Monmouth, NJ), p. 225 (1978).
- [89] J. J. Harrahy, "Assessment of Plastic, Commercial Grade IC Failure Rates Achieved in Field Operation," *Proc. Symp. Plastic Encapsulated/Polymer Sealed Semiconductor Devices for Army Equipment* (US Army ERADCOM, Fort Monmouth, NJ), p. 17 (1978).
- [90] R. W. Harriot, "Epoxy Testing for Hybrid Applications . . . How Reliable Is It?," *Proc. 1978 Int. Microelectron. Symp.*, p. 61, ISHM (Sept. 1978).
- [91] B. Harris and P. B. P. Phipps, "The Role of Adsorbed Water in Atmospheric Corrosion," *Electrochem. Soc. Ext. Abstr.*, 79(2), p. 626 (Oct. 1979).
- [92] L. B. Harris, "Change in pH Near the Cathode During the Electrodeposition of a Bivalent Metal. Analysis," *J. Electrochem. Soc.*, 120, p. 1034 (Aug. 1973).
- [93] J. C. Harrison, "Control of the Encapsulation Material as an Aid to Long Term Reliability in Plastic Encapsulated Semiconductor Components (PEDs)," *Microelectron. Reliab.*, 16(3), p. 233 (1977).
- [94] K. Heid, "Nichrome Passivation Coatings—Help or Hindrance?," *Proc. 27th Electronic Components Conf.*, p. 68 (May 1977).
- [95] T. P. Hoar, "On Corrosion Resistant Materials," *J. Electrochem. Soc.*, 117, p. 17C (Jan. 1970).

- [96] C. E. Holland, Jr., and C. A. West, "Navy High Reliability/Low Cost Integrated Circuit Program," *Proc. Symp. Plastic Encapsulated/Polymer Sealed Semiconductor Devices for Army Equipment* (US Army ERADCOM, Fort Monmouth, NJ), p. 120 (1978).
- [97] L. Holland, *The Properties of Glass Surfaces*, John Wiley & Sons, Inc., New York, 1964, p. 228.
- [98] P. H. Holloway, "Analysis of Corrosion Products with Surface and Near-Surface Sensitive Analytical Techniques," *Electrochem. Soc. Ext. Abstr.*, 78(2), p. 670 (Oct. 1978).
- [99] R. E. Honig, "Materials Characterization at RCA Laboratories," *Solid State Technol.*, 13(3), p. 59 (March 1970).
- [100] R. E. Honig, "Characterization of Materials at RCA Laboratories," *RCA Engineer*, 20(6), p. 62 (Apr./May 1975).
- [101] Von L. Horner and K. Meisel, "Corrosion Inhibitors 23: (1) Does There Exist a Structure-Efficiency Relation in the Organic Inhibitors of Aluminum Corrosion?," *Werkstoffe u. Korrosion*, 29, p. 654 (1978).
- [102] A. T. Hubbard and E. C. Anson, "The Theory and Practice of Electrochemistry with Thin Layer Cells," in Vol. 4 of J. Bard, ed., *Encyclopedia of Electrochemistry of the Elements*, Marcel Dekker, Inc., New York, 1975, pp. 129-214 (see p. 135).
- [103] H. Inayoshi, K. Nishi, S. Okikawa, and Y. Wakashima, "Moisture-Induced Aluminum Corrosion and Stress on the Chip in Plastic-Encapsulated LSIs," *17th Ann. Proc. Reliab. Phys.*, p. 113 (1979).
- [104] S. Iwata, A. Ishizaka, and H. Yamamoto, "Corrosion Test for Metallization for Plastic-Encapsulated IC's," *J. Electrochem. Soc.*, 126, p. 110 (Jan. 1979).
- [105] R. O. Jones, "Developments Likely to Improve the Reliability of Plastic Encapsulated Devices," *Microelectron. Reliab.*, 17, p. 273 (1978).
- [106] C. E. Jowett, "Failure Mechanisms and Analysis Procedures for Semiconductor Devices," *Microelectron. J.*, 9(3), p. 5 (Jan./Feb. 1979).
- [107] V. S. Kale, "Interaction of Parylene and Moisture in Hermetically Sealed Hybrids," *Proc. 28th Electronic Components Conf.*, p. 344 (April 1978).
- [108] V. S. Kale and T. J. Riley, "A Production Parylene Coating Process for Hybrid Microcircuits," *Proc. 27th Electronic Components Conf.*, p. 245 (May 1977); *IEEE Trans. Parts Hybr. Pkg.*, PHP-13, p. 273 (Sept. 1977).
- [109] W. Kern, "Characterization of Localized Structural Defects in

- Dielectric Films," *RCA Rev.*, **34**, p. 655 (Dec. 1973).
- [110] W. Kern and R. B. Comizzoli, "Techniques for Measuring the Integrity of Passivation Overcoats on Integrated Circuits," NBS Spec. Publ. 400-31, U.S. Dept. of Commerce, March 1977.
- [111] W. Kern, R. B. Comizzoli, A. W. Fisher and G. L. Schnable, "Improved CVD Techniques for Depositing Passivation Layers on ICs," Technical Report AFML-TR-75-160, Final Report for the period April 1974-June 1975, Air Force Materials Laboratory (LTFE), Wright-Patterson AFB, Ohio 45433, Oct. 1975.
- [112] W. Kern and R. S. Rosler, "Advances in Deposition Processes for Passivation Films," *J. Vac. Sci. Technol.*, **14**, p. 1082 (Sept.-Oct. 1977).
- [113] W. Kern and G. L. Schnable, "Low-Pressure Chemical Vapor Deposition for Very Large-Scale Integration Processing—A Review," *IEEE Trans. Electron Devices*, **ED-26**, p. 647 (April 1979).
- [114] W. Kern, G. L. Schnable, and A. W. Fisher, "CVD Glass Films for Passivation of Silicon Devices: Preparation, Composition and Stress Properties," *RCA Rev.*, **37**, p. 3 (March 1976).
- [115] W. Kern, J. L. Vossen, and G. L. Schnable, "Improved Reliability of Electron Devices Through Optimized Coverage of Surface Topography," *11th Ann. Proc. Reliab. Phys.*, p. 214 (1973).
- [116] H. Khajezadeh and A. S. Rose, "Reliability Evaluation of Hermetic Integrated Circuit Chips in Plastic Packages," *13th Ann. Proc. Reliab. Phys.*, p. 87 (1975).
- [117] H. Khajezadeh and A. S. Rose, "Reliability Evaluation of Trimetal Integrated Circuits in Plastic Packages," *15th Ann. Proc. Reliab. Phys.*, p. 244 (1977).
- [118] H. Koelmans, "Metallization Corrosion in Silicon Devices by Moisture-Induced Electrolysis," *12th Ann. Proc. Reliab. Phys.*, p. 168 (1974).
- [119] H. Koelmans and H. J. Kretschman, "Water Droplet Formation During the Life Testing of IC's in a Humid Ambient," *J. Electrochem. Soc.*, **125**, p. 1715 (Oct. 1978).
- [120] S. C. Kolesar, "Principles of Corrosion," *12th Ann. Proc. Reliab. Phys.*, p. 155 (1974).
- [121] R. Kossowsky, "Analytical Techniques for Electronic Materials—A Comparative Evaluation," *16th Ann. Proc. Reliab. Phys.*, p. 112 (1978).
- [122] M. Koudelkva, J. Augustynski, and H. Berthou, "On the Composition of the Passivating Films Formed on Aluminum in Chromate Solutions," *J. Electrochem. Soc.*, **124**, p. 1165 (Aug. 1977).

- [123] J. Kruger, "New Approaches to the Study of Localized Corrosion," in R. Baboian, ed., *Electrochemical Techniques for Corrosion*, Natl. Assoc. Corrosion Engineers, 1977, pp. 35-41.
- [124] A. Kubovy and M. Janda, "The Influence of Residual Gas Pressure on the Stress in Aluminum Films," *Thin Solid Films*, **42**, p. 169 (1977).
- [125] D. J. Lando, J. P. Mitchell, and T. L. Welsher, "Conductive Anodic Filaments in Reinforced Polymeric Dielectrics: Formation and Prevention," *17th Ann. Proc. Reliab. Phys.*, p. 51 (1979).
- [126] G. Landrum, "Moisture Related Failures in Epoxy Packages," *Semiconductor Int.*, **2**(5), p. 68 (June 1979).
- [127] M. H. Lee, J. M. Eldridge, G. Scherer, W.-Y. Lee, and C. H. Ting, "Electrochemical Studies of Processing Effects on Permalloy Thin Film Corrosion," *Electrochem. Soc. Ext. Abstr.*, **78**(2), p. 666 (Oct. 1978).
- [128] W.-Y. Lee and J. Eldridge, "Oxidation Studies of Permalloy Films by Quartz Crystal Microbalance, AES, and XPS," *J. Electrochem. Soc.*, **124**, p. 1747 (Nov. 1977).
- [129] W.-Y. Lee, H. C. Siegmann, and J. M. Eldridge, "A Comparison of the Mass and Resistance Change Techniques for Investigating Thin Film Corrosion Kinetics," *J. Electrochem. Soc.*, **124**, p. 1744 (Nov. 1977).
- [130] B. R. Livesay, "The Reliability of Electronic Devices in Storage Environments," *Solid State Technol.*, **21**(10), p. 63 (Oct. 1978).
- [131] R. K. Lowry, L. A. Miller, A. W. Jonas, and J. M. Bird, "Characteristics of a Surface Conductivity Moisture Monitor for Hermetic Integrated Circuit Packages," *17th Ann. Proc. Reliab. Phys.*, p. 97 (1979).
- [132] R. K. Lowry, C. J. Van Leeuwen, B. L. Kennimer, and L. A. Miller, "A Reliable Dry Ceramic Dual In-Line Package," *16th Ann. Proc. Reliab. Phys.*, p. 207 (1978).
- [133] N. Lycoudes, "Pressure Temperature Humidity Bias Method and System For Corrosion Studies of Plastic Encapsulated Integrated Circuits," *Proc. Inst. Environmental Sci.*, **23**, p. 213 (1977).
- [134] N. Lycoudes, "The Reliability of Plastic Microcircuits in Moist Environments," *Solid State Technol.*, **21**(10), p. 53 (Oct. 1978).
- [135] I. A. Maier and J. R. Galvele, "Localized Corrosion on Slip Steps of Aluminum Straining," *J. Electrochem. Soc.*, **125**, p. 1594 (Oct. 1978).
- [136] P. A. Malachuk, "Aluminum," in Vol. 6 of A. J. Bard, ed., *Encyclopedia of Electrochemistry of the Elements*, Marcel Dekker, Inc., New York, 1976, pp. 63-165.
- [137] J. E. Mann, W. E. Anderson, T. J. Raab, and J. S. Rollins, "Reli-

- ability of Deposited Glass," Technical Report RADC-TR-76-82, Final Report for the period March 1974–April 1975, for Rome Air Development Center by Rockwell International, March 1976.
- [138] F. Mansfield and J. V. Kenkel, "Laboratory Studies of Galvanic Corrosion of Aluminum Alloys," in *Galvanic and Pitting Corrosion—Field and Laboratory Studies*, ASTM STP 576, American Society for Testing and Materials, Phila., PA (1976), pp. 20–47.
- [139] A. D. Marderosian, "The Electrochemical Migration of Metals," *Proc. 1978 Int. Microelectron. Conf.*, p. 134, ISHM (Sept. 1978).
- [140] A. D. Marderosian and V. Gionet, "Water Vapor Penetration Rate into Enclosures with Known Air Leak Rates," *16th Ann. Proc. Reliab. Phys.*, p. 179 (1978).
- [141] A. D. Marderosian and C. Murphy, "Humidity Threshold Variations for Dendrite Growth on Hybrid Substrates," *15th Ann. Proc. Reliab. Physics*, p. 92 (1977).
- [142] A. D. Martin and K. J. McLean, "The Effect of Adsorbed Gases on the Surface Conductivity of Quartz," *J. Appl. Phys.*, 48, p. 2950 (July 1977).
- [143] J. J. Mazenko, "The Effect of MIL-STD-883 Screening and Stress Upon Beam Lead IC's," *Proc. 25th Electronic Components Conf.*, p. 65 (May 1975).
- [144] J. J. Mazenko, "How Reliable Are Plastic Encapsulated/Polymer Sealed Hybrids?," *Proc. Symp. Plastic Encapsulated/Polymer Sealed Semiconductor Devices for Army Equipment* (US Army ERADCOM, Fort Monmouth, NJ), p. 213 (1978).
- [145] W. J. McGarvey, "Autoclave vs. 85°C/85% R. H. Testing—A Comparison," *17th Ann. Proc. Reliab. Phys.*, p. 136 (1979).
- [146] P. S. McLeod and J. L. Hughes, "Effects of Sputter Etching and Process Techniques on the Properties of Sputtered Aluminum Films," *J. Vac. Sci. Technol.*, 16, p. 369 (Mar./Apr. 1979).
- [147] P. H. Melville, "Variation of Potential in Stress Corrosion Cracks," *Brit. Corrosion J.*, 14(1), p. 15 (1979).
- [148] C. G. Messenger, "Improved Reliability Through Dry and Hermetic Microcircuit Packaging," *Proc. 27th Electronic Components Conf.*, p. 172 (1977).
- [149] C. G. Messenger, "Moisture Syndromes in Microcircuit Packaging," *Proc. 1978 Int. Microelectron. Symp.*, p. 142, ISHM (1978).
- [150] K. W. Michael and R. C. Antonen, "The Properties of Silicone-Epoxy Electronic Grade Molding Compound," *Proc. Tech. Program Int. Microelectron. Conf.* (Anaheim, CA/New York, NY), p. 246 (1978).

- [151] G. Milazzo and S. Caroli, *Tables of Standard Electrode Potentials*, John Wiley & Sons, Ltd., Chichester, England (1978).
- [152] K. L. Mittal, Ed., *Surface Contamination—Genesis, Detection, and Control*, Vol. 1 and 2. Plenum Publishing Corp., N.Y., N.Y. (1979).
- [153] R. Y. Moss, "Comparative Field Warranty Experience with Unscreened Plastic and Hermetic Semiconductors in Electronic Instruments," *Proc. Symp. Plastic Encapsulated/Polymer Sealed Semiconductor Devices for Army Equipment* (US Army ER-ADCOM, Fort Monmouth, NJ), p. 33 (1978).
- [154] K. Mukai, A. Hiraiwa, S. Muramatsu, S. Takahashi, and S. Harada, "Mechanical Properties of Plasma-CVD Silicon Nitride Film," *Electrochem. Soc. Ext. Abstr.*, **79**(1), p. 268 (May 1978).
- [155] A. W. Mullendore, G. C. Nelson, and P. H. Holloway, "Surface Sensitive Analytical Techniques: An Evaluation," *Proc. Advanced Techniques in Failure Analysis*, p. 236 (Sept. 1977).
- [156] I. L. Muller and J. R. Galvele, "Pitting Potential of High Purity Binary Aluminum Alloys—I. Al-Cu Alloys, Pitting and Intergranular Corrosion," *Corrosion Sci.*, **17**, p. 179 (1977).
- [157] C. R. Murphy and D. E. Mitchell, "Investigation of RGA Test Results for Hybrids with Epoxy Die/Substrate Attachment," *Proc. 1978 Int. Microelectron. Symp.*, p. 107, ISHM (Sept. 1978).
- [158] F. Neighbour and B. R. White, "Factors Governing Aluminum Interconnection Corrosion in Plastic Encapsulated Microelectronic Devices," *Microelectron. Reliab.*, **16**, p. 161 (1977).
- [159] D. A. L. Nicklen and D. R. Gabe, "A. C. Anodizing of Aluminum in Sulphuric Acid," *Surface Technol.*, **7**, p. 353 (1978).
- [160] K. Nisancioglu and H. Holtan, "Measurement of the Critical Pitting Potential of Aluminum," *Corrosion Sci.*, **18**, p. 835 (1978).
- [161] K. Nisancioglu and H. Holtan, "The Protection Potential of Aluminum," *Corrosion Sci.*, **18**, p. 1011 (1978).
- [162] K. Nisancioglu and H. Holtan, "Correlation of the Open-Circuit and Electrochemical Measurements for the Pitting Corrosion of Aluminum in Chloride Media," *Werkstoffe u. Korrosion*, **30**, p. 105 (1979).
- [163] N. W. Nurnberg, ed., *Electroanalytical Chemistry*, Wiley-Interscience, New York, NY (1975).
- [164] A. E. O'Keefe and G. C. Oitman, "Primary Standards for Trace Gas Analysis," *Anal. Chem.*, **38**(6), p. 760 (1966).
- [165] R. C. Olberg and J. L. Bozarth, "Factors Contributing to the Corrosion of the Aluminum Metal on Semiconductor Devices Packaged in Plastics," *Microelectron. Reliab.*, **15**(6), p. 601

- (1976).
- [166] R. G. Oswald, J. M. Montante, and W. R. Rodrigues de Miranda, "Automated Tape Carrier Bonding for Hybrids," *Proc. Symp. Plastic Encapsulated/Polymer Sealed Semiconductor Devices for Army Equipment* (US Army ERADCOM, Fort Monmouth, NJ), pp. 143-167 (1978).
 - [167] W. M. Paulson and R. W. Kirk, "The Effects of Phosphorus-Doped Passivation Glass on the Corrosion of Aluminum," *12th Ann. Proc. Reliab. Phys.*, p. 172 (1974).
 - [168] W. M. Paulson and R. P. Lorigan, "The Effect of Impurities on the Corrosion of Aluminum Metallization," *14th Ann. Proc. Reliab. Phys.*, p. 42 (1976).
 - [169] D. S. Peck, "New Concerns about Integrated Circuit Reliability," *16th Ann. Proc. Reliab. Phys.*, p. 1 (1978).
 - [170] D. S. Peck and C. H. Zierdt, Jr., "Temperature-Humidity Acceleration of Metal-Electrolysis Failure in Semiconductor Devices," *11th Ann. Proc. Reliab. Phys.*, p. 146 (1973).
 - [171] K. L. Perkins and J. J. Licari, "Investigation of Moisture Effects on Selected Microelectronic Devices," *Proc. 1978 Int. Microelectron. Symp.*, p. 125, ISHM (Sept. 1978).
 - [172] P. W. Peterson, "The Performance of Plastic Encapsulated CMOS Microcircuits in a Humid Environment," *Proc. 29th Electronic Components Conf.*, p. 360 (May 1979).
 - [173] G. F. Piacentini and G. Minelli, "Reliability of Thin Film Conductors and Air Gap Crossovers for Hybrid Circuits: Tests, Results and Design Criteria," *Microelectron. Reliab.*, 15, p. 451 (1976).
 - [174] D. C. Porter and M. Bahan, "Failure Analysis of Plastic Encapsulated Custom LSI Circuits," *Proc. Symp. Plastic Encapsulated/Polymer Sealed Semiconductor Devices for Army Equipment* (US Army ERADCOM, Fort Monmouth, NJ), p. 42 (1978).
 - [175] M. Pourbaix, *Atlas of Electrochemical Equilibria in Aqueous Solutions*, Pergamon Press, Oxford, England (1966).
 - [176] M. Pourbaix, *Lectures on Electrochemical Corrosion*, translated by J. A. S. Green, Plenum Press, New York, NY (1973).
 - [177] M. Pourbaix, "Some Applications of Potential-pH Diagrams to the Study of Localized Corrosion," *J. Electrochem. Soc.*, 123, p. 25C (Feb. 1976).
 - [178] J. L. Prince, Jr., "Investigation of Factors Involved in Reliability Assurance of Plastic-Encapsulated Integrated Circuits," Dept. Electrical and Computer Eng., Clemson Univ., SC, Feb. 8, 1978.
 - [179] J. L. Prince, D. B. Bullard, and R. A. Hartman, "Investigation of

- Accelerated Testing of Plastic-Encapsulated CMOS Integrated Circuits," *GOMAC-78*, Monterey, CA, Nov. 14, 1978, p. 143.
- [180] A. Quach and W. L. Hunter, "A Study of Properties of Plastics Used for Semiconductor Encapsulation," *J. Electronic Mater.*, **6**, p. 319 (May 1977).
- [181] B. Reich, "Life Characteristics of Plastic Encapsulated Semiconductor Devices," *Microelectron. Reliab.*, **17** (5), p. 513 (1978).
- [182] B. Reich, "A Study of Accelerated Storage Test Conditions Applicable to Semiconductor Devices and Microcircuits," *IEEE Trans. Reliab.*, **R-27**, p. 178 (Aug. 1978).
- [183] B. Reich, "Reliability of Plastic Encapsulated Semiconductor Devices and Integrated Circuits," *Solid State Technol.*, **21** (9), p. 82 (Sept. 1978).
- [184] Reliability Analysis Center, "Microcircuit Reliability Bibliography," *MRB-78*, RADC, Griffiss AFB, NY (April 1978).
- [185] Reliability Analysis Center, "Search and Retrieval Index to IRPS Proceedings—1968 to 1978," *TRS-2*, RADC, Griffiss AFB, NY (1979).
- [186] F. H. Reynolds and J. W. Stevens, "Semiconductor Component Reliability in an Equipment Operating in Electromechanical Telephone Exchanges," *16th Ann. Proc. Reliab. Phys.*, p. 7 (1978).
- [187] L. T. Romankiw, "Technique For Measuring pH at Electrodes During Electrolysis," Preprint rec. Nov. 2, 1978.
- [188] R. Rosenberg, M. J. Sullivan, and J. K. Howard, "Effect of Thin Film Interactions on Silicon Device Technology," in J. M. Poate, K. N. Tu, and J. W. Mayer, eds., *Thin Films—Interdiffusion and Reactions*, Wiley-Interscience, New York, NY (1978).
- [189] R. S. Rosler, W. C. Benzing, and J. Baldo, "A Production Reactor for Low Temperature Plasma-Enhanced Silicon Nitride Deposition," *Solid State Technol.*, **19**(6), p. 45 (June 1976).
- [190] W. H. Safranek, *The Properties of Electrodeposited Metals and Alloys*, American Elsevier Publishing Co., New York, NY (1974), pp. 153-178.
- [191] A. N. Saxena and R. A. Powell, "Chemical State of Phosphorus in Deposited SiO₂ (P) Films," in S. T. Pantelides, ed., *The Physics of SiO₂ and Its Interfaces*, Pergamon Press, New York, NY (1978), pp. 195-199.
- [192] N. L. Sbar, private communication, 1978.
- [193] N. L. Sbar, "Bias-Humidity Performance of Encapsulated and Unencapsulated Ti-Pt-Au Thin-Film Conductors in an Environment Contaminated with Cl₂," *IEEE Trans. Parts Hybr. Pkg.*

- PHP-12, p. 176 (Sept. 1976).
- [194] N. L. Sbar, "Environmental Testing to Study Circuit Failure Mechanisms and Acceleration Factors," *Electrochem. Soc. Ext. Abstr.*, 78(2), p. 668 (Oct. 1978).
- [195] N. L. Sbar and L. G. Feinstein, "Performance of New Copper Based Metallization Systems in an 85°C 80 Percent RH Cl₂ Contaminated Environment," *IEEE Trans. Parts Hybr. Pkg.*, PHP-12, p. 208 (1976).
- [196] N. L. Sbar and R. P. Kozakiewicz, "New Acceleration Factors for Temperature, Humidity, Bias Testing," *16th Ann. Proc. Reliab. Phys.*, p. 161 (1978).
- [197] G. M. Schmid and M. E. Curley-Fiorino, "Gold," in Vol. 4 of A. J. Bard, ed., *Encyclopedia of Electrochemistry of the Elements*, Marcel Dekker, Inc., New York, 1975, pp. 87-178.
- [198] G. L. Schnable, "Reliability of MOS Devices in Plastic Packages," *Proc. Tech. Program Int. Microelectron. Conf. (West/East)*, p. 82 (1976).
- [199] G. L. Schnable, "State of the Art in Semiconductor Materials and Processing for Microcircuit Reliability," *Solid State Technol.*, 21(10), p. 69 (Oct. 1978).
- [200] G. L. Schnable, L. J. Gallace, and H. Pujol, "Reliability of CMOS Integrated Circuits," *Computer*, 11(10), p. 6 (Oct. 1978).
- [201] G. L. Schnable, W. Kern, and R. B. Comizzoli, "Passivation Coatings on Silicon Devices," *J. Electrochem. Soc.*, 122, p. 1092 (Aug. 1975).
- [202] G. L. Schnable, E. M. Reiss, and M. Vincoff, "Reliability of Hermetically-Sealed CMOS Integrated Circuits," *EASCON (Electronics and Aerospace Systems Convention) '76 Record*, p. 143-A (Sept. 1976).
- [203] G. L. Schnable and P. F. Schmidt, "Applications of Electrochemistry to Fabrication of Semiconductor Devices," *J. Electrochem. Soc.*, 123, p. 310C (Sept. 1976).
- [204] P. wh Schuessler, "Polymer Sealed Devices in IBM Military Products," *Proc. Symp. Plastic Encapsulated/Polymer Sealed Semiconductor Devices for Army Equipment (US Army ERADCOM, Fort Monmouth, NJ)*, p. 240 (1978).
- [205] R. A. Schwartz, "Plastic Encapsulated Semiconductor Field Removal Data for Commercial Test and Measurement Equipment," *Proc. Symp. Plastic Encapsulated/Polymer Sealed Semiconductor Devices for Army Equipment (US Army ERADCOM, Fort Monmouth, NJ)*, p. 1 (1978).
- [206] S. Shabde, J. Edwards, and W. Meuli, "Moisture Induced Failure Mode in a Plastic Encapsulated Dynamic Timing Circuit," *15th*

- Ann. Proc. Reliab. Phys.*, p. 33 (1977).
- [207] S. P. Sharma, J. H. Thomas III, and F. E. Bader, "Development of a Gentle Accelerated Corrosion Test," *J. Electrochem. Soc.*, **125**, p. 2002 (Dec. 1978).
- [208] T. Shirasu and Y. Kosa, "Electrical Instability of Water-Absorbed CVD PSG Films," *Electrochem. Soc. Ext. Abstr.*, **79**(1), p. 462 (May 1979).
- [209] A. Shumka and R. Haack, "Moisture and Other Contaminants in Hybrid Packages," *Proc. 1978 Int. Microelectron. Conf.*, p. 128, ISHM (Sept. 1978).
- [210] A. Shumka and R. R. Piety, "Migrated-Gold Resistive Shorts in Microcircuits," *13th Ann. Proc. Reliab. Phys.*, p. 93 (1975).
- [211] D. W. Siitari and R. C. Alkire, "Experimental and Theoretical Modeling Studies on the Initiation of Crevice Corrosion," *Electrochem. Soc. Ext. Abstr.*, **79**(2), p. 618 (Oct. 1979).
- [212] L. G. Sillen and A. E. Martell, "Stability Constants of Metal-Ion Complexes," Spec. Publ. No. 17, The Chemical Society, London, 1964.
- [213] S. P. Sim and R. W. Lawson, "The Influence of Plastic Encapsulants and Passivation Layers on the Corrosion of Thin Aluminum Films Subjected to Humidity Stress," *17th Ann. Proc. Reliab. Phys.*, p. 103 (1979).
- [214] J. D. Sinclair, "An Instrumental Gravimetric Method for Indexing Materials, Contaminants, and Corrosion Products According to Their Hygroscopicity," *J. Electrochem. Soc.*, **125**, p. 734 (May 1978).
- [215] A. K. Sinha, H. J. Levinstein, and T. E. Smith, "Thermal Stresses and Cracking Resistance of Dielectric Films (SiN, Si₃N₄ and SiO₂) on Si Substrates," *J. Appl. Phys.*, **49**, p. 2423 (April 1978).
- [216] A. K. Sinha, H. J. Levinstein, T. E. Smith, G. Quintana, and S. E. Haszko, "Reactive Plasma Deposited Si-N Films for MOS-I:SI Passivation," *J. Electrochem. Soc.*, **125**, p. 601 (April 1978).
- [217] A. K. Sinha and T. T. Sheng, "The Temperature Dependence of Stresses in Aluminum Films on Oxidized Silicon Substrates," *Thin Solid Films*, **48**, p. 117 (1978).
- [218] J. M. Smith and S. M. Stuhlbarg, "Hybrid Microcircuit Tape Chip Carrier Materials/Processing Trade-Offs," *IEEE Trans. Parts Hybr. Pkg.*, **PHP-13**, p. 257 (Sept. 1977).
- [219] P. J. Smith, H. S. Wildman, and A. Leighton, "Pitting Corrosion in Al-Cu Thin Films," *Electrochem. Soc. Ext. Abstr.*, **79**(2), p. 640 (Oct. 1979).
- [220] D. T. Somerville, "The Role of Hybrid Construction Techniques on Sealed Moisture Levels," *15th Ann. Proc. Reliab. Phys.*, p. 107

- (1977).
- [221] N. A. Soos and D. Jaffe, "Encapsulation of Large Beam Leaded Devices," *Proc. 28th Electronic Components Conf.*, p. 213 (April 1978).
 - [222] R. W. Staehle, "Marcel J. N. Pourbaix—Palladium Award Medalist," *J. Electrochem. Soc.*, **123**, p. 23C (Feb. 1976).
 - [223] Staff Article, "Quality Control for Epoxy Encapsulants," *Circuits Manufacturing*, **18**(3), p. 18 (March 1978).
 - [224] Staff Article, "Fairchild Molds MOS Devices Faster, Better with Silicone/Epoxy Compound," *Dow Corning Material News*, p. 3 (Mar./Apr. 1979).
 - [225] H.-H. Strehblow and C. J. Doherty, "Examination of Aluminum Copper Films During Anodic Oxidation—I. Corrosion Studies," *J. Electrochem. Soc.*, **125**, p. 30 (Jan. 1978).
 - [226] R. E. Sulouff, "A Study of Leak Rate Versus Reliability of Hybrid Packages," *Proc. 1978 Int. Microelectron. Symp.*, p. 121, ISHM (Sept. 1978).
 - [227] M. E. Sweet, "Assessment of Moisture Permeation of an Epoxy Sealed Test Module," *Proc. 28th Electronic Components Conf.*, p. 33 (April 1978).
 - [228] C. H. Taylor, "Just How Reliable Are Plastic Encapsulated Semiconductors for Military Applications and How Can the Maximum Reliability Be Obtained?," *Microelectron. Reliab.*, **15**(2), p. 131 (1976).
 - [229] C. H. Taylor and B. C. Roberts, "Evaluation of a UK Specification for the Procurement of Plastic Encapsulated Semiconductor Devices for Military Use," *Proc. Symp. Plastic Encapsulated/Polymer Sealed Semiconductor Devices for Army Equipment* (US Army ERADCOM, Fort Monmouth, NJ), p. 55 (1978).
 - [230] R. E. Thomas, V. Winchell, K. James, and T. Scharr, "Plastic Outgassing Induced Wire Bond Failure," *Proc. 27th Electronic Components Conf.*, p. 182 (May 1977).
 - [231] R. W. Thomas, "Moisture, Myths and Microcircuits," *IEEE Trans. Parts Hybr. Pkg.*, **PHP-12**, p. 167 (Sept. 1976).
 - [232] P. A. Totta, "Abstract: In-Process Intergranular Corrosion of Al Alloy Thin Films," *J. Vac. Sci. Technol.*, **13**, p. 26 (Jan./Feb. 1978).
 - [233] R. K. Traeger, "Organics Used in Microelectronics: A Review of Outgassing Materials and Effects," *Proc. 27th Electronic Components Conf.*, p. 408 (May 1977).
 - [234] H. H. Uhlig, *Corrosion and Corrosion Control*, John Wiley & Sons, Inc., New York, NY (1963).
 - [235] H. H. Uhlig, "Advances in Corrosion Over the Past 25 Years," *J.*

- Electrochem. Soc.*, 125, p. 58C (Feb. 1978).
- [236] T. Valand and G. Nilsson, "The Influence of F⁻ Ions on the Electrochemical Reactions on Oxide-Covered Al," *Corrosion Sci.*, 17, p. 449 (1977).
- [237] M. Vandenberg, "Properties of Plasma Deposited Silicon Oxide," *Electrochem. Soc. Ext. Abstr.*, 79(1), p. 262 (May 1979).
- [238] M. Vandenberg and M. S. Hassan, "Cracking of Plasma Deposited Si-N Films After Subsequent Anneal," *Electrochem. Soc. Ext. Abstr.*, 79(1), p. 234 (May 1979).
- [239] E. P. G. T. van de Ven and H. Koelmans, "The Cathodic Corrosion of Aluminum," *J. Electrochem. Soc.*, 123, p. 143 (Jan. 1976).
- [240] R. W. Vasofsky, "Water Vapor Sorption of Package Sealants," *17th Ann. Proc. Reliab. Phys.*, p. 91 (1979).
- [241] R. Vasofsky, A. W. Czanderna, and K. K. Czanderna, "Abstract: Water Vapor Sorption by Cured Commercial Epoxies," *J. Vac. Sci. Technol.*, 16, p. 716 (March/April 1979).
- [242] J. L. Vossen et al., "Bibliography on Metallization Materials and Techniques for Silicon Devices, I to V," Thin Film Div., American Vacuum Society, New York, NY (1974-1979).
- [243] J. L. Vossen and W. Kern, eds., *Thin Film Processes*, Academic Press, New York, NY (1978).
- [244] J. L. Vossen, G. L. Schnable, and W. Kern, "Processes for Multi-level Metallization," *J. Vac. Sci. Technol.*, 11, p. 60 (Jan./Feb. 1974).
- [245] B. L. Weigand, J. J. Licari, and I. H. Pratt, "Detection of Conductive Condensates Resulting from Adhesive Outgassing in Hybrid Microcircuits," *Proc. 28th Electronic Comp. Conf.*, p. 217 (April 1978).
- [246] J. K. Whittington, G. T. Malloy, A. R. Mastro, and R. D. Hutchens, "Internal Conformal Coatings for Microcircuits," *IEEE Trans. Components, Hybr. Mfg. Technol.*, CHMT-1, p. 416 (Dec. 1978).
- [247] R. E. Williams, "Improvements in Plastic Integrated Circuits—Molding Compounds. Assembly Techniques and Reliability," *Proc. Symp. Plastic Encapsulated/Polymer Sealed Semiconductor Devices for Army Equipment* (US Army ERADCOM, Fort Monmouth, NJ), p. 184 (1978).
- [248] D. B. Willmott, "Investigation of Metallization Failures of Glass Sealed Ceramic Dual Inline Integrated Circuits," *15th Ann. Proc. Reliab. Phys.*, p. 158 (1977).
- [249] J. C. Wright, "Reliability Improvements of Plastic Semiconductors Using Gold Metallization," *11th Ann. Proc. Reliab. Phys.*, p. 224 (1973).

- [250] K. D. Zastrow, "Artillery Fuze Experience with Plastic Encapsulated Semiconductor Devices," *Proc. Symp. Plastic Encapsulated/Polymer Sealed Semiconductor Devices for Army Equipment* (US Army ERADCOM, Fort Monmouth, NJ), p. 54 (1978).
- [251] C. H. Zierdt, Jr., "Procurement-Specification Techniques for Plastic-Encapsulated Semiconductor Devices and Integrated Circuits," *Proc. Symp. Plastic Encapsulated/Polymer Sealed Semiconductor Devices for Army Equipment* (US Army ERADCOM, Fort Monmouth, NJ), p. 84 (1978).
- [252] C. H. Zierdt, Jr., "Accelerated Life Testing for LSI Failure Mechanisms," *16th Ann. Proc. Reliab. Phys.*, p. 76 (1978).

Recent References (Not Alphabetically Listed)

- [253] T. Smith and G. Lindberg, "Surface Tools for Automated Non-Destructive Inspection of Contamination," *Surface Technol.*, **9**, p. 1 (July 1979).
- [254] H. A. Katzman and G. M. Malouf, R. Baner and G. W. Stupian, "Corrosion-Protective Chromate Coatings on Aluminum," *Appl. Surf. Sci.*, **2**, p. 416 (Mar. 1979).
- [255] H. Leidheiser, ed., *Corrosion Control by Coatings*, Science Press, Princeton, NJ (1979).
- [256] R. Comizzoli, W. Kern, G. Schnable and L. White, "Corrosion of Metal Films with Defective Protection Layers", Final Report on Contract No. F-30602-78-C-0276 prepared by RCA Labs for Rome Air Development Center, Griffiss Air Force Base, New York, Oct. 1979.
- [257] R. B. Comizzoli, W. Kern, G. L. Schnable, L. K. White, D. A. Peters, E. Tracy, and R. D. Vibronek, "Corrosion of Aluminum IC Metallization with Defective Surface Passivation Layer," to be published.
- [258] K. Nisancioglu and H. Holtan, "Cathodic Polarization of Commercially Pure Aluminum," *Corrosion Science*, **19**, No. 8, p. 537 (1979).
- [259] R. P. Frankenthal and W. H. Becker, "Corrosion Failure Mechanisms for Gold Metallizations in Electronic Circuits," *J. Electrochem. Soc.*, **126**, p. 1718 (Oct. 1979).
- [260] R. P. Frankenthal and J. Kruger, eds., *Passivity of Metals*, The Electrochem. Soc., Princeton, NJ (1979).
- [261] B. L. Wensink, "Improved Technique for Decapsulation of Epoxy-Packaged Semiconductor Devices and Microcircuits," *Solid State Technol.*, **22**(10), p. 107 (Oct. 1979).

- [262] *Reliability Handbook*, National Semiconductor Corp., Santa Clara, CA (1979).
- [263] R. S. Rosler and G. M. Engle, "LPCVD-Type Plasma-Enhanced Deposition System," *Solid State Technology*, **22**(12), p. 88 (Dec. 1979).
- [264] A. Hiraiwa, K. Mukai, S. Harada, T. Yoshimi and S. Itoh, "Fast Etching Phenomena of Plasma-Silicon Nitride Films over Substrate Steps," *Japn. J. Appl. Phys.*, **18**, p. 191 (Jan. 1979).
- [265] "Advanced Techniques in Failure Analysis, 1978," *Proc. ATFA-78*, IEEE Cat. No. 78CH1407-6 REG 6, 1978.
- [266] L. K. White, R. B. Comizzoli, C. A. Deckert, and G. L. Schnable, "The Decoration of Corrosion Phenomena with pH-Sensitive Fluorescent Dyes on Aluminum and Gold Metallized IC Devices," to be published.
- [267] T. R. Beck and R. C. Alkire, "Occurrence of Salt Films During Initiation and Growth of Corrosion Pits," *J. Electrochem. Soc.*, **126**, p. 1662 (Oct. 1979).
- [268] A. J. Learn and R. S. Nowicki, "Methods for Minimizing Silicon Regrowth in Aluminum Films," *Appl. Phys. Lett.*, **35**, p. 611 (Oct. 15, 1979).
- [269] T. H. Nguyen and R. T. Foley, "On the Mechanism of Pitting of Aluminum," *J. Electrochem. Soc.*, **126**, p. 1855 (Nov. 1979).
- [270] F. L. Givens and W. J. Daughton, "Measuring Dielectric Film Integrity: An Application," *Semiconductor International*, **2** (9), p. 63 (Nov. 1979).
- [271] A. R. Reinberg, "Plasma Deposition of Inorganic Thin Films", in *Annual Review of Materials Science*, **9**, p. 341, ed. by R. A. Huggins, Annual Reviews Inc., Palo Alto, CA (Aug. 1979).
- [272] B. Mattison and T. Thompson, "Productivity Increase in A Planar Plasma Deposition System," *Solid State Technol.*, **22**(11), p. 81 (Nov. 1979).

Patents Issued to RCA Inventors—Third Quarter 1979

July

- A. A. Ahmed Voltage Regulators (4,160,201)
- A. A. Ahmed Current Amplifier Capable of Selectively Providing Current Gain (4,160,944)
- C. H. Anderson and F. J. Marlowe System and Method for Keying Video Information to Electron Beam Deflection (4,160,194)
- B. W. Beyers, Jr. and A. J. Suchko Television System Scheduler (4,162,513)
- G. W. Carter Mixer Injection Voltage Compensation Circuit (4,160,213)
- W. R. Curtice Exclusive-Or Circuit (4,160,919)
- W. F. Dietz Regulator with Short Circuit Protection (4,162,434)
- A. G. Dingwall Method of Making a Substrate Contact for an Integrated Circuit (4,159,561)
- A. H. Firester and M. E. Heller Apparatus for the Determination of Focused Spot Size and Structure (4,160,598)
- A. M. Goldschmidt and L. V. Hedlund Tracking Servo System for VideoDisc Player/Recorder (4,160,270)
- J. J. Hanak Inverted Amorphous Silicon Solar Cell Utilizing Cermet Layers (4,162,505)
- D. F. Hopta and H. R. Beellitz Switched Current Regulator (4,160,943)
- S. T. Hsu Floating Gate Solid-State Storage Device (4,162,504)
- E. O. Keizer Keel-Tipped Stylus for VideoDisc Systems (4,162,510)
- M. G. Kovac CCD Electrode and Channel Structure for 180 Degree Turn (4,160,262)
- D. P. Marlnelli Apparatus for Depositing Epitaxial Semiconductor From the Liquid Phase (4,159,694)
- F. J. Marlowe and R. H. Dawson Digital Memory Addressing System (4,160,273)
- L. W. Martinson Correlator/Convolver Using a Second Shift Register to Rotate Sample Values (4,161,033)
- D. D. Mawhinney, A. Rosen, Z. Turski, and H. J. Wolkstein Microwave Power Limiter Comprising a Single-Gate FET (4,162,412)
- T. E. Molinar Printed Circuit Impedance Transformation Network with an Integral Spark Gap (4,160,210)
- A. M. Morrell Cathode Ray Tube Having Corrugated Shadow Mask With Slits (4,162,421)
- J. L. Smith Magnetizing Apparatus and Method for Producing a Statically Converged Cathode Ray Tube and Product Thereof (4,162,470)
- V. Stachejko Precision Microwave Delay Circuit and Method (4,160,220)
- E. M. Sulphin, Jr. Ignition Spark Zone Duration Circuit (4,163,192)
- M. Toda, Y. Matsumoto, and S. Osaka Velocity Correction System for VideoDisc Player (4,162,511)
- C. M. Tomasetti and A. F. McDonie Red Sensitive Photocathode Having an Aluminum Oxide Barrier Layer (4,160,185)
- L. A. Torrington VideoDisc Package (4,159,827)
- M. H. Wardell, Jr. CRT with Tension Band Adapted for Pusher-Type Tensioning and Method for Producing Same (4,160,510)
- C. E. Weitzel and J. H. Scott, Jr. Planar Semiconductor Devices and Method of Making the Same (4,160,260)
- R. Williams and A. Bloom Process for Storing Solar Energy in the Form of an Electrochemically Generated Compound (4,160,816)

August

- A. A. Ahmed Television Kinescope Protection Circuit (4,164,687)
- J. A. Calamari, Jr. Method for Salvaging the Light-Absorbing Matrix and Support of a Luminescent Screen (4,165,396)
- D. E. Carlson and C. R. Wronski Schottky Barrier Amorphous Silicon Solar Cell with Thin Doped Region Adjacent Metal Schottky Barrier (4,163,677)
- C. A. Catanese Image Display Device with Ion Feedback Control and Method of Operating the Same (4,164,681)
- W. R. Curtice Time Interval Measurement (4,165,459)
- R. A. Dischert and S. L. Bendell Video Image Highlight Suppression Circuit with Delayed Compensation (4,166,281)

- K. Katagi Reduction of Target Shift in Coordinate Converter (4, 164,739)
- Y. Matsumoto VideoDisc Pickup Apparatus (4, 164,755)
- Y. Matsumoto Method for Manufacturing a Diamond Stylus for VideoDisc Players (4, 165,560)
- J. I. Nubani and R. L. Muenkel Stem-Sealing Method for Assembling Electron Tubes Including Improved Cullet Collection (4, 165,227)
- C. E. Profera Antenna Feed System (4, 163,974)
- T. O. Stanley Phosphor Screen for Flat Panel Color Display (4, 166,233)
- S. A. Steckler and A. R. Balaban Tuning System Including a Memory for Storing Tuning Information with User Controls Arranged to Facilitate Its Programming (4, 164,711)
- M. C. Stewart Locking Mechanism for Record Package (4, 164,782)
- M. Toda, Y. Matsumoto, and S. Osaka Disc Record Groove Skipper (4, 164,756)
- D. H. Willis Switching Regulator for a Television Apparatus (4, 163,926)
- O. M. Woodward Rotary Joint (4, 163,961)

September

- A. A. Ahmed Inverting Buffer Circuit (4, 166,964)
- O. E. Bessette and J. S. Griffin Rotating Head Recorder with Different Recording and Playback Speeds (4, 167,023)
- T. W. Burrus Noise Reduction Apparatus (4, 167,749)
- D. E. Carlson Amorphous Silicon Solar Cell Allowing Infrared Transmission (4, 166,919)
- S. L. Corsover Film Guide for Optical Scanners (4, 168,506)
- W. R. Curtice Threshold Gate (4, 166,965)
- R. A. Dischert and L. J. Thorpe Setup Control Unit for Television Cameras (4, 167,022)
- R. A. Gange Cathode and Method of Operating the Same (4, 167,690)
- J. J. Hanak Cermet Layers for Amorphous Silicon Solar Cells (4, 167,015)
- D. D. Holmes Suppression of Luminance Signal Contamination of Chrominance Signals in a Video Signal Processing System (4, 167,020)
- D. D. Holmes Suppression of Chrominance Signal Contamination of the Luminance Signal in a Video Signal Processing System (4, 167,021)
- G. Kaganowicz Method of Depositing a Silicon Oxide Layer (4, 168,330)
- S. K. Khanna PVC Molding Composition (4, 168,256)
- G. E. Nostrand and J. J. Hanak Method of Removing the Effects of Electrical Shorts and Shunts Created During the Fabrication Process of a Solar Cell (4, 166,918)
- P. Nyul Electroluminescent Semiconductor Device Having Optical Fiber Window (4, 167,744)
- J. C. Peer, W. F. Dietz, R. J. Gries, and L. W. Nero Overvoltage Protected De-Boost Regulator (4, 169,241)
- C. J. Petrizio AC Voltage Regulator (4, 168,476)
- D. H. Vilkomerson Pulse-Echo Ultrasonic-Imaging Display System Having Time-Variied Effective Aperture (4, 168,628)
- R. Williams and M. H. Woods Method of Testing Radiation Hardness of a Semiconductor Device (4, 168,432)
- D. H. Willis Automatic Peak Beam Current Limiter (4, 167,025)
- H. J. Wolkstein, J. Goel, and A. Rosen Microwave Power Limiter Comprising a Dual-Gate FET (4, 167,681)

AUTHORS



Kern K. N. Chang received his BS degree from National Central University, Chungking, China, in 1940, his MS degree in Electrical Engineering from the University of Michigan in 1948, and his PhD degree from the Polytechnic Institute of Brooklyn, New York, in 1954. Since 1948, Dr. Chang has been a Member of Technical Staff at RCA Laboratories, Princeton, N.J. From 1962 to 1971, he was Head of Solid State Microwave Devices. In 1967, he was appointed a Fellow of RCA Laboratories. He has been engaged in research on TV receivers, magnetrons, traveling-wave tubes, beam-focusing devices, parametric amplifiers, tunnel-diode devices, Hall effect solid-state devices, bulk light-emitting sources, avalanche diodes, and display devices. He is currently doing research on TV kinescopes. His significant technical contributions have included a pioneering effort on periodic field focusing that culminated in a commercial line of traveling-wave tubes, original work on parametric and tunnel diodes as amplifiers and converters for military and industrial applications, and discovery of a new mode of high-power and high-efficiency operation of avalanche diodes for radar application. Dr. Chang holds 32 U.S. patents in the field of microwave tubes and solid-state devices and is the author of the book *Parametric and Tunnel Diodes* (Prentice Hall, Inc.). He was the recipient of three RCA Laboratories Achievement Awards, for outstanding theoretical and experimental research on electron-beam focusing, on parametric and tunnel-diode devices, and on avalanche diodes. He was also the 1964 Achievement Award winner of the Chinese Institute of Engineers, New York, Inc., and in 1967 he received the David Sarroff Outstanding Achievement Individual Award in Science. Dr. Chang is a member of Sigma Xi.



Robert B. Comizzoli received a BS degree in Physics, summa cum laude, from Boston College in 1962 and was awarded Wilson, Danforth, and National Science Foundation fellowships. He attended Princeton University from 1962 to 1966, receiving a PhD in Physics in 1967. His thesis work involved polarization effects in photoconductors. He joined RCA Laboratories, Princeton, New Jersey, in 1966. His research experience includes color centers in alkali halides, atomic beams, neutron interactions with polarized nuclei, photoconductivity, electrophotography, silicon device surface effects, and dielectric breakdown evaluations. He has developed new techniques for the study of surface and bulk charge in high-resistivity semiconductors, and has contributed to the understanding of electrophotographic parameters as affected by substrate-interface electrical breakdown. Dr. Comizzoli has studied glass passivation of silicon devices; he has developed novel methods for the deposition of thick-glass-passivating films and has related device performance to thick-glass passivation properties. He originated a useful method for decorating localized defects in insulating films over conductors or semiconductors. He has studied failure mechanisms of bipolar and CMOS integrated circuits, and has made important contributions to understanding and eliminating these failure mechanisms. In November 1979, he was appointed Manager, Quality Assurance and Special Projects, at the Solid State Technology Center of RCA Laboratories in Somerville, N.J.

Dr. Comizzoli received a 1973 RCA Laboratories Achievement Award for his contributions to the glass passivation of silicon device structures, and a 1978 RCA Laboratories Achievement Award for contributions to integrated circuit reliability. He is a Senior Member of IEEE and a member of the Electrochemical Society.



and the IEEE.

Richard S. Crandall received a B.S. degree in physics from Cornell University in 1960, an M.S. in physics in 1962, and a Ph.D. in physics from the University of Illinois. He joined RCA Laboratories in 1964 and has worked in the fields of Electron and phonon transport in insulators and semiconductors, electron surface states on liquids, electrochromics, macro ions in solution, and is now engaged in studies of amorphous silicon solar cells. Dr. Crandall received an RCA Achievement Award for work on the electron-photon interaction and spent the year from 1971 to 1972 at the Zurich Laboratories of RCA. He is a member of The American Physical Society



Werner Kern received his education in chemistry at universities in Switzerland and the U.S.A. The research thesis he published in 1947 on the discovery of fluorescing carcinogenic hydrocarbons in soil established an important new branch of environmental science. He was research chemist with Hoffmann-LaRoche in Switzerland and New Jersey, and with Nuclear Corporation of America where he became chief chemist directing research in radiation chemistry. He joined RCA Electronic Components and Devices Division in 1959 to investigate semiconductor processes by radiochemical methods, was project scientist and consultant on several research projects, and was in charge of radiological safety. Since 1964 he has been at RCA Laboratories in Princeton, N.J. as a Member of the Technical Staff in semiconductor process research, specializing in chemical vapor deposition, etching processes, characterization, and device applications of dielectric films. From 1974 to 1979 he was project scientist for government-sponsored research contracts on glass passivation, dielectric defects, and silicon solar cells. Mr. Kern is a member of the American Chemical Society, the American Vacuum Society, the Electrochemical Society, the Research Honorary Society of Sigma Xi, and is listed in "American Men and Women of Science" and "Who's Who in the East". He holds five U.S. patents, and has presented numerous invited technical lectures, as well as organizing several scientific symposia. He received an RCA Achievement Award in 1966 for his work in integrated circuit process research, and is the recipient of the Callinen Award for 1971 of the Electrochemical Society, in recognition of his pioneering work in chemical vapor deposition research. He received a 1973 RCA Laboratories Outstanding Achievement Award for his team contributions to glass passivation of silicon device structures. In 1978 he completed coediting and coauthoring a book on thin film processes, published by Academic Press.



Wendell M. Lee received the B.S. degree in Chemistry from Virginia Union University in 1953. From 1953 to 1955 he did graduate studies at Howard University. In 1955, he joined the Plastics Section of the National Bureau of Standards, where his surface chemistry studies on glass reinforced plastics led to the development of an automatic tensiometric method for measuring the surface tensions of liquids. Dr. Lee matriculated at the Polytechnic Institute of Brooklyn in 1959, receiving the Ph.D. degree in Polymer Chemistry in 1967. His Ph.D. thesis dealt with the uses of nuclear magnetic resonance (nmr) spectroscopy in determining the microtacticities and molecular motions of new methacrylate polymers with highly fluorinated side groups, and, in part, with the theoretical and experimental nmr spectra of five proton, AMX_3 , spin systems (methacrylate monomers). In 1966, Dr. Lee joined the RCA Laboratories. His work in electrophotography led him to the invention of metal ion complexing dye classes that are highly efficient spectral sensitizing materials for certain inorganic photoconductors. Dr. Lee's involvement in other research activities includes materials research for prerecorded-video systems and

assisting RCA's Consumer Electronics Division in successfully meeting the current safety standards for the TV industry. His current research activities include polymer rheology, injection molding, and the properties and testing of plastics.

Dr. Lee is a member of Sigma Xi, Phi Lambda Upsilon, the Society of Plastics Engineers and the American Chemical Society and its Polymer and Organic Coatings and Plastics Chemistry Divisions.



George L. Schnable received a B.S. degree in Chemistry from Albright College, Reading, Pa., in 1950, and M.S. and Ph.D. degrees in Chemistry from the University of Pennsylvania, in 1951 and 1953 respectively. From 1953 until 1971, he was employed by Philco-Ford Corporation, where he became Manager of the Advanced Materials and Processes Department in the R & D Operation of the Microelectronics Division. In 1971, Dr. Schnable joined RCA Laboratories, Princeton, N.J., as Head, Process Research, in the Process and Applied Materials Research Laboratory, where he supervised projects dealing with thin-film dielectrics and metallization, silicon

device fabrication technology, ion-implantation technology, and silicon device reliability. In 1977, he was named Head, Solid State Process Research. He is presently Head, Device Physics and Reliability in the Integrated Circuit Technology Center of RCA Laboratories. Dr. Schnable holds 20 U.S. Patents and is listed in American Men and Women of Science. He is a Member of the American Chemical Society, the Electrochemical Society, the Franklin Institute, the Pennsylvania Academy of Science, Alpha Chi Sigma, Phi Lambda Upsilon, and Sigma Xi; a Senior Member of the American Association for the Advancement of Science and the Institute of Electrical and Electronics Engineers; and a Fellow in the American Institute of Chemists.



Lawrence K. White received an A.B. degree from Earlham College (1970) and a Ph.D. degree in physical chemistry (1975) from the University of Illinois (Urbana). He joined RCA Labs in 1978 where he became involved in IC device processing and reliability research. Dr. White is a member of Phi Lambda Upsilon, Sigma Xi, Alpha Chi Sigma, the American Chemical Society, and the Electrochemical Society.



Richard Williams received the A.B. in chemistry from Miami University and his Ph.D. in physical chemistry from Harvard University. He joined RCA Laboratories, Princeton, N.J., in 1958. He has worked in numerous areas, including semiconductor-electrolyte interfaces, liquid crystals, internal photoemission, and insulator physics. He was group leader in Insulator Physics from 1967 to 1970 and in Quantum Electronics from 1970 to 1972; in 1972, he was made a Fellow. He has received several achievement awards and shared in the David Sarnoff Team Award in Science in 1969. He was a visiting scientist at the RCA Zurich laboratory in 1963 and has been

a Fulbright Lecturer in Sao Carlos, Brazil, a summer school lecturer at Instituto Politécnico Nacional in Mexico, and a visiting lecturer at Princeton University.

Index Volume 40, 1979

March

- 3 **A Computer Evaluation of Colorimetric Effects of Differential Gain and Differential Phase Distortions in Color TV Receivers Having Phosphors and Demodulation Matrices Different from NTSC**
T. M. Wagner
- 22 **High-Power Low-Loss PIN Diodes for Phased-Array Radar**
A. Rosen, R. U. Martinelli, A. Schwarzmann, G. J. Brucker, and G. A. Swartz
- 59 **On the Limits of the Electrophotographic Process**
H. Kiess
- 96 **Patents**
- 99 **Authors**

June

- 103 **A Temperature-Compensated Laser Module for Optical Communications**
M. Ettenberg, D. R. Patterson, and E. J. Denlinger
- 115 **The Adherence of Chromium and Titanium Films Deposited on Alumina, Quartz, and Glass—Testing and Improvement of Electron-Beam-Deposition Techniques**
Martin Caulton, William L. Sked, and Francis S. Wozniak
- 129 **Doppler Servo Tracker With Frequency Synthesizer Feedback**
M. I. Rozansky
- 140 **An Optimized Grid Design for a Sun-Concentrator Solar Cell**
A. R. Moore
- 153 **Optimum Grid Design for a Nonuniformly Illuminated Sun-Concentrator Solar Cell**
A. R. Moore
- 166 **Response of Diazoquinone Resists to Optical and Electron-Beam Exposure**
Michael Kaplan and Dietrich Meyerhofer
- 191 **The Effect of Rain on Satellite Communications Above 10 GHz**
R. S. Engelbrecht
- 230 **Correction Notice**
- 231 **Patents**
- 234 **Authors**

September

- 241 **Low-Loss Charge-Coupled Device**
Walter F. Kosonocky and Donald J. Sauer
- 278 **Analysis of the Effective Transfer Losses in a Low-Loss CCD**
Donald J. Sauer

- 295 Review and Analysis of Laser Annealing**
A. E. Bell
- 339 Laser Annealing to Round the Edges of Silicon Structures**
C. P. Wu and G. L. Schnable
- 345 Optical Recording With the Encapsulated Titanium Trilayer**
A. E. Bell, R. A. Bartolini, and F. W. Spong
- 363 Patents**
- 365 Authors**

December

- 371 Carrier Generation, Recombination, and Transport in Amorphous Silicon Solar Cells**
Richard Williams and Richard S. Crandall
- 390 Collimated Electron Trajectory in a Nonuniform Transverse Magnetic Field**
K. K. N. Chang
- 397 Shear Viscosity-Temperature-Shear Rate Relations for Flame Retardant Impact Polystyrene Melts**
Wendell M. Lee and Hollis V. Becker
- 415 A Survey of Corrosion Failure Mechanisms in Microelectronic Devices**
George L. Schnable, Robert B. Comizzoli, Werner Kern, and Lawrence K. White
- 447 Patents**
- 449 Authors**
- 452 Index to Volume 40, 1979**

Index to Authors, Volume 40, 1979

- R. A. Bartolini** Optical Recording with the Encapsulated Titanium Trilayer, Sept., p. 345
- Hollis V. Becker** Shear Viscosity-Temperature-Shear Rate Relations for Flame Retardant Impact Polystyrene Melts, Dec., p. 397
- A. E. Bell** Review and Analysis of Laser Annealing, Sept., p. 295
—Optical Recording with the Encapsulated Titanium Trilayer, Sept., p. 345
- G. J. Brucker** High-Power Low-Loss PIN Diodes for Phased-Array Radar, March, p. 22
- Martin Caulton** The Adherence of Chromium and Titanium Films Deposited on Alumina, Quartz, and Glass—Testing and Improvement of Electron-Beam-Deposition Techniques, June, p. 115
- K. K. N. Chang** Collimated Electron Trajectory in a Nonuniform Transverse Magnetic Field, Dec., p. 390
- Robert B. Comizzoli** A Survey of Corrosion Failure Mechanisms in Microelectronic Devices, Dec., p. 415
- Richard S. Crandall** Carrier Generation, Recombination, and Transport in Amorphous Silicon Solar Cells, Dec., p. 371
- E. J. Denlinger** A Temperature-Compensated Laser Module for Optical Communications, June, p. 103
- R. S. Engelbrecht** The Effect of Rain on Satellite Communications Above 10 GHz, June, p. 191
- M. Ettenberg** A Temperature-Compensated Laser Module for Optical Communications, June, p. 103
- Michael Kaplan** Response of Diazoquinone Resists to Optical and Electron-Beam Exposure, June, p. 166
- Werner Kern** A Survey of Corrosion Failure Mechanisms in Microelectronic Devices, Dec., p. 415
- H. Kless** On the Limits of the Electrophotographic Process, March, p. 59

- Walter F. Kosonocky** Low-Loss Charge-Coupled Device, Sept., p. 241
- Wendell M. Lee** Shear Viscosity-Temperature-Shear Rate Relations for Flame Retardant Impact Polystyrene Melts, Dec., p. 397
- R. U. Martinelli** High-Power Low-Loss PIN Diodes for Phased-Array Radar, March, p. 22
- Dietrich Meyerhofer** Response of Diazoquinone Resists to Optical and Electron-Beam Exposure, June, p. 166
- A. R. Moore** An Optimized Grid Design for a Sun-Concentrator Solar Cell, June, p. 140
—Optimum Grid Design for a Nonuniformly Illuminated Sun-Concentrator Solar Cell, June, p. 153
- D. R. Patterson** A Temperature-Compensated Laser Module for Optical Communications, June, p. 103
- A. Rosen** High-Power Low-Loss PIN Diodes for Phased-Array Radar, March, p. 22
- M. I. Rozansky** Doppler Servo Tracker With Frequency Synthesizer Feedback, June, p. 129
- Donald J. Sauer** Low-Loss Charge-Coupled Device, Sept., p. 241
—Analysis of the Effective Transfer Losses in a Low-Loss CCD, Sept., p. 278
- G. L. Schnable** Laser Annealing to Round the Edges of Silicon Structures, Sept., p. 339
—A Survey of Corrosion Failure Mechanisms in Microelectronic Devices, Dec., p. 415
- A. Schwarzmann** High-Power Low-Loss PIN Diodes for Phased-Array Radar, March, p. 22
- William L. Sked** The Adherence of Chromium and Titanium Films Deposited on Alumina, Quartz, and Glass—Testing and Improvement of Electron-Beam-Deposition Techniques, June, p. 115
- F. W. Spong** Optical Recording With the Encapsulated Titanium Trilayer, Sept., p. 345
- G. A. Swartz** High-Power Low-Loss PIN Diodes for Phased-Array Radar, March, p. 22
- T. M. Wagner** A Computer Evaluation of Colorimetric Effects of Differential Gain and Differential Phase Distortions in Color TV Receivers Having Phosphors and Demodulation Matrices Different from NTSC, March, p. 3
- Lawrence K. White** A Survey of Corrosion Failure Mechanisms in Microelectronic Devices, Dec., p. 415
- Richard Williams** Carrier Generation, Recombination, and Transport in Amorphous Silicon Solar Cells, Dec., p. 371
- Francis S. Wozniac** The Adherence of Chromium and Titanium Films Deposited on Alumina, Quartz, and Glass—Testing and Improvement of Electron-Beam-Deposition Techniques, June, p. 115
- C. P. Wu** Laser Annealing to Round the Edges of Silicon Structures, Sept., p. 339

4237